Progress in Materials Science 125 (2022) 100891

Contents lists available at ScienceDirect

Progress in Materials Science

journal homepage: www.elsevier.com/locate/pmatsci

Nanofabrication through molding

Ze Liu [a,*,1], Naijia Liu [b,1], Jan Schroers [b,*]

[a] Department of Engineering Mechanics, School of Civil Engineering, Wuhan University, Wuhan, Hubei 430072, China
[b] Department of Mechanical Engineering and Materials Science, Yale University, New Haven, CT 06511, USA

ARTICLE INFO

Keywords:
Nanomolding
Nanofabrication
Diffusion
Dislocation slip
Single crystal
Viscous flow

ABSTRACT

Nanomolding usually refers to a top-down fabrication method by which a formable or moldable material is shaped using a mold of nanoscale dimensions. Nanomolding is the underlying mechanism for a wide range of nanofabrication methods including template-based deposition, extrusion, nanoembossing, soft lithography, nanoimprint lithography, thermomechanical nanomolding, and nanoimprinting. Its suitability for nanofabrication in a wide range of materials and states of matter makes it one of the most versatile nanofabrication methods. It offers solutions for the fabrication of a wide range of nanomaterials for applications including catalysts, energy, devices, and a wide range of surface functionalization as well as improvements of lithography techniques. This review discusses the various physical mechanisms underlying the nanomolding process, and how they relate to the specifics of the states of matter and the material classes. Nanofabrication methods will then be categorized based on their underlying mechanism, materials that they can fabricate, and technological characteristics such as scalability, costs, precision, and versatility. This will help the reader navigate the numerous, often very specific, methods of this advanced field, and identify the most appropriate process and state of matter for a specific application. A general discussion on nanomolding follows, from accomplishments to date and the challenges that lie ahead in realizing the many potential nanodevices and structures that researchers have envisioned. Particularly the recent advances of nanomolding have resulted in a paradigm shift of nanofabrication in which the design of nanodevices is no longer limited by material and nanostructured geometries but can be selected from a very wide palette of materials.

1. Introduction

Nanofabrication is a crucial requirement in the development of solutions to challenges in a variety of areas including water desalination [1,2], batteries [3,4], fuel cells [5], cellular response [6,7], antibacterial [8], hydrophobic [9-11], de-icing [12], plasmonics [13-16], photovoltaics [17], biosensors [18,19], catalysis [20,21], adhesion regulation [22], flexible electronics [23], storage devices [24], nanogenerators [25], nanopore sequencing [26], nanomechanics [27], lab-on-chip systems [28], surface-enhanced Raman spectroscopy (SERS) [29,30], medical diagnosis [18], biomedicine [31], and metasurfaces [32]. One of the overreaching motivations for nanofabrication is to fabricate nanodevices and structures with very large surface/volume or surface/footprint ratios in order to enhance the chemical reactions occurring on the surfaces. Typically, the nanostructures simply multiply the materials required for specific applications through their enlarged surface area. Very different from this general nanoscale effect, in some cases the

* Corresponding authors.
E-mail addresses: ze.liu@whu.edu.cn (Z. Liu), jan.schroers@yale.edu (J. Schroers).
[1] These authors contributed equally to this work.

https://doi.org/10.1016/j.pmatsci.2021.100891
Received 12 March 2021; Received in revised form 30 October 2021; Accepted 3 November 2021
Available online 14 November 2021

Nomenclature

symbol	definition
σ_{flow}	flow stress
$\dot{\gamma}$	strain rate in liquids
$\dot{\varepsilon}$	Strain rate in solids
η	viscosity
ρ	density
γ	surface tension
θ	wetting angle
d	character size/diameter
F_G	gravity force
F_p	pressure force
F_d	dislocation slip force
F_y	capillary force
F_η	viscos force
τ_y	shear strength
p_y	pressure induced by capillary force
p_η	pressure induced by viscous force
D	diffusion coefficient
D_L	lattice diffusivity
D_I	interface diffusivity
δ	interface diffusion layer thickness
G	shear modulus
b	Burgers vector
k_B	Boltzmann constant
T_g	glass transition temperature
T_x	crystallization temperature
T_m	melting temperature
$\overline{u}$	Mean flow velocity of liquid
V	volume of nanowire
L	length of nanowire
L_m	maximum length by dislocation-based molding
S	cross section area of nanowire
J	atomic flux
Ω	average atomic volume
N_d	number of dislocations
p_c	minimum molding pressure required for dislocation-based nanomolding

material itself changes its properties when its size is reduced to the nanoscale [33-39]. Yet another motivation for the nanoscale is to match length scales of physical phenomena. This is used to tune the optical, electrical, and mechanical properties of a material by matching the sample size with the characteristic length scale of a specific physical phenomenon [27,40,41].

Nanofabrication can be traced back to circa 1860, when Michael Faraday chemically synthesized gold nanoparticles [42] and observed that the color of such colloidal gold nanoparticle solution can vary drastically from the bulk color of gold, and can change with the size of the nanoparticles (Fig. 1). This observation stimulated great interest in the chemical synthesis of nanoparticles [65,66]. However, the morphologies of synthesized nanoparticles are difficult to control due to the complex physical mechanisms underlying their nucleation and growth [66,67]. Hence the preparation of precise nanopatterns has relied on lithography techniques, such as photolithography and electron/ion beam lithography [46,47,68], which were developed for the fabrication of microelectronics. Spontaneous growth methods were introduced to semiconductors in the 1960 s, by applying metallic catalysts, when whiskers/nanowires growth with a Vapor-Liquid-Solid (VLS) mechanism has been developed. In the 1970s, mica templates were first introduced into electrochemical synthesis, to prepare 1D nanostructures [48,69] where the growth of nanostructures is constrained to follow the cavities in the template. Direct fabrication of nanopatterns into soft polymers by nanoimprinting was achieved in 1995 and was considered an effective manufacturing method for ICs [53,54,70]. Following these advances, soft nanolithography techniques such as microcontact printing [71,72], replica molding [73,74], microtransfer molding [75,76], micromolding in capillaries [54,77], and solvent-assisted micromolding [78,79] have been proposed. These soft nanolithography methods are best suited for the liquid state of matter. In the following 10 years, a large number of nanofabrication methods were developed. These methods are either based on gas or liquid processes, and include dip-pen lithography [59,80], solid state de-wetting [81], self-assemble [82], and nanomolding [60]. In 2009, nanomolding of amorphous metals was demonstrated. Very recently (2017–2020), thermomechanical nanomolding of metals in their crystalline state was introduced for a very broad range of metals and alloys [60-64] as high-aspect-ratio single crystal nanowires

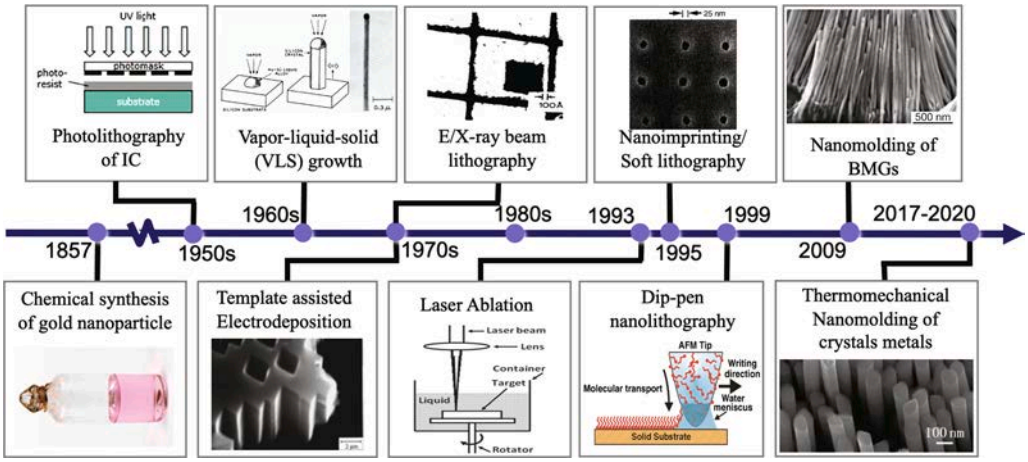

Fig. 1. Timeline of major milestones in nanofabrication. Preparation of Au nanoparticles by chemical synthesis in 1857 [42] is often referred to as the "birth of modern nanofabrication." Photolithography has enabled the microelectronic revolution through the precise and scalable fabrication of Integrated Circuits in the 1950s [43] (Copyright 2020, Elsevier). Breakthroughs in the vapor–liquid-solid (VLS) growth in the 1960s has provided solutions for the growth of semiconductor single crystal nanowires [44,45] (Copyright 2004, AIP Publishing [44]). E/X-ray beam lithography [46,47] (Copyright 1976, AIP Publishing [47]) and template-assisted electrodeposition [48] (inset [49], Copyright 1999, AIP Publishing [49]) in the 1970s has been used in the fabrication of integrated electronics. In 1993, laser ablation-based synthesis of nanoparticles was demonstrated [50-52] (Copyright 2012, John Wiley and Sons [52]). Direct imprinting of nanopatterns into soft polymers by using hard molds was demonstrated in 1995 [53-58] (Copyright 1996, The American Association for the Advancement of Science [56]). Dip-pen nanolithography was proposed in 1999 as a way to directly "write" nanopatterns in substrates by using atomic force microscope tips [59] (Copyright 1999, The American Association for the Advancement of Science). Direct thermomechanical nanomolding of metals/alloys to prepare nanostructures was achieved in 2009 for metallic glasses [60] (Copyright 2009, Springer Nature) and in 2017–2020 for crystalline metals and alloys [61-64] (Copyright 2019, American Physical Society [62]).

[61-64].

In principle, all nanofabrication techniques can be classified into two categories: top-down, in which a large work piece is shaped or reduced into nano-dimensions, and bottom-up, in which small building blocks build up the nanostructure. Today's nanofabrication methods can go down to below 10 nm, and some can fabricate hierarchical structures [83-88]. However, each technique has its own

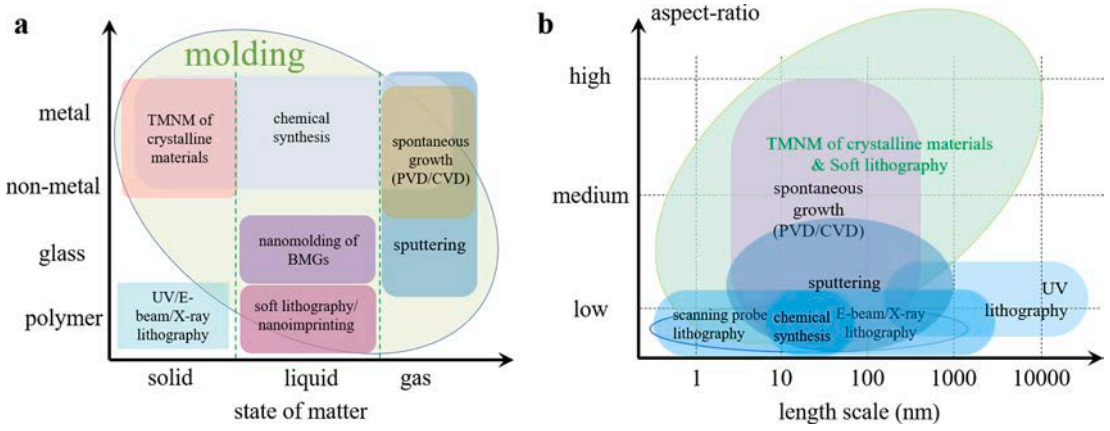

Fig. 2. Classification of common nanofabrication techniques. (a) Comparison of typical nanofabrication techniques in terms of material types and the state of matter. Metal and non-metal (e.g., semiconductors, ceramics, and ordered phases) nanostructures can be prepared by solid-based TMNM, chemical synthesis methods, gas-based physical vapor depositions (PVD), and chemical vapor deposition (CVD) by spontaneous growth and gas phase sputtering. Nanostructured glass materials such as metallic glasses are widely prepared by liquid-based nanomolding. Polymer materials are generally patterned by solid-based lithography (e.g., UV/E-beam/X-ray) and liquid-based soft lithography such as microcontact printing or nanoimprinting. Indicated by the green background are all the nanofabrication methods in which molding constitutes the underlying mechanism which covers all states of matter and materials. (b) Classification of the nanofabrication techniques by their length scale and aspect ratio. Chemical synthesis and scanning probe lithography have excellent resolution down to the molecular level, but the aspect ratio of prepared nanostructure is usually low. Lithography (UV/E-beam/X-ray) allows preparation of regular nanofeatures from sub-10 nm to microns, but they are also limited to small aspect ratios. Overall, TMNM, nanomolding of BMGs and soft lithography are most versatile in terms of length scales and aspect ratios. (For interpretation of the references to color in this figure legend, the reader is referred to the web version of this article.)

advantages and limitations such as the optimal state of matter, the material it can fabricate on the nanoscale, size limitations, dimensional precision and control, scalability, robustness, and costs. For example, chemical synthesis of nanomaterials allows the fabrication of metal and non-metal nanostructures down to very small length scales in massive production. But the fabricated geometry of these methods is always limited to nanoparticles, often referred to as zero-dimensional nanoparticles with no dimension >100 nm. An additional limitation is that the size distribution of nanoparticles cannot be precisely controlled. Lithography (i.e., UV/E-beam/X-ray lithography) is the most advanced and widespread nanofabrication technology and offers the ability to achieve complex human-designed nanopatterns with excellent dimensional precision and control. Resolution limitations of lithography originate from diffraction effects of the pattern caused by electromagnetic radiation. Additional limitations derive from the etching process, which limits the geometry to perpendicular site walls. Scanning probe lithography (e.g. dip-pen lithography [59]) can attain molecular-level resolution, but suffers from limited scalability. This review will discuss the wide range of techniques and their characteristics in detail, with a focus on the nanomolding technique and the underlying various physical mechanisms.

A useful classification of nanofabrication methods is by the materials they can fabricate, and the state of matter of that material during fabrication (Fig. 2a). In most common nanofabrication methods, metal and non-metals such as semiconductors, ceramics, and ordered phases, can be prepared by solid-based TMNM, chemical synthesis methods, and gas-based physical vapor depositions (PVD) and chemical vapor deposition (CVD) by spontaneous growth and gas phase sputtering. Nanostructured glass materials such as metallic glasses and particularly the subset of metallic glasses with high processability, so called bulk metallic glasses (BMGs), are widely prepared by liquid-based nanomolding. Polymer materials are generally patterned by solid-based lithography (e.g., UV/E-beam/X-ray) and liquid-based soft lithography such as microcontact printing or nanoimprinting. Nanofabrication methods in which molding constitutes the underlying mechanism cover all states of matter and materials.

Another useful comparison of nanofabrication methods is by their length scale and aspect ratio (Fig. 2b). In principle, chemical methods can achieve very fine resolution (atomic scale) because it is a “bottom-up” method. Lithography (UV/E-beam/X-ray) covers the length scale from sub-10 nm to microns, but the aspect ratio of prepared nanostructures and their shape is limited due to beam scattering. Scanning probe lithography (including dip-pen nanolithography) can obtain feature size as small as the molecular scale, but the fabricated aspect ratio is low as it is relying on probe scanning. Among the nanofabrication techniques, both TMNM and soft lithography can prepare nanostructures with high aspect ratio as well as small feature size.

These comparisons of nanofabrication methods reveal that molding is by far the most versatile method in terms of materials, state of matter, and length scales. This recognition of the versatility and wide usage of nanofabrication methods based on molding has been the motivation for this review. Within this review, we will discuss nanomolding in terms of the different states of matter (gas, liquid, crystal) and the various material classes that can be fabricated (metals, polymers, glasses). We will further consider the specific requirements (temperature, pressure, reactivity with environment), achievable length scales, and applications and potential applications specific nanofabrication are best suited for. Finally, we will suggest, based on the above discussion, research that we consider critical to unleash the potential of nanomolding to realize the many applications that have been envisioned.

2. Nanomolding essentials

2.1. Molding

Nanomolding is based on the same principles as molding, a 6000-year-old manufacturing process [89]. Typically in molding, a moldable material is shaped using a mold as a rigid form-giving tool (Fig. 3(a)). A bias, which is typically a pressure gradient, a chemical gradient, or an electric field, is the driving force for the moldable material to fill the mold cavity. As deformation should be limited to the moldable material, the mold must have a significant higher strength (or viscosity) than the moldable material at the

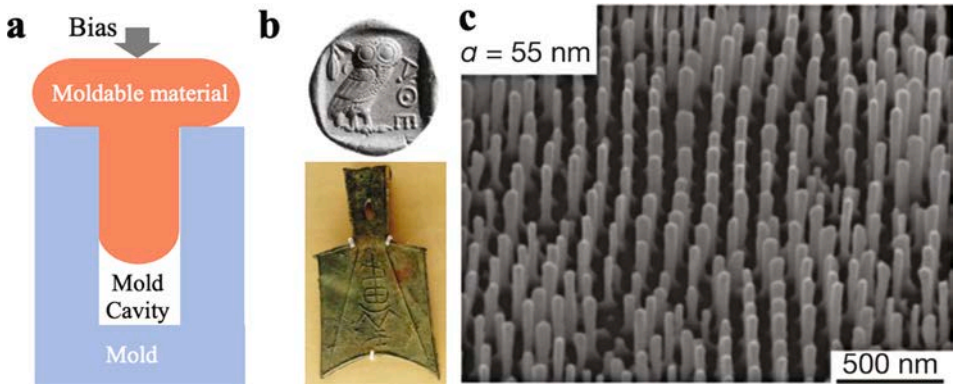

Fig. 3. Principle of molding. (a) A moldable material is typically formed under a bias, such as a pressure gradient into a hard mold to fill the mold cavity. (b) Molded ancient coin from the Spring and Autumn period of China, 770–476 BCE. This particular part was molded by pouring liquid bronze, CuSn, into a coin mold. (c) Using the same molding principle, metallic glass nanorod arrays are molded into mold cavities of 55 nm in diameter [60] (Copyright 2009, Springer Nature).

molding temperature. The requirement for significant higher strength is difficult to define in a general sense, as it depends on the specifics of the molding process. As an estimate, one order of magnitude higher strength in the mold than in the moldable material is a reasonable general guideline. Requirements for the pressure gradient or general bias are (i) that it is sufficiently large to drive the moldable material to fill the mold cavity on a desirable time scale and (ii) that it is sufficiently small so as not to exceed the yield strength of the mold. For example, considering that the flow stress of a liquid scales with the strain rate as $\sigma_{\text{flow}} = \dot{\gamma} \times \eta$ (σ_{flow} : flow stress, η: viscosity, $\dot{\gamma}$: strain rate), obeying the requirement (i) requires high strain rate; this leads to high flow stress, which requires high applied pressure, which may exceed the yield strength of the mold. Hence, requirements (ii) cannot simultaneously be obeyed. As molding is often carried out at elevated temperatures, the mold material must be able to withstand applied forming pressure at such temperatures.

2.2. From Macroscopic molding to nanomolding

Essentially, the mechanism for nanomolding is the same as for macroscopic molding. However, due to the different scaling of the involved forces with the characteristic size, the dominant force controlling the molding mechanism changes (Fig. 4). Taking the mold diameter d as the characteristic size, their scaling can be expressed as:

$$\begin{cases} F_G \propto d^3 \\ F_p \propto d^2 \\ F_d \propto d^2 \\ F_\eta \propto d^2 \\ F_\gamma \propto d \end{cases} \tag{1}$$

Here, F_G is the gravity force and scales with the volume, hence d^3. F_p is the pressure force applied on the moldable material, and scales with the area over which the applied pressure acts, hence d^2. Both the yielding force, F_d, and the viscous force, F_η , are resisting the molding process. F_d scales with d^2 as described by the Schmid law (slip deformation of single crystals). F_η scales with d^2 as described by the Hagen-Poiseuille equation. The capillary force, F_γ can either promote or resist molding, depending on the wettability of the moldable material on the mold. F_γ scales with the circumference of the mold cavity, the length of the intersection between mold, and the free surface of the moldable material. To compare the contributions of the various forces, we assume typical values for metals: for density $\rho = 1000\text{kg/m}^3$, surface tension $\gamma = 1\text{N/m}$, viscosity of supercooled liquid $\eta = 10^7\text{Pa•s}$, shear strength of ~ 10 MPa, under an applied pressure of ~ 1 GPa, and formed nanowires with $L/d = 5$ on a practical time scale of 100 s. The quantitative results of these forces as a function of the characteristic length scales are plotted in Fig. 4.

In addition to geometric scaling (eq.1), materials may also change their properties. For example, crystalline metals (solids) increase their strength when the sample size is reduced to nanoscale dimensions. This has been explained by a dislocation starvation process [27,90-94]. The increase of the already high strength of crystalline metals has led to the general opinion that nanomolding of crystalline metals is impractical [60,95,96]. Material property changes have also been reported for liquids, where a change in viscosity has been observed when the liquid is confined to length scales comparable to their intrinsic length scales [97-99]. Intrinsic length scale depends on the material and can be set by the chain length of polymers, the shear transformation zones in metallic glasses, or particle size in granular materials [100]. Such size effects in properties can be significant, and hence must be considered in nanomolding.

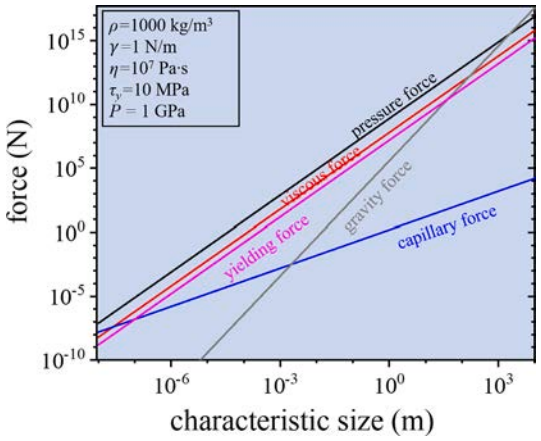

Fig. 4. Scaling of the involved forces during molding with the molding diameter (characteristic length scale). The forces are calculated according to$F_G = \rho g V$, $F_p = p\pi d^2/4$, $F_d = \tau_y \pi d^2/4(cos45^\circ)^2$, $F_\eta = 8\eta\pi L^2/t$, and $F_\gamma = \pi d\gamma cos\theta$. Whereas applied pressure force and resisting viscous and yielding force exhibit same scaling, and hence their relative importance is size independent, gravity force dominates at large scales while the capillary force dominates at very small scales.

2.3. State of matter of moldable materials for nanomolding

Nanomolding has been carried out with materials in all three states of matter: solid, liquid, and gas. It is generally carried out under a combination of pressure and temperature. Pressure takes the role of the driving force for the molding process, and temperature the enabler, to reduce viscosity or flow stress of the moldable materials. The main differentiator for the nanomolding process in the three states of matter is the viscosity and diffusivity (the change in shear modulus of solids is small in comparision). The viscosity changes by over 16 orders of magnitude, from a glass below its glass transition of $> 10^{12}$ Pa•s, and liquids including supercooled liquids spanning from 10^{12} to 10^{-3} Pa•s, to gases with a viscosity below 10^{-5} Pa•s. For solids including crystals, the lattice diffusion coefficient varies from $D \sim 10^{1}$ nm^2/s at around $0.5T_m$ to $\sim 10^{7}$ nm^2/s near T_m. It is this wide variation of viscosity and diffusivity that defines the flow resistance stress (Fig. 5), and thus determines the requirements for a specific nanomolding technique dependent on the state of matter.

Separate nanomolding techniques exist for low and high viscous liquids. For low viscous liquids, capillary forces dominate viscous forces (see Fig. 4). High viscous liquids, such as supercooled liquids, are controlled by viscous forces. Only when very small dimensions are molded capillary forces must also be considered [60,102]. For supercooled liquids, which can be present in amorphous materials such as polymers and metallic glasses, the viscosity of the liquid decreases exponentially with increasing temperature in the supercooled liquid region between the glass transition temperature, T_g, and the crystallization temperature, T_x [103,104]. Practically accessible viscosities are in the range of 10^{5}-10^{12} Pa•s [103,105-110]. Viscosities in polymers are in the range of 10^{2} and 10^{5} Pa•s [111,112]. As most polymers don't readily crystallize, constrains on processing time are not a general limitation. For metallic glasses this is different as they readily crystallize, and access to low viscosity is limited with impractically short processing times and fast strain rates [105,109,113-116].

Solid state matter-based nanomolding has been dismissed as impractical until recently, due to the high strength of solids [27,90,117-122]. An additional challenge results from the size dependent deformation mechanisms in metals (Fig. 13). Hence, effective deformation mechanisms which take place on the macroscale, such as the motion of existing mobile dislocations or cross-slip, are not available on the nanoscale [62] due to dislocation starvation [92,94,123]. Such scaling of deformation mechanisms in metals also reflects in the "Hall-Petch" effect, in which nanoscale metals approach theoretical strength ($\sim Y/10$, Y is the elastic modulus), as well as changes in the deformation mechanisms from highly localized to homogeneous deformation in amorphous metals [27,90,117-122,124,125].

Recently however, a nanomolding method based on atomic diffusion was introduced which can be applied to essentially all metals [61], alloys [62,63,126], and, even to many ordered phases [64]. Such diffusion-based molding is only effective on the nanoscale, as diffusion lengths are too short for macroscale dimensions. As the rapid diffusion path is generally on the mold/moldable interface, the effectivity of such a diffusion-based molding process scales with the ratio of the circumference/cross sectional area, $1/d$. Hence, diffusion-based deformation is highly effective on the nanoscale but can be neglected on the macroscale at the expense of other more effective deformation mechanisms (see details in Fig. 13).

Numerous solution and gas-based nanomolding techniques have been developed in the past two decades (Fig. 6c) [127,128]. The required bias, such as a gradient in concentration, pressure, chemical potential or electrical potential for solution-based and gas-based nanomolding, is usually very low. Such low bias originates from the very low viscosities, $\sim 10^{-3}$ Pa·s for solution, and $\sim 10^{-5}$ Pa·s for

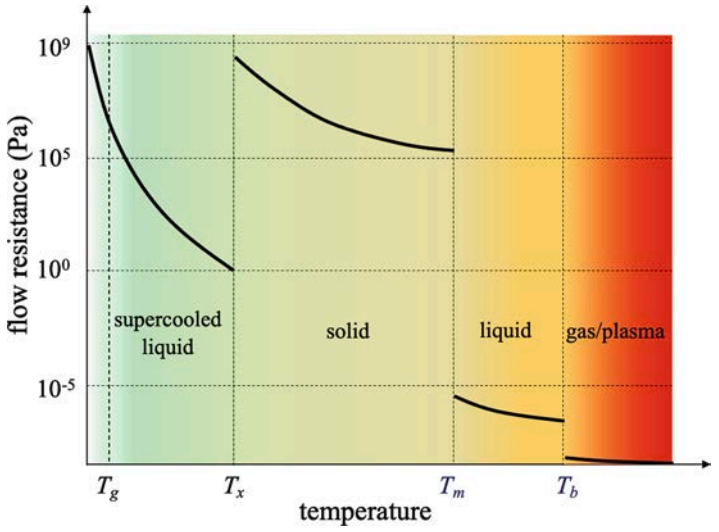

Fig. 5. Flow resistance as a function of temperature for the three states of matter. The flow resistance of liquid (including supercooled liquid) and gas (including plasma) is estimated through $\sigma = \eta \cdot \dot{\gamma}$, where η and $\dot{\gamma}$ represent viscosity and strain rate, and the flow stress (creep stress) of solids (including crystal) as $\sigma = \left(\frac{k_B T G^2 \dot{\varepsilon}}{Db}\right)^{1/3}$ [61,101], where D, G, b, and k_B represent the diffusion coefficient, shear modulus, magnitude of the Burgers' vector and the Boltzmann constant, respectively. The strain rate is taken as $\dot{\varepsilon} = 10^{-3}$ s^{-1}.

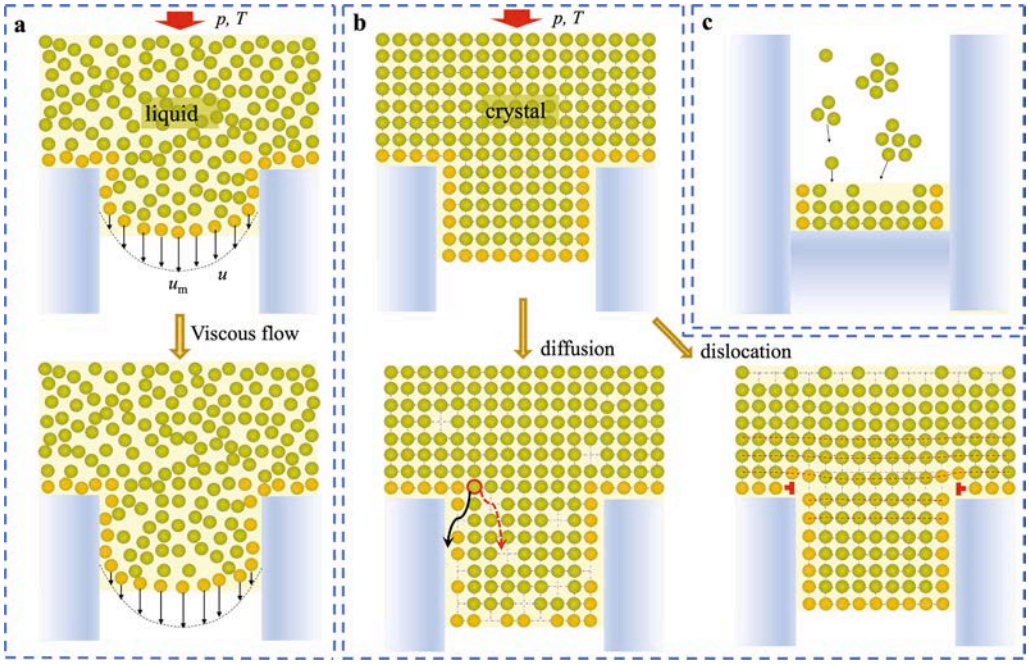

Fig. 6. Underlying microscopic mechanisms for the nanomolding of liquid, crystal, gas, and diluted solutions. (a) Viscous flow of a liquid into a mold cavity. The required driving force must overcome the internal friction force of the liquid. For typical non-slip boundary condition with a finite mold/liquid material friction coefficient, the velocity of liquid atoms varies from a small value (zero for an infinite friction coefficient) at the liquid/mold interface, to a maximum value at the center of the mold cavity. (b) Thermomechanical nanomolding (TMNM) of solids is based on diffusion as the transport mechanism at high homologous temperature, $T > 0.4\ T_m$, and dislocation slip at low homologous temperature, $T < 0.4\ T_m$. (c) Nanomolding in gas and solution phases. Atoms, ions, or clusters are driven by a bias such as a gradient in concentration, pressure, electric field, or chemical potential gradient into the mold, and form nanostructures which dimensions are controlled through the confinement provided by the mold.

gas, compared to the viscosities of supercooled liquids, $> 10^5$ Pa·s. For example, pressure gradients of $\sim 10^5$ Pa/cm and electrical field gradients of $\sim 10^2$ V/cm are sufficient to achieve the biased particle velocity to fill mold nanocavities on a practical time scale [129]. Like in any molding process, for solution- and gas/plasma-based nanomolding, the mold serves as a geometrical confinement, shaping and confining the forming nanocrystals [130-132] (Fig. 6). Solution-based and gas-based nanomolding are both versatile, scalable, and practical. Limitations for solution-based nanomolding are given by the selection and availability of precursor compounds, and the limitation of the number of components which can be used simultaneously, which is usually limited to three [133]. Gas-based nanomolding is often slow due to the small material flux rate, especially for nanostructures with high-aspect ratios. High-aspect ratio nanostructures pose an additional challenge, which originates from the divergence of the material transport preventing filling of long and narrow cavities. The synthesize efficiency can be enhanced through the use of catalysts, which have to be applied into the mold cavity prior to molding [128,134].

3. Nanomolding mechanisms

The developed nanomolding techniques are dictated by the states of matter of the molded material. A summary of the dominant mechanisms enabling nanomolding of liquids and solids are shown in Fig. 6. The flow mechanism behind the nanomolding of liquids is generally viscous and/or capillary-flow dominated (Fig. 6a). The flow mechanism of solid states under molding can either be dominated by diffusion or dislocation motion (Fig. 6b), depending on temperature and pressure. For high-temperatures, $T > 0.4T_m$, nanomolding is diffusion dominated, while for low-temperatures, $T < 0.4T_m$, nanomolding is dominated by dislocation motion [63]. Gas-phase nanomolding is based on the transport of individual particles following a bias into the mold cavity (Fig. 6c). The bias is typically realized through a gradient in pressure, electrical, or magnetic field.

3.1. Nanomolding of liquids: Viscous flow and capillary flow

Generally, viscous force and capillary force are the intrinsic forces related to the flow of liquids. Viscous force always resists flow into the mold cavity, while capillary force can either drive the flow into the mold or resist it, depending on the wettability of the liquid on the mold surface. Such wettability is quantified by the contact angle of the liquid/mold interface. Therefore, nanomolding of liquids requires an applied force to balance the flow resistance forces. For a steady-state flow of a Newton fluid into a cylindrical mold cavity of diameter *d*, the required applied force is:

$$F_p = F_\eta + F_\gamma = 8\pi\eta\bar{u}L - \pi d\gamma\cos\theta \tag{2}$$

with $\bar{u} = u_m/2$ as the mean flow velocity of the fluid in the mold cavity (Fig. 6(a)). Eq. (2) is valid for viscous flow with a small Reynolds number ($\mathrm{Re} = \frac{\rho\bar{u}d}{\eta} \ll 1$). For nanomolding of high viscous liquids such as polymers and BMGs in their supercooled state, the small Reynolds number requirement, which results in laminar flow, is always present. If in addition to laminar flow, interface slipping is suppressed, and $\bar{u} \approx L/t$ can be approximated, mold filling can be quantified by a modified Hagen-Poiseuille equation containing a capillary term [60,61]:

$$p_0 = p_\eta + p_\gamma = \frac{32\eta}{t}\left(\frac{L}{d}\right)^2 - \frac{4\gamma\cos\theta}{d} \tag{3}$$

p_η and p_γ are pressure terms that correspond to flow resistance force and capillary force, respectively. Examples of nanostructures which have been molded according to Eq. (3) comprise a wide range of materials and length scales, including those that can be

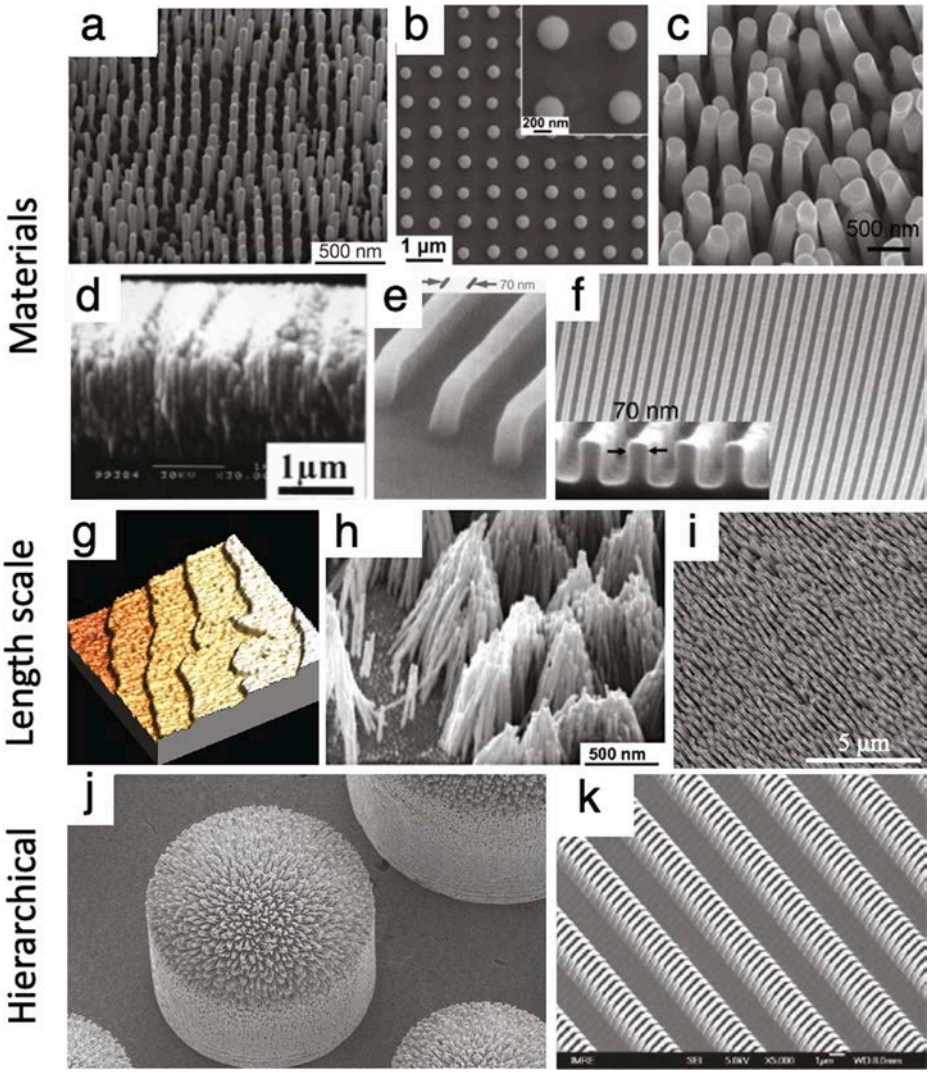

Fig.7. Examples of viscous flow-based nanomolding. (a)-(f) Nanomolding of different materials (a) $Pt_{57.5}Cu_{14.7}Ni_{5.3}P_{22.5}$ BMG [60] (Copyright 2009, Springer Nature). (b) $Pd_{40.5}Ni_{40.5}Si_{4.5}P_{14.5}$ BMG [135] (Copyright 2015, Elsevier). (c) $Zr_{35}Ti_{30}Cu_{8.25}Be_{26.75}$ BMG [102] (Copyright 2015, IOP Publishing). (d) TiO_2 nanowires [136] (Copyright 2001, AIP Publishing). (e) PDMS [56] (Copyright 1996, The American Association for the Advancement of Science). (f) PMMA [137] (Copyright 2007, John Wiley and Sons). (g)-(i) Nanomolding on a different length scale. (g) Atomic-size resolution in nanoimprinting of metallic glasses demonstrated through replication of atomic steps in $Pt_{57.5}Cu_{14.7}Ni_{5.3}P_{22.5}$ surface [138]. (h) 13 nm in diameter nanowire arrays of $Pt_{57.5}Cu_{14.7}Ni_{5.3}P_{22.5}$ BMG [60] (Copyright 2009, Springer Nature). (i) 200 nm in diameter nanowire arrays of $Pt_{57.5}Cu_{14.7}Ni_{5.3}P_{22.5}$ BMG. (j)-(k) Hierarchical structures. (j) BMG hierarchical nanostructures combining micron- and nano-length scales [83] (Copyright 2015, American Chemical Society). (k) PMMA hierarchical nanostructure combining micron- and nano-length scales [139] (Copyright 2006, IOP Publishing).

combined into hierarchical structures (Fig. 7).

3.1.1. Viscous flow of highly viscous liquid-based nanomolding

Though both viscous force and capillary force generally contribute to the nanomolding of liquids (Eq. (3)), their relative contribution can vary dramatically, to the extent that one force essentially dominates the process (Fig. 4). For highly viscous liquids such as supercooled liquids of BMG forming alloys and polymers, $F_\eta \gg F_\gamma$, since $\eta \gg \frac{\gamma|\cos\theta|}{\bar{u}} \frac{d}{L}$. In order to estimate the situations that result in viscous- or capillary-dominated behavior, the forces in the viscosity-mold diameter parameters space using Eq. (3) are calculated (Fig. 8). For this, typical values were assumed: $|\cos\theta| = 0.5$, $L/d = 5$, and a practical time scale of $t = 100$ s. For large mold diameter and high viscosity, nanomolding is viscous force dominated. On the other hand, for small mold diameters and low viscosity, nanomolding of viscous liquids is dominated by capillary forces. In the transition region both forces have to be considered. For example, for $d = 10^2$ nm and $\eta = 10^7$-10^8 Pa•s, viscous force and capillary force contribute approximately equivalently to the flow into the nanomold cavity.

Capillary force-dominant nanomolding is typically present in polymers and sol–gel materials [56,140-144], whereas viscous force-dominated namomolding is present in metallic glasses [60,102,145-155]. However, it has been observed that when nanomolding metallic glass into smaller sizes, < 100 nm, capillary forces have to be considered, and for $d < 20$ nm, capillary forces dominate the molding process (Fig. 9) [60]. In the case of nanomolding BMGs into small sizes, < 100 nm, appropriate mold/moldable materials have to be identified to achieve a contact angle below 180° (Fig. 9) [156,157]. Otherwise, the required forming pressures are impractically high to realize nanomolding [60,102]. It is worth noting that for $\theta < 90°$ capillary force promotes nanomolding, but to date such a condition has not been realized.

For viscous force-dominated nanomolding (Fig. 8), the viscosity is the controlling material parameter (Fig. 10). The required molding pressure is essentially defined by the viscous flow term in Eq. (3):

$$p_0 = p_\eta = \frac{32\eta}{t}\left(\frac{L}{d}\right)^2 \tag{4}$$

To provide some typical requirements for the forming pressure, we assume a molding time of $t \sim 100$ s, a mold cavity of $d = 100$ nm, and an aspect ratio of $L/d = 10$. For polymeric liquids ($\eta \sim 10^3$ Pa•s), these conditions require a forming pressure of $p_0 \sim 0.01$ MPa. For metallic glass liquids, the viscosity is on the order of 10^7 Pa•s [103], and thus the required forming pressure under the same conditions is $p_0 \sim 100$ MPa. In addition, considering that metallic glasses are metastable in nature, the available processing time generally limits the molding time. Substituting a typical crystallization time for BMGs (with viscosity of $\sim 10^7$ Pa•s) of $t_{cryst} \sim 300$ s [158], and a typical molding pressure of 100 MPa, into Eq. (4), the maximum aspect ratio that can be obtained is $\frac{L}{d} = \sqrt{\frac{p_0 t_{cryst}}{32\eta}} = \sqrt{\frac{100\times10^7\times300}{32\times10^7}} = 30$, which can be considered a medium-high aspect ratio.

In summary, nanomolding based on viscous flow offers a solution to fabricate nanostructures from highly viscous liquids. It can be realized with a variety of material classes including BMGs [60,159], sol-gels [136], and polymers [56,137] (Fig. 7). In terms of geometry, it covers length scales down to sub nanometers [152,160], and allows the fabrication of hierarchical micro/nanostructures

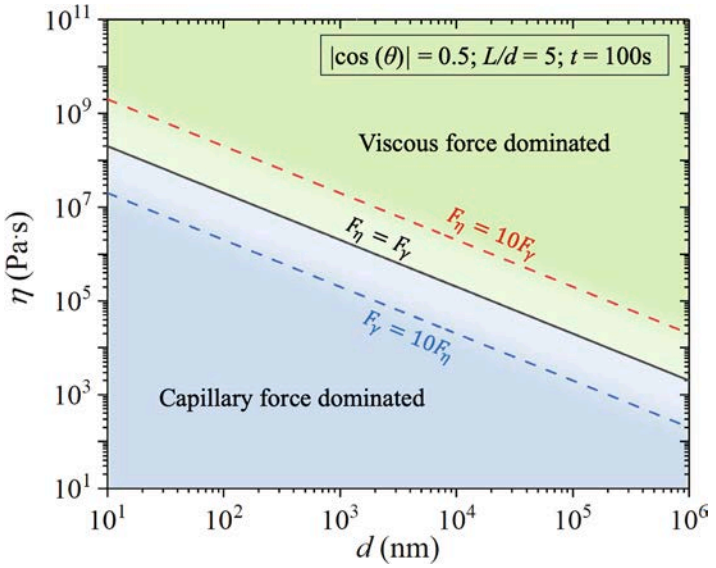

Fig. 8. Viscous force or capillary force-dominated nanomolding regions as a function of mold diameter and viscosity. Values are calculated according to $p_0 = p_\eta + p_\gamma = \frac{32\eta}{t}\left(\frac{L}{d}\right)^2 - \frac{4\gamma\cos\theta}{d}$, assuming typical conditions: $|\cos\theta| = 0.5$, $L/d = 5$, and $t = 100$ s. For small diameters and low viscosity, nanomolding is dominated by capillary forces, and for high viscosity and large diameters, nanomolding is dominated by viscous forces. The transition region requires consideration of both forces.

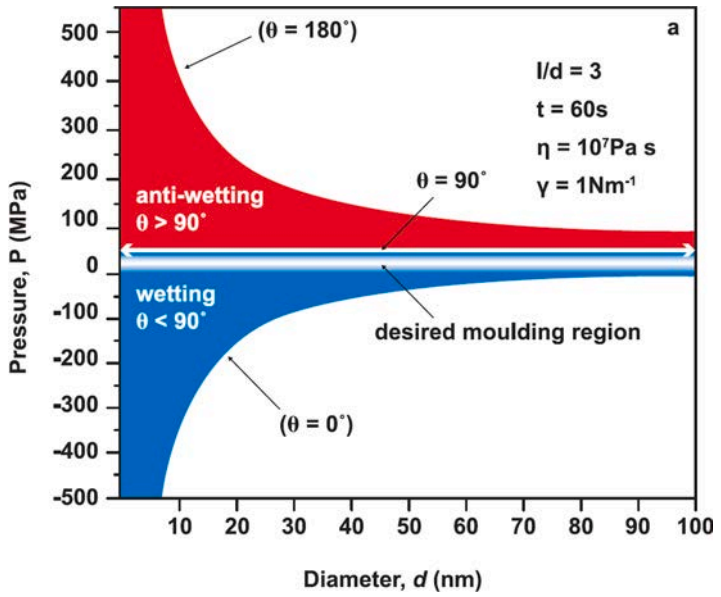

Fig. 9. Required pressure for nanomolding of supercooled liquids as a function of mold diameter. For mold cavities smaller than ~ 100 nm capillary forces become significant. The wetting behavior drastically increases ($\theta > 90°$) or decreases ($\theta < 90°$) the required forming pressure for small mold diameters [60] (Copyright 2009, Springer Nature).

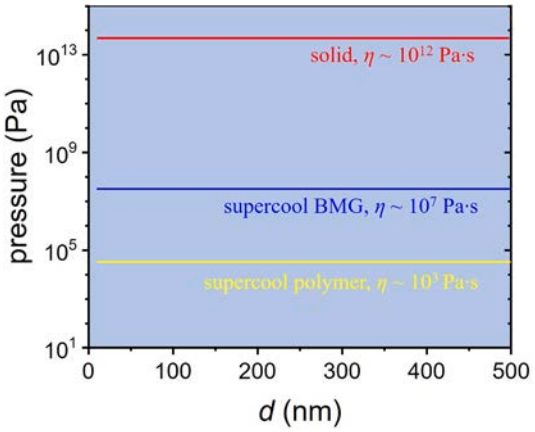

Fig. 10. Required forming pressure to nanomold solids. Materials considered include BMGs at room temperature or crystalline materials, BMGs in their supercooled liquid state and polymers. Equation (4) is performed with: $t = 100$ s, $L/d = 10$, and a typical viscosity for polymer of ~ 10^3 Pa•s, BMG in supercooled liquid (~10^7 Pa•s), and a solid (~10^{12} Pa•s).

[83,139] (Fig. 7). Whereas polymers and sol-gels nanomolding is capillary force-controlled metallic glasses nanomolding is viscous force-controlled. Only on the small scale (< ~100 nm) must the contribution of capillary force be considered, as it becomes dominant at ~ 20 nm in the nanomolding of metallic glasses (Fig. 9 and Fig. 10). The versatility of this process has led to a large range of applications spanning from fuel cells, catalysis, force sensors, waveguides, magnetic storages, and structural color filters (Fig. 11).

3.1.2. Capillary force controlled nanomolding

In the case of capillary force-controlled nanomolding, the wetting of the moldable material on the mold plays an important role (Fig. 9 and Fig. 12). The pressure required for capillary force-controlled nanomolding is defined by the capillary term in Eq. (3):

$$P_0 \approx P_\gamma = -\frac{4\gamma\cos\theta}{d} \tag{5}$$

For $\Theta > 90°$ (dewetting), formation of additional interface requires energy. Hence, the capillary force resists molding. As a consequence, P_γ increases with decreasing mold cavity (the black line in Fig. 12(a)). Under dewetting conditions, an external force is thus required for nanomolding. However, for $\Theta < 90°$ (wetting), formation of an additional interface lowers the energy of the system,

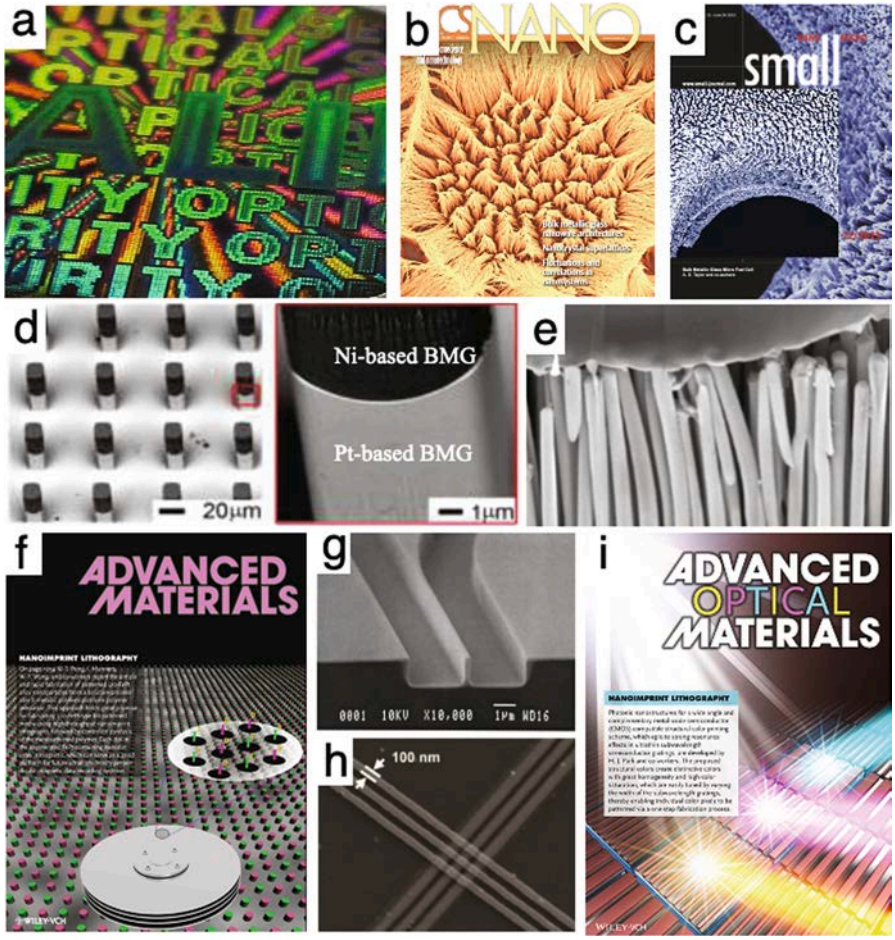

Fig. 11. Applications of viscous flow-based nanomolding. (a) diffraction patterns to generate color on metallic glass surfaces [100] (Copyright 2010, John Wiley and Sons), (b)-(c) catalyst fuel cells [5,161] (Copyright 2012, John Wiley and Sons [5]. Copyright 2011, American Chemical Society [161]), (d) metal–metal Janus nanostructures [162] (Copyright 2016, American Chemical Society), (e) nanopatterns as a cell traction force sensor [19] (Copyright 2017, American Chemical Society), (f) bit-patterned media for high-density magnetic data storage [163] (Copyright 2012, John Wiley and Sons), (g) Polymer waveguides [164] (Copyright 2002, American Vacuum Society), (h) metallic cross bars for nanocircuits [165] (Copyright 2009, American Chemical Society), (i) structural color filters with subwavelength semiconductor gratings [166] (Copyright 2016, John Wiley and Sons).

which leads to spontaneous wetting and molding (the dashed blue line in Fig. 12(a)).

Capillary force-controlled nanomolding can be present when filling liquids with a viscosity below $\sim 10^6$ Pa·s into nanocavities below 100 nm (Fig. 8). This can be realized in polymers [167], sol-gels [136], and liquid metals [77]. For example, it has been demonstrated that liquid lead spontaneously fills into carbon nanotubes through capillary forces (Fig. 12(c)) [77]. To fabricate low aspect-ratio nanofeatures from polymers such as photoresists, capillary forces have been utilized to develop capillary-force lithography [167,168]. Capillary forces can also be utilized to fabricate semiconductor oxide nanofibers/nanowires, even those of high-aspect ratio based on the sol–gel method [169]. It should be mentioned that for supercooled polymers and metallic glasses, nanomolding is often controlled by a combination of viscous and capillary forces (see Figs. 7 and 8)[60].

In summary, liquid-based nanomolding is generally controlled by viscous and capillary forces. It can be quantified by the Hagen-Poiseuille law (Eq. (3)) when extended to include a capillary pressure term. For high viscosities ($>10^8$ Pa·s) and larger mold cavities (>100 nm), viscous force controls nanomolding (Fig. 8). Capillary forces can be dominating (depending on the wetting angle) for low viscosities ($<10^6$ Pa·s) and/or small mold cavities (<100 nm).

Liquid-based nanomolding can be used to fabricate metal, polymer, and even ceramic nanostructures by using liquid metals, supercooled metallic glasses, polymers, or sol-gels. It is a stable process, which can be precisely controlled, is readily scalable, and robust. It has been widely explored in the commercial arena for nanoimprint lithography (NIL) in applications including semiconductors, nanophotonics, displays, light-emitting diodes, solar cells, optical communication, semiconductor integrated circuits, data storage, biotechnology, pharmaceuticals, medicines, and security features [56,137,144,170-178].

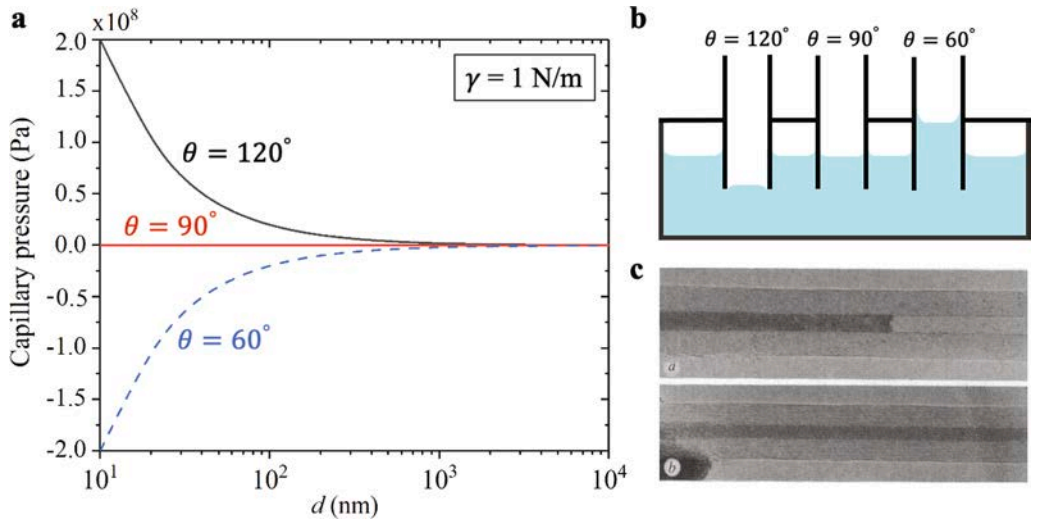

Fig. 12. Capillary force-dominated nanomolding of liquids. (a) Capillary force can be either a driving force or resistance force to molding, depending on the contact angle of the liquid/mold interface. (b) Liquids immersed in tubes with different wetting angles of 120°, 90°, and 60°. A wetting angle below 90° causes the capillary force to counteract gravity force and pull the liquid up. (c) Molten lead spontaneous fills carbon nanotubes through the action of a capillary force ($\theta < 90°$) [77] (Copyright 1993, Springer Nature).

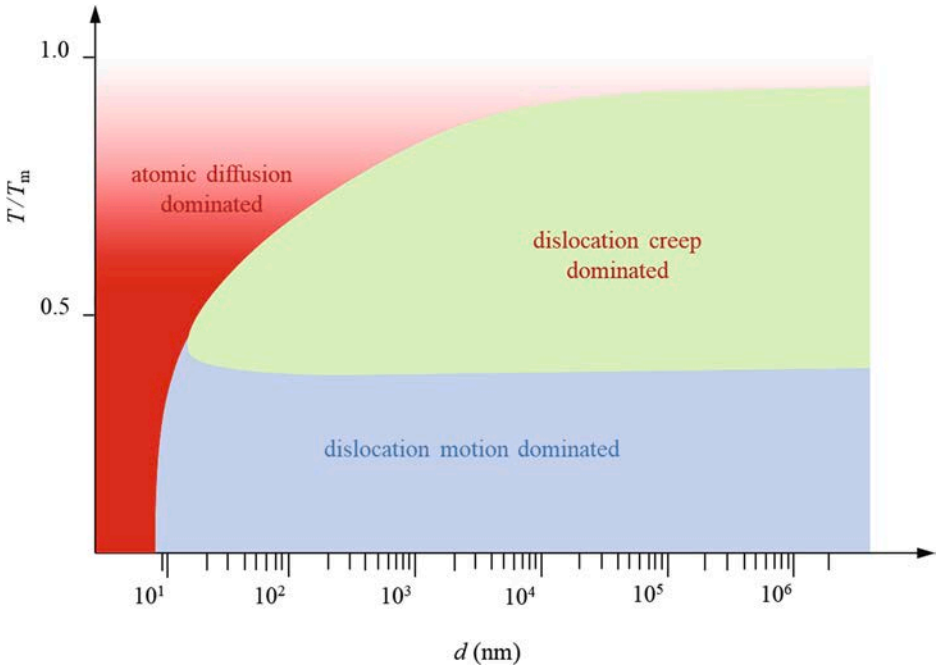

Fig. 13. Deformation mechanism map for typical crystalline metals. The dominant deformation mechanism is indicated as a function of temperature and sample dimension (mold diameter). For macroscopic samples, diffusion-based deformation mechanisms such as diffusion-assisted dislocation motion (e.g., dislocation climb) and diffusion-induced grain boundary migration dominate at high temperatures. On the very small scale, atomic diffusion dominates the underlying deformation mechanism, even at low temperatures including room temperature) (atomic diffusion dominated region). This is because the relative interface area of single digit nanosized metals is very high, and the interface diffusivity is by several orders of magnitude higher than that of lattice (bulk) diffusion. With increasing sample dimension, at low temperatures, dislocation motion (dislocation nucleation and dislocation propagation) is the main deformation mechanism controlling TMNM of metals. This is because atomic diffusion decreases exponentially with temperature and becomes less effective due to a decrease in interface/volume area.

3.2. Nanomolding of solids

In this discussion of the nanomolding of solids, the material class we will focus on is metals, with its wide range of deformation mechanisms. However, due to their practical importance, some non-metal materials will also be discussed. In crystalline metals the prominent deformation mechanism is a strong function of the sample size and temperature (Fig. 13). The basic underlying mechanisms are atomic diffusion and dislocation motion. With decreasing length scale, dislocation slip [179] ceases to operate due to the reduction of required space either to form dislocations (dislocation starvation) [93] or due to the lack of presence of dislocations [90,180,181]. As a consequence, plasticity, and hence nanomolding ability based on dislocation slip, is expected to be limited on the nanoscale [93,181]. Therefore, one can expect that, on the nanoscale, bulk diffusion (Nabarro-Herring creep) [62] and interface diffusion (Coble creep) [61,182,183] deformation mechanisms play a dominant role for metals. It is important to note that temperature plays an important role in the plastic deformation of metals, because it controls grain boundary sliding and assists dislocations to cross energy barriers. Generally, dislocation-based deformation becomes dominant with increasing grain size and at low temperatures, typically below 0.4 T_m. At high temperatures $> 0.4\ T_m$, deformation is dominated by diffusion. This is because the temperature dependence of atomic diffusion is controlled by the exponential temperature dependence of vacancy concentration. In contrast, the resistance to the sliding of a dislocation, which is directly proportional to the shear modulus, is almost temperature independent for $T < 0.4\ T_m$.

To conclude, atomic diffusion as an atomic transport mechanism dominates at the nanoscale, and diffusion-assisted dislocation motion, grain boundary sliding, migrating (i.e. diffusion creep) becomes dominant with increasing characteristic length scale [101,184] (Fig. 13). In general, for macroscopic samples, diffusion-based deformation mechanisms such as diffusion-assisted

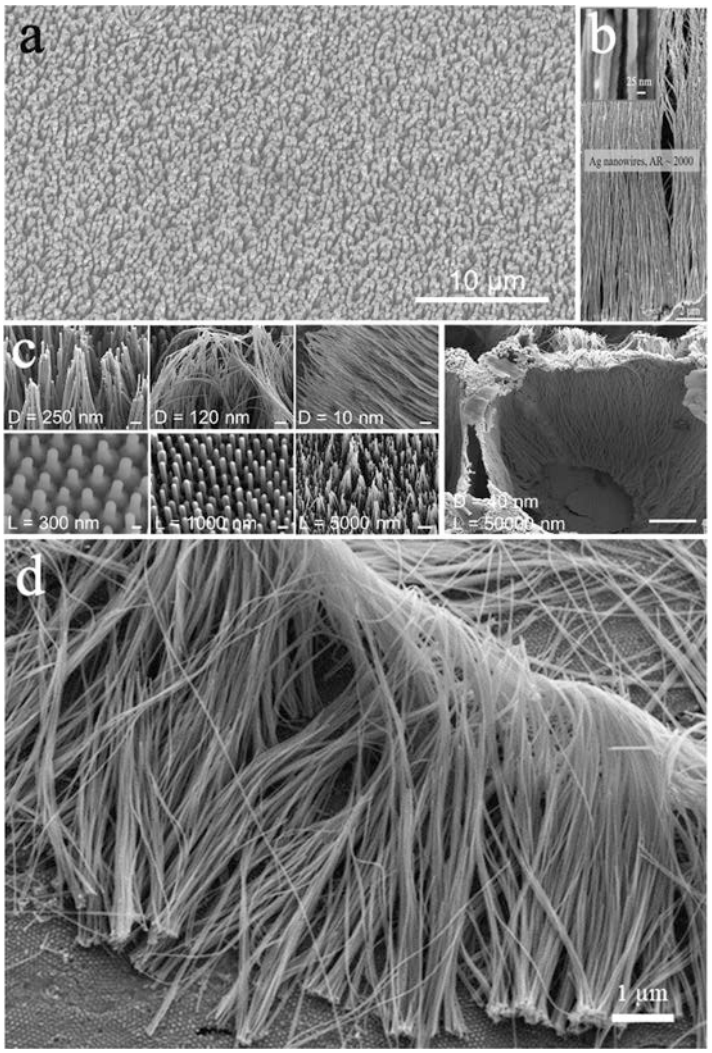

Fig. 14. Examples of materials and geometries that can be fabricated through thermomechanical nanomolding (TMNM). (a) High throughput fabrication of Au nanowire arrays with TMNM. (b) Long Ag nanowires with aspect ratio of ~ 2000 [61]. (c) and (d) Fabricated ordered phases nanowire arrays (Au_2Al) with controlled diameters and aspect ratios [64] (Copyright 2020, American Physical Society).

dislocation motion (e.g., dislocation climb) and diffusion-induced grain boundary migration dominate at high temperatures. However, for very small sample dimensions, < 10 nm, the very high interface/bulk atom ratio and the significantly higher interface diffusivity versus bulk diffusivity enables a diffusion-dominated deformation mechanism even at low temperatures, including room temperature. At larger sample dimensions, the increase in temperature rapidly enhances diffusivity, and for dimensions up to ~ 100 mm, diffusivity takes over dislocation-mitigated deformation at ~ 0.4 T_m. For sample sizes larger than the nanoscale, metal deformation is a diffusion-enabled dislocation mechanism. One has to keep in mind that the boundaries of the various deformation regions do shift with applied stress. Independent of the underlying mechanism (diffusion vs. dislocation), nanomolding of solids using temperature and pressure is generally referred to as thermomechanical nanomolding (TMNM) [62]. We will show below that TMNM is a highly versatile nanofabrication method which spans a wide range of length scales and geometries, and can be realized with most pure metals, alloys, and ordered phases (Fig. 14).

Below we will show that for higher homologous temperature ($T > 0.4T_m$), atomic diffusion becomes an effective transport mechanism when considering nanoscale dimensions. We will further discuss how dislocation motion can be sufficient to enable dislocation-based TMNM mechanism.

3.2.1. Diffusion-Based TMNM of solids

Atomic diffusion is generally involved in the deformation of macroscopic-sized metals, but it is often not the dominant mechanism. For example, atomic diffusion can assist dislocation motion perpendicular to their slip planes, so called "climb," which enhances overall dislocation mobility. Atomic diffusion is also involved in grain boundary sliding, the prominent macroscopic deformation mechanism for metals at elevate temperatures. These mechanisms form the basis of creep deformation on the macroscale. On the nanoscale, atomic diffusion can become the dominant atomic transport or deformation mechanism. This can be rationalized when considering random one-dimensional walk in a crystal. The diffusion distance can be estimated as $L \sqrt{Dt}$, where D is the atom's diffusivity. Substituting typical values for diffusion in solid metals at intermediate temperature ~ $0.5T_m$ of $D \sim 10^{-18}$ m^2/s and a timescale of $t = 100$ s yields a diffusion distance of $L \sim 10$ nm. Even though negligible for macroscale molding, this estimation suggest that diffusion-based material transport can be significant on the nanoscale [61,62].

We will see now that when a bias is present, such as a pressure gradient, practical conditions can result in significant and rapid net-flux of atoms. Diffusion-based TMNM can be quantified when considering the grows through a volume change of a nanowire, dV/dt, as a result of the diffusion flux of atoms, J, through the cross-section area of nanowire, S, as:

$$\frac{dV}{dt} = S \bullet \mathbf{J} \tag{6}$$

According to Fick's Law, in the case that atomic diffusion is controlling atomic flux, $J = \frac{D}{k_B T} \nabla p \Omega$, with D as the diffusivity, Ω as the

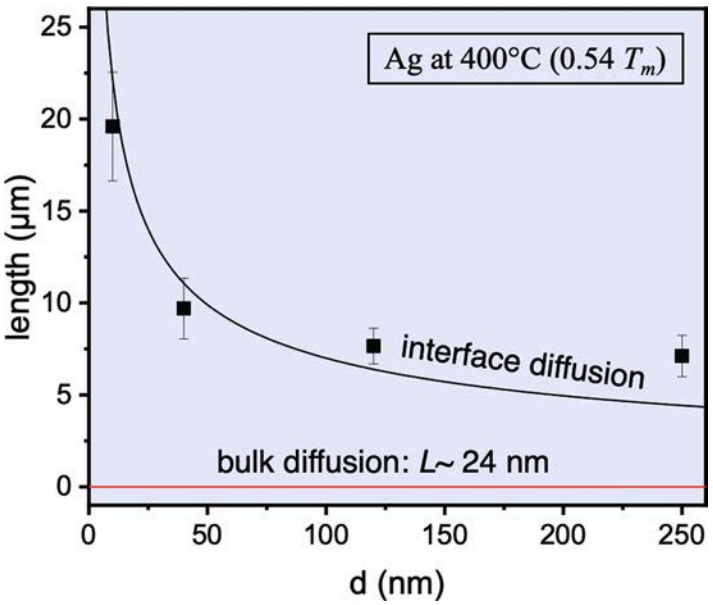

Fig. 15. Scaling experiments revealing interface diffusion as the underlying mechanism for TMNM at high temperature. Nanomolding of silver at 400°C (~0.54 T_m) for 300 s at a pressure of 1.6 GPa into mold cavities of various diameters [185]. The nanowire length increases with decreasing d according to $L \propto d^{-1/2}$. This scaling matches interface diffusion controlled nanomolding (eq. 10). For comparison, bulk diffusion controlled nanomolding is also plotted (eq. 9, red line), which predicts that the nanowire length is independent of mold diameter and approximately three orders of magnitude shorter than the experimental measurements. (For interpretation of the references to color in this figure legend, the reader is referred to the web version of this article.)

mean atomic volume and ∇p as the pressure gradient along the nanowire. Rewriting the volume as $V = S\bullet\mathrm{L}$, and $\nabla p = \frac{dp}{dL} = p/L$ with L as the nanowire length gives:

$$\frac{dL}{dt} = \frac{Dp\Omega}{Lk_BT} \tag{7}$$

Integrating eq. (7) and assuming $L_{(t=0)} = 0$ gives:

$$L = \sqrt{\frac{8SDp\Omega t}{\pi d^2 k_B T}} \tag{8}$$

Eq. (8) takes different forms for nanomolding based on bulk diffusion and interface diffusion. To describe nanomolding based on bulk diffusion, where diffusing atoms travel across the entire cross section of the nanowire requires substitution of $S = \frac{1}{4}\pi d^2$ and $D = D_L$, with D_L as the lattice diffusivity, which results in:

$$L = \sqrt{\frac{2D_L p\Omega t}{k_B T}} \tag{9}$$

For nanomolding based on interface diffusion, diffusing atoms travel across a thin nanowire/mold interface layer with an interface diffusivity, $D_I = D$. In this case, the cross section of atomic flux is $S = \pi d\delta$ where δ is the thickness of the interface layer. Substituting in eq. (8) gives:

$$L = \sqrt{\frac{8D_I p\Omega t}{k_B T}}\frac{\delta}{d} \tag{10}$$

The scaling of the nanowire length with its diameter, $L(d)$ has different forms for nanomolding based on bulk diffusion (eq. 9) or interface diffusion (eq. 10). In the case of bulk diffusion controlled nanomolding, the length of the nanowire is independent of its diameter (set by the mold cavity diameter), $L \propto d^0$. Instead, for interface diffusion controlled nanomolding, nanowire length scales with the wire diameter, $L \propto d^{-1/2}$. Due to this inverse relation, TMNM has been described as "the smaller the easier" [62]. In order to reveal the underlying diffusion process for diffusion-based TMNM, scaling experiments have been carried out [185] (Fig. 15). Using silver at 0.54 T_m and mold cavity diameters ranging 10–250 nm, $L(d)$ reveal that the underlying mechanism for diffusion-based TMNM is interface diffusion. This can be concluded from the fact that the scaling of $L(d)$ follows a $d^{-1/2}$ behavior and the absolute length are approximately three orders of magnitude longer than suggested for bulk diffusion. Bulk diffusion, due to the 4–6 orders of magnitude lower diffusivity [186], plays only a negligible role in diffusion controlled TMNM [185,187].

The consequences of an interface diffusion-based mechanism in TMNM are that nanomolding becomes "easier" with decreasing nanorod diameter [62]. Easier is quantified by the required forming pressure to nanomold a certain aspect ratio L/d, where with decreasing d the required forming pressure decreases to mold a certain L/d. Or, in other words, for the same pressure, with decreasing d, longer nanowires can be formed (Fig. 15). Diffusion-based TMNM can be realized with a vast range of materials as "significant" atomic diffusion is present in a broad range of materials at least at a homologous temperature, $T/T_m > 0.4$ (see 3.4).

3.2.2. *Dislocation-based TMNM of solids*

At low homologous temperature < $0.4T_m$, diffusion-based nanomolding is generally no longer effective because the diffusivity decreases exponentially with temperature. Taking Ag as an example, its bulk diffusivity is $\sim 2.2 \times 10^{-18}$ m^2/s at $0.3T_m$, about five

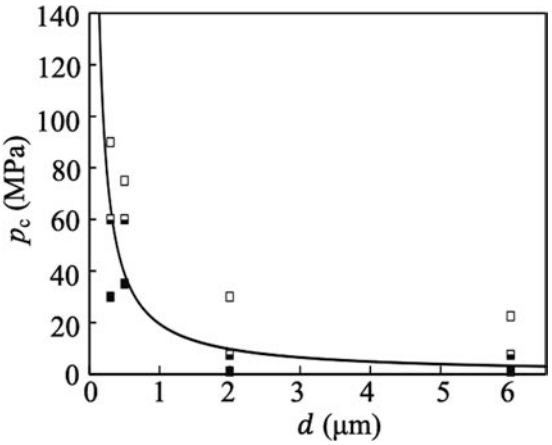

Fig. 16. Required minimum molding pressure for dislocation-based TMNM of crystalline aluminum [189]**.** Size-dependent critical forming pressure to nucleate an edge dislocation loop in Al. Dots and line are corresponding to the experimental data and theory (eq. (11)), respectively (Copyright 2020, IOP Publishing).

orders of magnitude smaller than its diffusivity at 0.54 T_m (~5.6×10^{-13} m^2/s) [188]. The predicted Ag nanowire length (eq. 10) would be 2–3 orders of magnitude shorter at $0.3T_m$ than at $0.54T_m$ (Fig. 16). Due to the ineffectively of the diffusion mechanism at low homologous temperature, dislocation mitigated nanomolding takes over.

As the grain size in metals of typically ~ 10 μm is much larger than the mold nanocavities, the vast majority of mold nanocavities contact with a single crystal. In the dislocation dominated low temperature nanomolding, nanorods grow by dislocation sliding [63,185]. We consider the simplest dislocation-based nanomolding model in Fig. 6(c) and (e). First, the applied pressure must overcome the energy barrier of dislocation loop nucleation (Fig. 6(e)). Equating the energy required to generate an edge dislocation loop [189] and the external work, the minimum molding pressure required for dislocation-based nanomolding is:

$$p_c = \frac{\alpha G b}{d} \tag{11}$$

where b is the magnitude of the Burgers vector and α is a constant which depends on the specifics of the material. Eq. (11) predicts that the required minimum molding pressure at low temperature increases with the mold cavity size. Such a scaling behavior has been experimentally verified by TMNM of gold [63] and aluminum (Fig. 16(a)) [189].

Furthermore, once the metal deforms into a mold nanocavity by dislocation sliding, the friction resistance from the cavity wall requires additional pressure. Therefore, the required molding pressure is

$$p = \frac{\alpha G b}{d} + \frac{\tau_s(\pi d L)}{S} \tag{12}$$

where the second term originates from the wall friction, τ_s is the shear strength of the wall/metal interface. Substituting $S = \frac{1}{4}\pi d^2$ into eq. (12) gives:

$$p = \frac{\alpha G b + 4\tau_s L}{d} \tag{13a}$$

$$\text{or } L = \frac{pd}{4\tau_s} - \frac{\alpha G b}{4\tau_s} \tag{13b}$$

Eq. (13) predicts that the length of a metal nanorod increases linear with the mold cavity size, which is in agreement with experimental observations (Fig. 17). The required molding pressure increases with decreasing mold cavity diameter and with increasing length of the forming nanorods. Due to the ineffectively of dislocation-based nanomolding, molded nanowires are usually limited to low aspect ratios below five (Fig. 17 and Fig. 18).

In summary, nanomolding of solids, with a focus on crystalline metals is based either on diffusion or dislocation mitigated material flux. At low homologous temperature, i.e., $T/T_m < 0.4$, dislocation mitigated nanomolding dominates. With increasing homologous temperature, diffusion becomes more effective and takes over the materials transport mechanism. As "significant" diffusion is present in a vast range of materials, this vast range of materials should be suitable for nanomolding as we will discuss in the following section.

3.3. Materials for nanomolding through TMNM

As different applications require different materials, a nanomolding method that can be applied to a wide range of materials has a major advantage. In this section, the various material classes that are suited for TMNM as a nanomolding process will be discussed.

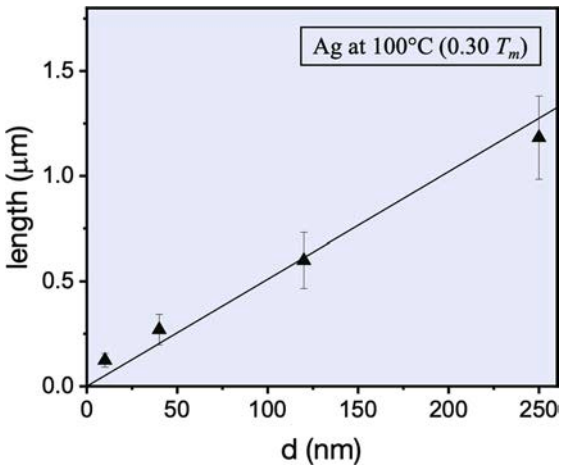

Fig. 17. Scaling of nanomolding length with diameter for Ag at 100 °C (~0.3 T_m). Experimental results reveal a linear increase of L with increasing d, the solid line is fitted by an dislocation dominated mechanism according to eq. (13b) [185].

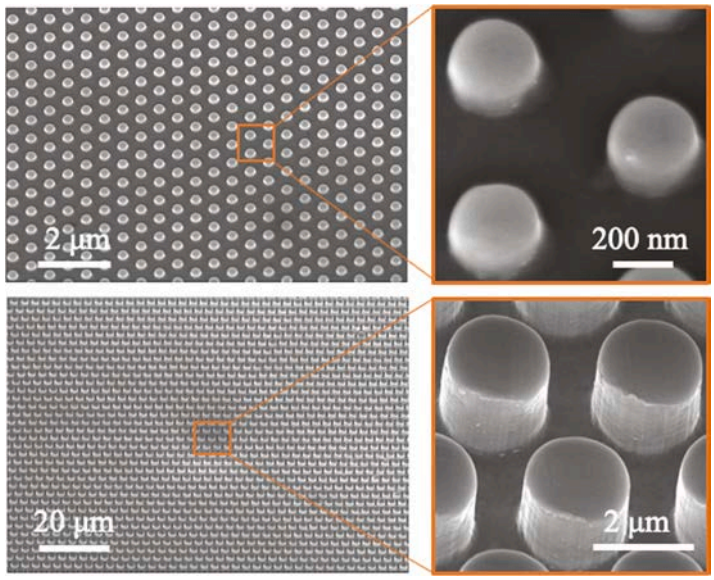

Fig. 18. Samples of dislocation-based nanomolding. Short Al nanorods and microrods arrays fabricated [189] (Copyright 2020, IOP Publishing).

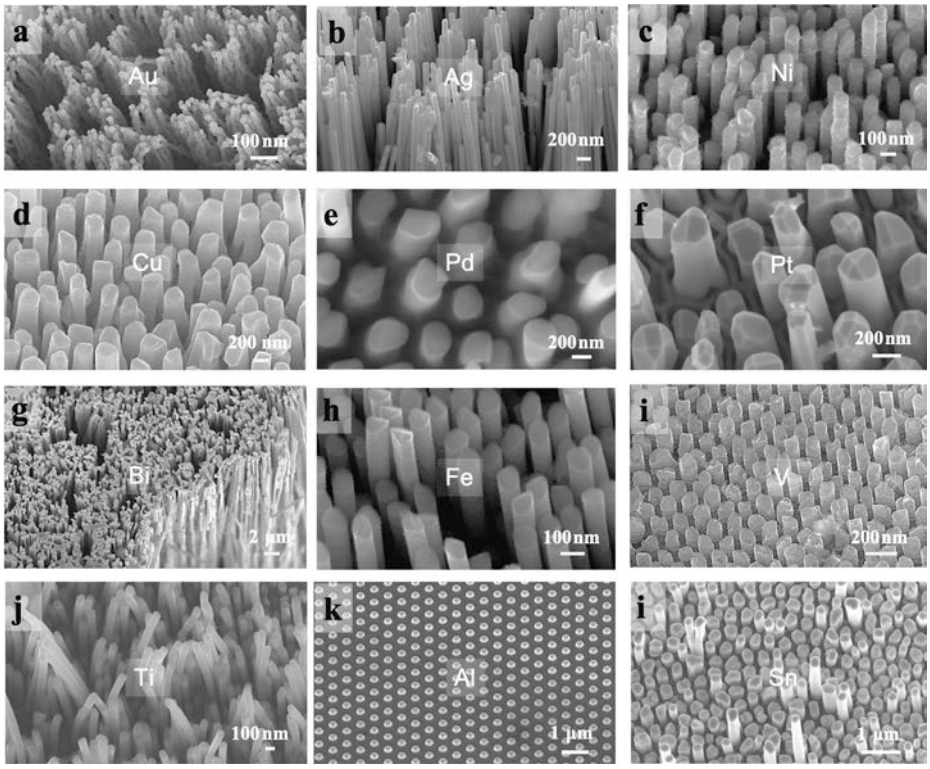

Fig. 19. Examples of pure metal nanowires. Nanowire arrays which have been fabricated through diffusion-based TMNM of pure metal at temperatures above 0.4 T_m [62,189] (Copyright 2019, American Physical Society [62]. Copyright 2020, IOP Publishing [189]).

Pure metals: A wide range of pure metals have been used in TMNM (Fig. 19). The reason for the suitability of pure metals for TMNM is that they exhibit high diffusivity at high homologous temperature, $T/T_m > 0.4$ [186]. In addition to diffusion, which is present in all solid materials, dislocation slip is also available as a deformation mechanism in pure metals. For example, Au nanorods have been fabricated through TMNM, where the controlling mechanism is based on dislocation slip for temperature of −60 °C ($T/T_m <$ 0.16) [63] and based on diffusion transport for temperatures above 660 °C ($T/T_m > 0.7$) [63]. To date, pure metals with FCC and BCC

structure have been nanomolded by TMNM, including In, Sn, Zn, Pb, Al, Au, Ag, Cu, Fe, Ni, Pt, Pd, Ti, V, Bi. Some of these metals, including In, Sn, Zn, Pb and Al are challenging to demold as they dissolve in KOH (KOH is generally used as an etchant to dissolve the AAO mold), and hence require other etchants or mechanical demolding (Fig. 19k-l).

In the case of diffusion-based nanomolding, the feasibility of molding specific feedstock materials into nanowires depends on the diffusivity of that material. Under practical molding conditions, for example, $p = 400$ MPa, $t < 10$ min, $d = 40$ nm, an interface diffusivity $> \sim 10^{-17}$ m^2/s, is required to form nanorods with aspect ratio $L/d > 1$. For pure metals, this requirement is achieved at homologous temperature $> 0.4\ T_m$. For example, at $0.4\ T_m$ (262 °C) the interface diffusivity of pure gold is $\sim 10^{-15}$ m^2/s [186]. For some metals with high melting temperature, such as W ($T_m = 3422$ °C), Ta ($T_m = 2980$ °C), Mo ($T_m = 2623$ °C), and Nb ($T_m = 2477$ °C), it is experimentally challenging to achieve the required absolute temperatures to realize homologous temperatures of $0.4\ T_m$.

Non-metals: Non-metals such as B, Si, C, P exhibit very different properties compared to pure metals. They exhibit low electrical conductivity, are brittle, and their diffusivity is generally low. These qualities originate predominately from their strong directional bonds. For example, the diffusivity of silicon at $T \sim 0.4\ T_m$ is $\sim 10^{-28}$ m^2/s [190]. Therefore, atomic transport through diffusion is essentially negligible even on the nanoscale. The directional bonds also drastically inhibit the formation and slip of dislocations; hence non-metals are generally brittle materials. Therefore, TMNM is not a suited process to fabricate nanosized elemental non-metals. Alternatively, by increasing the molding temperature to above the melting temperature of non-metals, liquid-based nanomolding of Si has been achieved [191].

Solid Solutions: Solid solutions (e.g., Au-Ag, Au-Cu, Ni-Cu, and Fe-Al) show very similar properties to pure metals. Their crystal structure is the same than that of the constituent solvent metal and they randomly occupy this lattice with two or more elements. Both mechanisms, dislocation slip, and diffusion transport operate the same way as in pure metals. Hence, they can be fabricated through TMNM in a similar way as pure metals. Examples of TMNM of solid solutions include Cu-Al, Pd-Cu, Ag-Ge, Au-Ag, Cu-Zn-Sn, and PdCuNiPtRhIr [62,64,192] (Fig. 20).

However, as the diffusion-based TMNM process depends on the atomic diffusivity (eq. (6)), one can expect that when the diffusivities differ for the constitutive elements in a solid solution that the composition in the nanorod differs from the nominal composition in the feedstock. Specifically, the composition in the nanorod will be enhanced by the faster moving constituent element, and accordingly, depleted by the slower moving constituent element.

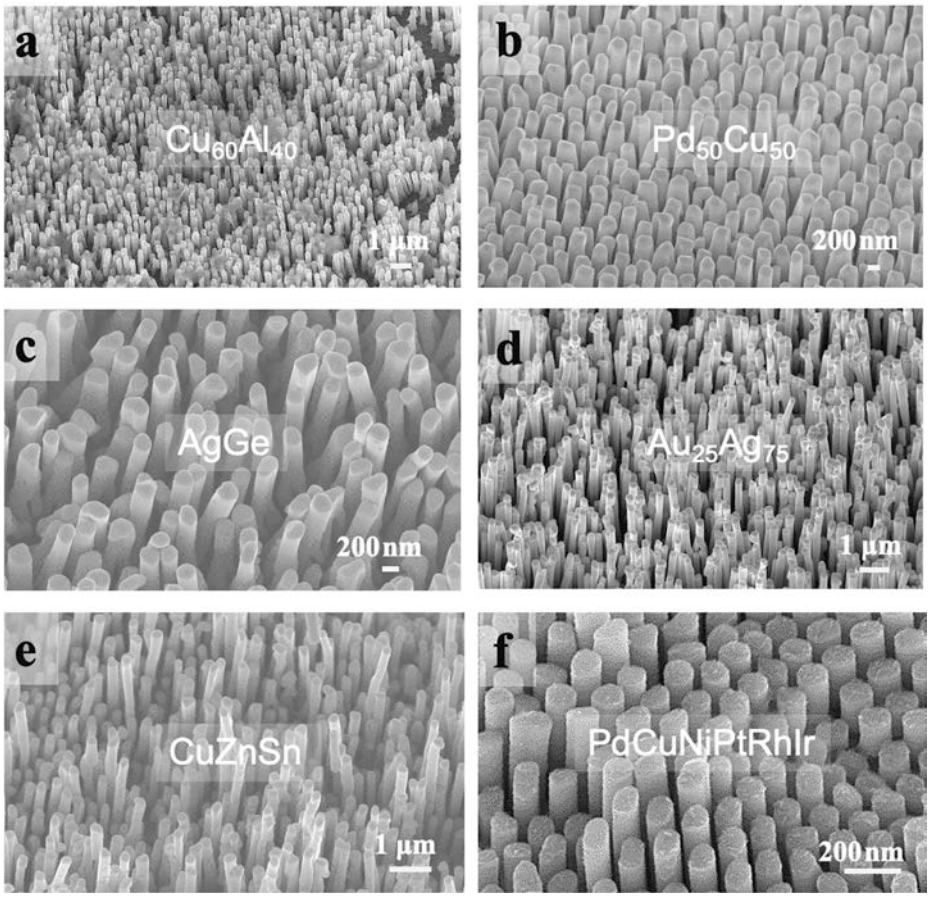

Fig. 20. Examples of solid solution metal nanowires. Nanowire arrays which have been fabricated through diffusion based TMNM of solid solutions at temperatures above $0.4\ T_m$ [62] (Copyright 2019, American Physical Society).

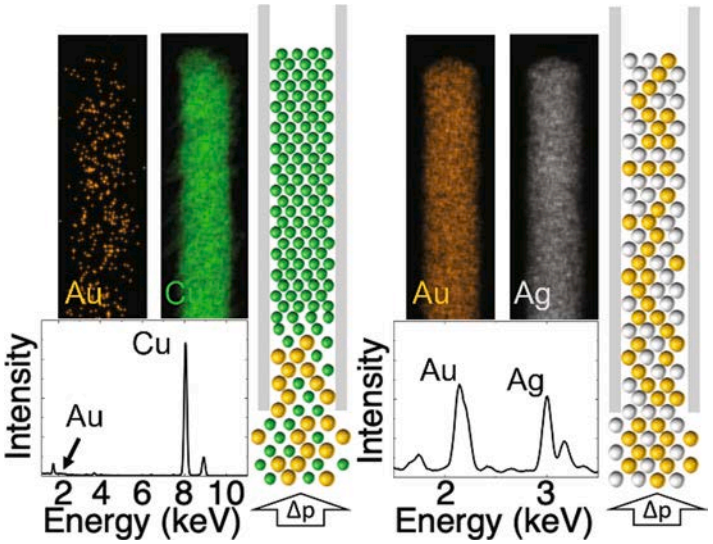

Fig. 21. TMNM with solid solutions $Au_{50}Cu_{50}$ and $Au_{50}Ag_{50}$ [64]. (a). When using $Au_{50}Cu_{50}$ as a feedstock material, the composition changes towards essentially pure Cu due to the higher diffusivity of Cu compare to Au. (b) For $Au_{50}Ag_{50}$ feedstock, the composition remains $Au_{50}Ag_{50}$ throughout the nanowire due to the similar diffusivity of Au and Ag (Copyright 2020, American Phys9ical Society).

For example, when TMNM of $Au_{50}Cu_{50}$, where the diffusivity for Cu, $D_{Cu} \sim 3.1 \times 10^{-13}cm^2/s$ is higher than the diffusivity for Au, $D_{Au} \sim 1.7 \times 10^{-14}cm^2/s$, the composition within the nanowire changes rapidly from initial $Au_{50}Cu_{50}$ to approach pure Cu after<500 nm (Fig. 21(a)). The situation is different in $Au_{50}Ag_{50}$ where the diffusivities are more similar, $D_{Ag} \sim 1.6 \times 10^{-14}cm^2/s$ and $D_{Au} \sim 1 \times 10^{-14}cm^2/s$ (Fig. 21(b)). Here, the composition in the nanowire remains that of the nominal composition of $Au_{50}Ag_{50}$.

Besides diffusivities, which control the kinetic aspect of the composition of the nanowires for solid solutions formed through TMNM, other contributions may also have to be considered. For example, heat of mixing and strain energy can act as thermodynamic contributions that can enhance or reduce the kinetic tendency to change composition in the nanowire. More research is required to develop a quantitative understanding of TMNM of solid solutions. Today's understanding suggests that diffusivities of the solid solutions constituents, relative atomic radius, heat of mixing and strain energies, and the mold material, can all have an effect on the TMNM of solid solutions.

Ordered Phases: Ordered phases such as intermetallics are phases that comprise multiple sublattices occupied selectively by the different atomic species. Ordered phases are a very broad class of materials and comprise essentially all functional materials including high temperature superconductors [193-195], semiconductors [196,197], ferromagnets [198], plasmonic materials [199], phase change materials [200-202], and topological insulators [203-205]. As the sublattices are exclusively occupied by one specific constitutive element, ordered phases are stable over very narrow compositional ranges. This characteristic of a very narrow compositional stability range distinguishes ordered phases from solid solutions. Solid solutions are often stable over very broad compositional ranges, which can encompass the entire compositional range in their corresponding alloy system.

The constituents of ordered phases typically differ significantly from each other in size, electron configuration and crystal structure. Such dispersity is much larger than in solid solutions where the constituents are similar. This suggest that ordered phases cannot be nanomolded through TMNM as the different constituents diffuse with highly different rates which would alter the composition out of their stable range and other phases would form. However, nanowires of a wider range of ordered phases have been successfully nanomolded through TMNM (Fig. 22(a)) [64]. Further, it has been shown that the chemical composition throughout the molded nanowires is uniform and identical to the composition of the feedstock material. It has been argued that the reason that ordered phases can indeed be nanomolded is rooted in their characteristic narrow Gibbs free energy curves and hence the composition dependent chemical potential, $\mu(c) = \frac{\partial G}{\partial c}$ (Fig. 22(b)). These narrow curves prevent compositional changes. This is because as soon as the composition changes slightly, the energy increases drastically and surpasses the energy gain from the nanowire growth. Specifically, assuming the two constituents, A, B of an ordered phase AB which exhibit different diffusivities, e.g., $D_A > D_B$. A can therefore diffuse faster and hence would change the composition in the nanowire. This will destabilize the AB phase (see Fig. 22(b). If $\mu > \mu_p$, no driving force for further growth exists. Only B, the slower diffuser, balances the composition towards AB (in Fig. 22(b) so that $\mu < \mu_p$ and growth continues. Hence, the nanomolding kinetics of ordered phases is controlled by the slower diffuser to maintain the stoichiometry AB and provide a driving force for nanomolding.

In summary, nanorods and nanowires can be fabricated through diffusion dominated TMNM from essentially all metals, solid solutions, and a large number of ordered phases. The diffusivity of the materials' constituents controls the molding process. Generally, the diffusivity has to be higher than 10^{-19} m^2/s so that nanorods can be fabricated through TMNM under practical conditions. For pure metals and solid solutions, higher diffusivities are always present for homologous temperatures $> 0.4\ T_m$. In solid solutions, a difference in the diffusivities of the constituents can change the composition of the nanowire relative the original composition of the

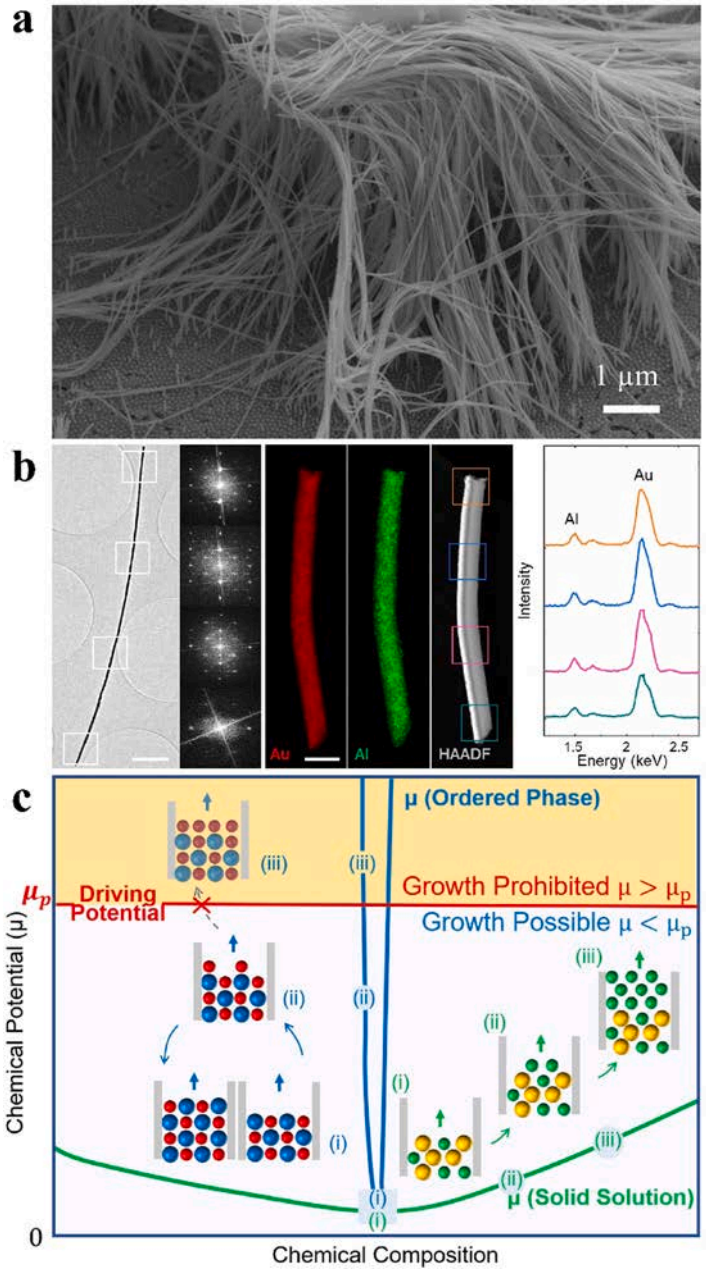

Fig. 22. TMNM of ordered phases [64]. (a) Fabricated Au_2Al ordered phases nanowires by TMNM. (b) Uniform chemical composition and a single crystalline structure of the entire nanowire is verified by EDS mapping and electron diffraction at different selected regions. (c) The competition between chemical potential, μ and the externally applied pressure gradient, μ_p, maintains the composition to stay within the narrow stability range of the ordered phase during TMNM (Copyright 2020, American Physical Society).

feedstock. Such compositional changes do not occur during TMNM of ordered phase. This is because the kinetic motifs to change the composition during nanorod formation due to the different diffusivities, are overwritten by the thermodynamic driving force controlled by the narrow stability range of the ordered phase.

3.4. Crystal structure of TMNM nanowires

One important feature of a nanofabrication method is its ability to produce nanostructures (such as nanowires) of controlled crystallographic orientation and further if this orientation is present throughout the entire nanowire (single crystal formation). It has been observed that the vast majority of nanowires formed through TMNM are essentially single crystals (Fig. 23) [61,62,64,398].

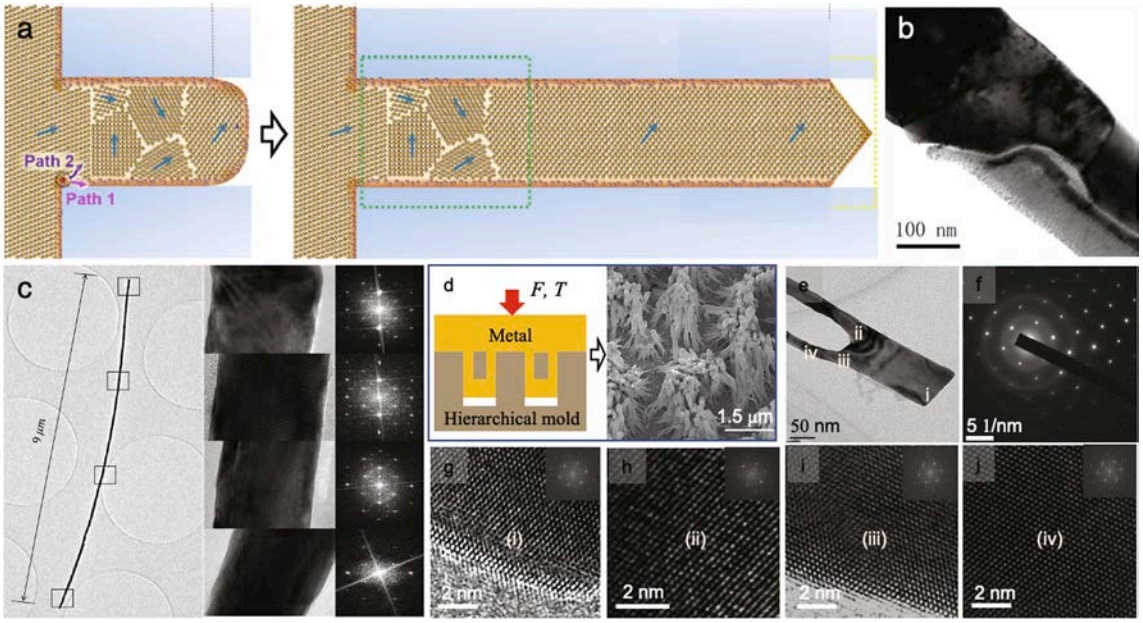

Fig. 23. Single crystal nanowires by TMNM. (a) Schematic of the entry effect during TMNM. Several crystals typically form at the entrance of nanocavities until the desired growth orientation is established. From here on the nanowire grows as a single crystal [62] (Copyright 2019, American Physical Society). (b) HRTEM image of the root of a Au nanorod, revealing several crystals formed at the mold entrance. (c) Ordered phase Au_2Al single crystal nanowire [64] (Copyright 2020, American Phys9ical Society). (d)-(i) The single crystal during TMNM forms even along complicated molds. When using a hierarchical nanomold (d), even merging nanowires continue in the same orientation to form a single crystal (f-i) [61].

However, for a randomly oriented feedstock crystal, the entry into the nanomold cavity is generally associated with a reorientation of the crystal (Fig. 23(a)-(c)). Hence, several crystals with various orientations form before eventually a long single crystal is formed. For example, for FCC materials the single crystal grows in ⟨1 1 0⟩ [62]. It has been suggested that the ⟨1 1 0⟩ orientation of an FCC nanowire originates from the low surface energy associated with this orientation of the forming nanowire [206]. Specifically, the surface energy is 10% lower on a (1 1 1) FCC surface (the surface of a single crystal growing along ⟨1 1 0⟩), than the surface energy of any other differently oriented surfaces. Hence, a FCC nanowire grows along ⟨1 1 0⟩ to generate (1 1 1) surfaces.

For ordered phase such as Au_2Al, similar behavior has been observed than for the FCC case discussed above [64]. Once the single crystal grows in its preferred orientation, its growth is surprisingly robust. For example, if the nanocavity change it shape, angle, or

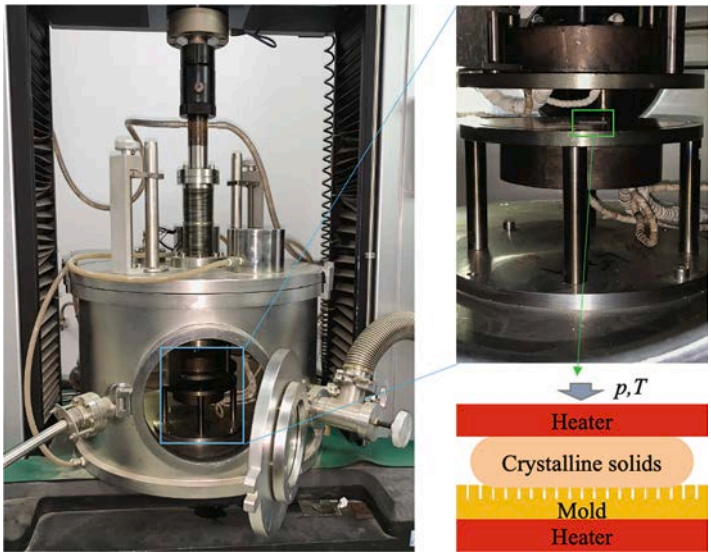

Fig. 24. TMNM setup. Typical experimental set-up for TMNM of solids [61] (Copyright 2019, American Physical Society).

diameter, the single crystal orientation remains unchanged (Fig. 23 d-i) [61].

3.5. *Experimental realization of TMNM of solids*

TMNM uses pressure and temperature to form the moldable material into the mold cavity (Fig. 24). Forming pressure, which is typically in the range of 10^2 MPa, can be readily applied by a standard press like a universal testing machine or even a simpler press. Required forming temperature depends strongly on the material. For example, ideal forming temperatures are in the range of $T/T_m \sim 0.5$ which for tungsten corresponds to 1711°C whereas for tin is 116°C. Therefore, heating systems are specific for the material. For temperatures below ~ 800°C, resistant heaters such as cartridge heaters and furnace can be used. For higher temperatures, RF-heating, also known as dielectric-heating is typically used.

In a typical TMNM experiment, a solid moldable material with a lateral dimension of typically ~ cm^2 is used and pressed against a

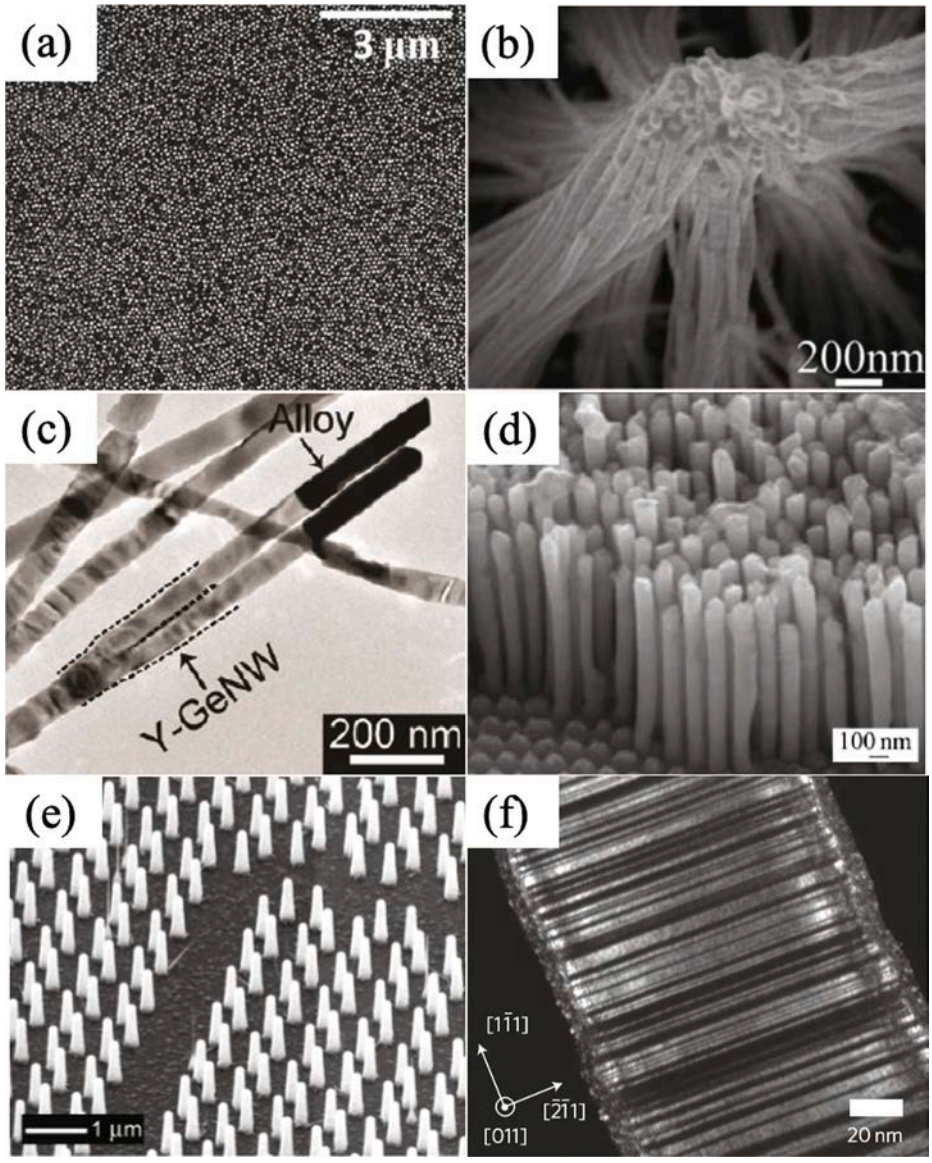

Fig. 25. Nanostructures fabricated by gas (a-e) and solution (f) based nanomolding. (a) Top view of a Si nanowire array fabricated by template assisted CVD [128] (Copyright 2009, John Wiley and Sons), (b) Large aspect ratio CrO_2 nanowire array fabricated by template assisted CVD [210] (Copyright 2011, IOP Publishing), (c) Ge nanowires with designed Y-brunch structure, which has been fabricated by template assisted CVD [209] (Copyright 2011, American Chemical Society), (d) Cu/Ni/Fe multilayer nanowire arrays fabricated by templated assisted electrochemical deposition [214] (Copyright 2009, Elsevier), (e) Free standing InP nanowire arrays with a designed pattern fabricated by template assisted vapor deposition followed by a second VLS growth process [134] (Copyright 2004, American Chemical Society), (f) nanotwinned Cu nanowire fabricated template assisted electrochemical deposition [212] (Copyright 2012, Springer Nature).

hard mold comprising of pre-defined nanocavities. A molding profile, controlling force and temperature is applied (Fig. 24(a)). By varying molding parameters such as pressure (~10^2 MPa), temperature ($T > 0.4T_m$), and molding time (~10^0-10^3 s), uniform nanowires of diameters set by the chosen mold cavity ranging ~ 10^0 – 10^2 nm with high aspect ratios of up to 10^3 can be fabricated [61,62].

A surprising advantage of TMNM is that it can be carried out in air. Even though not entirely understood why at $T_m/T \approx 0.5$ for most reactive materials oxidation would not take over and prevent the formation of metal nanowires it has been speculated that material transport of oxygen into the nanocavity prevents large amounts of oxygen available to form oxides instead of a metal nanowire.

3.6. Gas-phase and diluted solution-based nanomolding

Nanomolding can also be realized using gas-phase and diluted solutions as "feedstock" (Fig. 25). Here, individual atoms, ions, or small clusters of moldable materials are driven into the mold cavity, where they solidify and replicate the mold cavity. Gas-phase-based nanomolding includes template assisted vapor deposition methods (PVD/CVD). Here, atoms receive kinetic energy either through bombarding a target by high energy argon plasma (sputtering-based PVD [207,208]), pressurized inflow of reaction gases (CVD [128,209,210]), heating the target to evaporate (evaporation), or migrating ions by an electric field (electrochemical deposition [211,212]). Due to the similarities of ions in a diluted solution and atoms in a gas phase that are biased to fill a mold, we combine the discussion here on gas-phase and diluted solution-based nanomolding [211,212].

Molds that can be used for gas-phase and diluted solution-based nanomolding do not require to be able to withstand high driving pressures. Hence, more mold choices are available including polymers [212].

The underlying mechanism for gas-phase and solution-based molding differs. In template assisted PVD and electrochemical depositions, solid nanostructures confined in mold cavities are synthesized by direct deposition and condensation of atoms/clusters on a substrate. By carefully controlling the conditions, either polycrystalline, single crystalline or other designed nanostructures, e.g., nano twinned wires and heterogeneous nanostructures can be fabricated. In a template assisted CVD process, in addition to direct condensation, the formation of solid nanostructures can also involve nucleation and epitaxial growth of the moldable material from a

Table 1
Nanomoldable materials, mold materials used to mold them, deformation mechanism for state of matter and minimum feature size that can be molded.

material class	technique	mold	state of material	mechanism	minimum feature size	specific example material
pure metals	TMNM	AAO, Si, SiC, BMGs, polymers	solid	diffusion dislocation	atomic scale grain size	Au, Ag, Cu, Fe, Ni, Pt, Pd, Ti, Al, V, Ir, Bi [61,62] Au, Ag, Cu, Pt, Pd, Fe, Ti, Al [63]
	template-assisted electro deposition	AAO, polymers	solution	deposition	atomic scale	Ag, Cu, Ni, Fe, Zn, Co [212,214]
non-metals	template-assisted vapor deposition	AAO, polymers	gas	spontaneous growth	atomic scale	Si [128,215,221,222], Ge [209]
solid solutions	TMNM	AAO, Si, SiC, BMGs, polymers	solid	diffusion dislocation	atomic scale grain size	AuCu, AuAg, NiTi, AgGe, CuZnSn, PdCuNi, (PdCuNiPtRhIr [62,64] AuAg, AlSnZn [63]
ordered phases	TMNM	AAO, Si, SiC, BMGs	solid	diffusion	atomic scale	InSb, AuIn, AuIn2, FeSe, In75Sn25, Cu7In3, SnTe, Au2Al, AuAl2, CuAl2, In2Bi, InBi, AuSn, Sb2Te3, GST [64]
metallic glasses	Nano-imprinting	AAO, STO, Si, BMGs, polymers	liquid	viscous flow	atomic scale	PtNiCuP [60,138], PdNiP [223,224], PdNiCuP [85,218], MgCuY [102], ZrTiCuBe [100,102], ZrTiCuNiBe [102], TiZrBeFe [225,226]
polymers	Nano-imprinting	Si, AAO, Polymers	liquid	viscous flow	~ 1 nm	poly(methylmethacrylate) (PMMA) [53], polystyrene (PS) [216,227], polycarbonate (PC) [217], PPM [228], PBM [229], Polydiallyl Phthalate (PDAP) [228], phenyl-C61-butyric acid methyl ester (PCBM) [230,231], poly(3-hexylthiophene) (P3HT) [231], propylene glycol mono ether acetate (PGMEA) [232,233], poly(vinylidene fluoride-trifluoroethylene) [P(VDF-TrFE)] [234], Trichloroethylene (TCE) [235], TDPTD [236], trimethylopropane triacrylate (TMPTA) [237], acrylated poly(dimethylsiloxane) [238], Thiol-ene photopolymers [239], Polymerizable nematic liquid crystal [240]
ceramics, oxides, carbon NTs	template-assisted vapor deposition	AAO, polymers	gas	spontaneous growth	atomic scale	ZnO [241-243], SnO_2 [244], CrO_2 [210,245], ZnS [246,247], Cu_2S [248], InP [249], GaN [250], SiC [251], Pb/Sn based perovskite [219], CNT [213,220]
	template-assisted electro deposition		solution	deposition	atomic scale	ZnO [211]

Table 2
Summary of common nanofabrication methods.

	method	description	bottom-up or top-down	materials	throughput	uniformity	aspect ratio	smallest feature size	advantages	disadvantages	ref.
direct writing/mask less lithography	focused ion-beam milling	direct writing of nanopatterns or 3D nanostructures by milling a substrate material with scanning ion-beam, also called focused ion beam lithography	top-down	any material in its solid phase	very low	uniform	medium	~ 10 nm	complicated 3D nanostructure, no mask needed	• complex ion–solid interactions • very slow process • high cost	[252-255]
	e-beam lithography	direct writing on resist by e-beam and transfer pattern to substrate through etching, also called e-beam writing	top-down	mainly polymers (resists), semiconductors	low	uniform	< 5	~ 10 nm	• versatile patterns possible high precision	• high cost and low speed/throughput • limited to low aspect ratio 2D nanopatterns	[256,257]
	p-beam writing	focused beam of fast protons writing directly into a resist and transfer pattern to substrate through etching	top-down	mainly polymers (resists), semiconductors	low	uniform	medium	~ 20 nm	• higher aspect ratio than E-beam writing	• high cost and slow process • lower spatial resolution than E-beam writing • no commercially available user-friendly system available	[43,258, 259]
	scanning probe lithography (SPL)	direct writing of nanopatterns by STM or AFM tips, writing mechanism either indentation or deposition, includes dip-pen lithography	top-down	polymers, semiconductors, metals	low	uniform	< 5	~ 10 nm	• low-cost equipment	• slow process and not scalable	[260]
	FIB -CVD	CVD on selective locations guided by focused ion beam	bottom-up	carbon/diamond	very low	uniform	high	tens of nm	• can fabricate complicated 3D nanostructure	• very slow and high-cost process • not scalable	[130]
	EB-CVD	CVD on selective locations guided by electron beam	bottom-up	metals	very low	uniform	high	tens of nm	• can fabricated complicated 3D nanostructure	• very slow and high-cost process • not scalable	[261]
mask lithography/ nano-lithography (including projection printing and contact printing)	photolithography, UV lithography	large area light, UV exposure through mask, projection on resist and transfer pattern to substrate, also called optical	top-down	mainly polymers (resists) and semiconductors	high	uniform	< 5	~ 10–20 nm (for contact printing); ~ micrometers (for projection printing)	• versatile nanopattern fabrication • commercially established	• high-cost process • mask/prototype fabrication involves additional processes • requires contact printing process	[43]

(*continued on next page*)

Table 2 (*continued*)

	method	description	bottom-up or top-down	materials	throughput	uniformity	aspect ratio	smallest feature size	advantages	disadvantages	ref.
		lithography or UV lithography								for high resolution patterning	
	projection E-beam lithography	e- beam exposure through mask, projection on resist and transfer pattern to substrate	top-down		medium	uniform	< 5	$\sim$ 10 nm	• versatile patterns with high precision	• requires additional technology for mask fabrication • high-cost process	[256]
	X-ray lithography	X-ray exposure through mask, projection on resist and transfer pattern to substrate	top-down		medium	uniform	$\sim$ 100 when using high energy photons	$\sim$ 10 nm	• in principle sub-nm features possible	• resist requires long-time exposure • large penetration length of X-ray requires thick mask • high-cost process	[43,262]
	ion projection lithography	ion beam exposure through mask, projection on resist and transfer pattern to substrate	top-down		medium	uniform	< 5	$\sim$ 50 nm	• higher resolution than photolithography	• requires robust mask to withstand exposure of heavy ions • lower throughput than photolithography	[43,263]
	extreme ultraviolet (EUV) lithography	use extreme UV light (wavelength $\sim$ 13.5 nm) instead of UV/visible light used in photo-lithography to achieve higher resolution	top-down		high	uniform	< 5	$\sim$ 10 nm	• high resolution with similar principle to commercial photolithography	• requires vastly expensive facilities	[264]
	plasmonic lithography	use near-field effect to bypass the far-field diffraction limit in photolithography, also called near-field lithography	top-down		high	uniform	< 5	$\sim$ 10–20 nm	• can achieve sub-wavelength resolution • use same commercial resist as photolithography	• plasma effect is very sensitive to surface roughness of substrate	[265]
	interference lithography	incident beam is transmitted and diffracted through a mask which consists of diffracting gratings, and interference to generate periodic patterns, method includes laser, EUV and X-ray	top-down		high	uniform	< 5	depends on beam source	• can be readily scaled up to fabricate periodic patterns	• coherent beam source required, • more complicated mask required than for photo-lithography	[262,266]

(*continued on next page*)

Table 2 (*continued*)

	method	description	bottom-up or top-down	materials	throughput	uniformity	aspect ratio	smallest feature size	advantages	disadvantages	ref.
	colloidal lithography/ nanosphere lithography	interference lithography lithography with self-assembled 2D colloidal pattern as mask	top-down		high	uniform	< 10	size of colloid particles, ~100 nm	• efficient to fabricate ordered nanostructure arrays • provide some versatility of possible patterns • low cost	• feature size large and depends on colloid particles ~ 100 nm • patterns are limited by self-assembly process	[267]
electro spinning	electro spinning	use electrical forces to draw an electrically charged jet from polymer solution or melt to form nanofiber, ceramic fibers can also be fabricated combined with sol–gel process	top-down	polymer, carbon, ceramics	high	low	high	~ 10 nm	• low-cost, fabrication of ultrathin fibers with large aspect ratio	• materials limited to polymers and colloids • low uniformity in length • individual nanowires	[268,269]
chemical synthesis of nanoparticles	solution based chemical reaction	chemical synthesis of metallic (chemical reduction), semiconductor (pyrolysis) and oxides (hydrolysis or condensation) nanoparticles, products are colloidal dispersions, also sol–gel process	bottom-up	metals, non-oxide semiconductors, oxides	very high	medium	1	particle size varies with the material and fabrication conditions, smallest size can be < 1 nm	• low-cost method for high-volume fabrication. • compatible for wider class of materials	• limited to nanoparticles which are dispersed in solution • nanoparticle size distribution not uniform	[270-273]
	vapor phase chemical reaction	synthesis of nanoparticles in vapor phase with same mechanism as solution base methods, particles are collected on a solid substrate	bottom-up	metals, non-oxide semiconductors, oxides	high	medium	1	particle sizes varies with the material and fabrication conditions, smallest size can be < 1 nm	• fabricated nanoparticles not dispersed in solution	• only small fraction of fabricated nanoparticles is collected on substrate • often nanoparticles agglomerate on substrate	[274]
	solid phase segregation	synthesis of metal/ semiconductor nanoparticles in a solid phase through same	bottom-up	metals, non-oxide semiconductors	very high	medium	1	particle size varies with the material and fabrication conditions,	• a low-cost method to fabricate nanoparticles	• nanoparticles are dispersed in glass	[275]

(*continued on next page*)

Table 2 (*continued*)

	method	description	bottom-up or top-down	materials	throughput	uniformity	aspect ratio	smallest feature size	advantages	disadvantages	ref.
		mechanism as solution base methods, nanoparticles are collected on a solid substrate						smallest size can be < 10 nm			
spontaneous growth through vapor deposition (CVD and PVD) or in solution base	vapor–solid process (VS)	1D nanostructures formed by vapor deposition onto a substrate, condensation and anisotropic growth of vapor into nanostructures is driven by reduction of Gibbs free energy	bottom-up	metals, semiconductors, oxides	high	not uniform in length and diameter	aspect ratio depends on material and processing conditions, can achieve high aspect ratios	depend on material and condition, can achieve ~ 10 nm	• easy and low-cost method to fabricate 1D nanostructures • high-throughput • high-quality single crystal nanostructures	• nanostructures not uniform in diameter and length • size change with material and conditions and size is difficult to control	[127,276]
	dissolution-condensation growth	nanostructures growth within solution via a similar process as VS methods	bottom-up	metals, semiconductors, oxides	high	not uniform in length and diameter	aspect ratio depends on material and processing conditions, can achieve high aspect ratios	depends on material and condition, can achieve ~ 10 nm	• easy and low-cost method to fabricate 1D nanostructures • high-throughput	• nanostructures not uniform in diameter and length • often low-purity	[277,278]
	vapor–liquid-solid process (VLS)	dissolution of vapor reactants into a nanosized liquid droplet (metal catalyst), nucleation and growth of nanowires	bottom-up	semiconductors, and oxides	medium	medium	high	size of catalyst (~10 nm)	• high quality single crystalline structures • easy and low-cost process	• rely on selection of appropriate catalyst • catalyst contaminates nanowire • limited to non-metallic materials	[127,279]
	solution-liquid–solid process (SLS)	1D nanostructures growth in solution via a similar mechanism as VLS	bottom-up	semiconductors, and oxides	high	low	high	size of catalyst (~10 nm)	• lower temperature process than VLS, • no vacuum required	• crystal quality control more difficult than with VLS • same issues than for VLS	[280]
	laser ablation	use laser to ablate target materials in vapor or solution phase, and induce condensation growth of nanostructures, include pulsed laser ablation (PLA) and laser	bottom-up	metals, semiconductors, oxides, ceramics	high	not uniform	high	~ 5 nm	• Low cost and easy to fabricate	• control of size and length difficult	[52,281]

(*continued on next page*)

Table 2 (*continued*)

	method	description	bottom-up or top-down	materials	throughput	uniformity	aspect ratio	smallest feature size	advantages	disadvantages	ref.
		ablation in liquid (LAL)									
self-assembly	static self-assembly	nanoparticles self-assemble to equilibrium structures motivated by energy minimization	bottom-up	molecules, macromolecules, colloidal particles, DNA and proteins	medium	uniform		size of colloid particle,~100 nm	• low-cost method to fabricate nanostructure arrays • ability to fabricate 2D/3D nanostructures	• limited range of nanopatterns • feature size limited by used nanoparticles, usually > 100 nm	[282]
	directed self-assembly	self-assembly that is directed by base (seed) pattern to set pattern of particles	bottom-up		medium	uniform	< 5	size of colloid particle, ~100 nm	• larger range of nanopatterns than with static self-assembly	• feature size limited by nanoparticles used, usually > 100 nm	[283,284]
	dynamic self-assembly	self-assembly that results in stable nonequilibrium structures with a constant supply of energy	bottom-up		medium	uniform		size of colloid particle, ~100 nm	• nanostructures can be dynamically controlled	• requires specific materials/ mechanisms to achieve dynamic control • complicated fabrication procedure	[285]
	block copolymer self-assembly	self-assembly process based on intermolecular interactions between individual blocks of block copolymers	bottom-up	block copolymers	high	uniform		< 10 nm	• high-throughput fabrication of nanostructures • can fabricate 2D/ 3D structures	• accurate control of the geometry of nanostructures depends on the structure of block copolymers.	[286-289]
	block copolymer self-assembly-directed sol gel strategy	self-assembly of inorganic precursors using block copolymers as structure-directing agents	bottom-up	metals, oxides, carbides, nitrides, etc.	high	uniform		< 10 nm	• nanofabrication of broad range of chemistries and functional materials	• successful assembly relies on the choice of pressors and precise control of the conditions.	[290-294]
molding	nanomolding: liquid phase	soft materials mold with mold of pre-defined pattern/ nanostructure, nanoimprinting lithography (NIL), soft lithography, contact molding, capillary force lithography, nano injection molding, nanomolding of BMGs	top-down	polymers, BMGs, molten metals	high	uniform	medium; some cases up to 100	~ 5 nm	• low cost & readily scaled-up	• material limited to thermoplastic polymers, BMGs, and molten metals • mold required	[53,60,295]
			top-down		high	medium	medium	~ 50 nm			

(*continued on next page*)

Table 2 (*continued*)

	method	description	bottom-up or top-down	materials	throughput	uniformity	aspect ratio	smallest feature size	advantages	disadvantages	ref.
	sol–gel method with template	nanowires are synthesized from sol-gel filling into mold cavities by capillary force		semiconductor oxides					• can do multi-component, doping easily • operates at low temperature	• limited material choice • mold required	[169,296-298]
	nanomolding: solution base	electro-deposit into nano-porous molds	bottom-up	metals, semiconductors, ceramic, conductive polymers	high	medium	high	~ 1.5 nm	• dimensions and compositions can be readily controlled	• challenging to control crystal structure • mold required	[127,129, 211,212, 214,299]
	nanomolding: gas phase	vapor deposition of atoms/clusters into nanomolds, includes template assisted CVD, and CVD /VLS/VSS with patterned seeds, PVD and ALD	bottom-up	metals, semiconductors, and oxides	medium	uniform	medium	~10 nm	• dimensions, shapes and compositions can be readily controlled	• requires complex procedure for catalysts deposition • mold required	[128,209, 300]
	nanomolding: TMNM	nanostructure grows in mold cavities through diffusion/ dislocation driven by applied pressure gradient, includes TMNM based on dislocation and diffusion mechanism	top-down	ordered phases, metals, semiconductors, solid solutions, alloys,	high	uniform	very high up to 2000	atomic level	• highly versatile in material selection, shape, and size • one-step fabrication of nanorod arrays • high-quality single crystals with defined orientation • low-cost process that can be readily scaled-up	• mold required	[61,62,64]

pre-deposited catalyst [134]. Here, orientated single crystal nanowire arrays are typically fabricated.

Gas/solution-based molding provides easy-to-handle solutions to fabricate nanostructures/nano-devices with high-quality single crystal structure, controlled size and crystalline orientation. A large number of nanostructures including semiconductors including Si, Ge, and ZnO, metals such as Cu, Zn, and Ag, and carbon nanotubes [213] have been fabricated (Fig. 25). By using multi precursors, nanowires with heterostructures have also been fabricated [214]. The aspect ratio in gas/solution base molding is essentially limited by the mold. When compared to other nanomolding techniques, gas/solution-based molding using AAO template can achieve similar aspect ratios than those achievable with techniques for nanomolding of solid and liquid phases. When using photoresist as a mold, due to the limitations imposed by lithography techniques, only low aspect ratio nanorods can be fabricated. To lift the restriction of a small aspect ratio, more involved lithography and lift-off processes have been developed, in which a subsequent second deposition step, such as VLS or VSS growth, is applied [134]. To date, these methods are limited to some selected materials. For example, template assisted CVD methods are mainly used for semiconductors.

4. Nanomolding as a nanofabrication category

4.1. Materials for nanomolding

In principle, any material that is stable at the processing temperature and pressure can be molded on the nanoscale either in its liquid, solid, or gas states. The range of materials that can be nanomolded is therefore very large. Table 1 summarizes the various material classes with specific example materials for the various classes, and summarizes the underlying mechanisms and nanomolding technique, state of matter during molding, scaling with mold diameter of the molding length and the minimum features size that can be achieved.

Pure metals can be fabricated by a range of techniques such as TMNM by either diffusion or dislocation and electrodeposition using a template [212,214]. Non-metal nanorod arrays including Si [215] and Ge [209] can be fabricated through template assisted vapor deposition in their gas phase. Soft materials, such as numerous thermoplastic polymers [53,216,217] and metallic glasses [60,218], are typically fabricated through nanoimprinting by viscous flow. Ordered phases, including many functional materials of superconductors, phase change materials, semiconductors and topological materials, can be fabricated through TMNM with a diffusion mechanism [64]. Ceramics [210,219] including oxides [211] and other materials such as carbon nanotubes [220] can also be fabricated by template assisted vapor and electrochemical deposition.

4.2. Comparison of nanomolding with other nanofabrication methods

Over the past decades, driven by ever increasing demands for nanomaterials and devices, a wide range of nanofabrication methods have been developed (Table 2). They cover different material categories, length scales, shapes and morphologies, scalability and fabrication environments. Each nanofabrication method has its specific advantages and drawbacks and thereby suitability for a specific application.

The various nanofabrication methods can be grouped into seven categories according to their fabrication principles (Fig. 26). These are:

1. Direct writing methods which use scanning beams (ions, electrons, protons) or probes (STM or AFM) to directly write nanopatterns on substrate, through either indentation, etching/milling, reaction or deposition. Many direct writing methods (such as e-beam lithography) generally work with polymers and semiconductors, while Focus Ion Beam (FIB) milling methods fabricate in principle any solid materials. Direct writing techniques are highly versatile to fabricate any designed 2D pattern (and also some 3D structures). Their mayor limitation is their very slow processing speed and fabrication throughput.

2. Lithography techniques that are using a pre-fabricated mask with designed patterns and radiation beams (photons, ions, electrons) project the patterns onto a resist. Through a subsequent dry or wet etching step, the pattern is transferred into the material of interest. Lithography is a high-throughput 2D nanofabrication techniques that has revolutionized the microelectronic industry. The main material class where lithography techniques are used for are semiconductors. The spatial resolution of mask lithography methods is defined by the diffraction limit of the used radiation. Limits are the high cost of facilities used in these techniques and fabrication of the masks.

3. Electrospinning uses electrical forces to draw an electrically charged jet from polymer solution or melts and form nanofibers. Ceramic fibers can also be fabricated combined with sol–gel process. Materials that are suited for nanofabrication through electrospinning are limited to polymers and colloids. Electrospinning produces single and free-standing nanowires.

4. Chemical synthesis methods fabricate nanoparticles by chemical reactions through processes comprising of supersaturation followed by nucleation and subsequent growth of the nanoparticles. Such processes can be carried out in a solution, gas or solid phase. A range of different chemical reaction routes are used to fabricate nanoparticles of metals, non-metals and oxides. Chemical synthesis-based nanofabrication is very high-throughput and low-cost and is widely used for commercial applications. Limitations of chemical synthesis-based nanofabrication is that mainly 0D nanoparticles can be fabricated with limited control over their size and shape.

5. Spontaneous growth methods, that fabricate 1D nanostructures (nanowires, nanorods, nanobelts, nanofibers, whiskers, etc.) via anisotropic growth along specific directions or crystallographic orientations. Condensation and anisotropic growth of vapor into nanostructures occurs for example on preferred crystal facets. Spontaneous growth methods are realized by vapor deposition, including physical vapor deposition (PVD) and chemical vapor deposition (CVD), solution base growth, or other techniques such as laser ablation in either gas phase or solution phase. Spontaneous growth methods fabricate a wide range of materials such as metals,

semiconductors, oxides, and ceramics. They allow medium fabrication throughput and can produce nanowires with high crystal quality, which is important when fabricating nanowires for applications of functional materials. Their limits include the lack of control over the length of the nanowires and the lack of the ability to fabricate nanorod arrays without the use of a template. Moreover, each technique to fabricate nanowires through spontaneous growth is limited in the range of materials it can use. For example, VLS method only works for non-metals and non-metal compounds.

6. Self-assembly methods can be used to fabricate 2D/3D nanostructures with nanoparticles and molecules as building blocks. The self-assembly process is driven by energy minimization of the system. Templates can also be used to guide the assembly process and to control the desired patterns. Self-assembly with molecules (including DNA and proteins), macromolecules, and colloidal particles exhibits high fabrication throughput at low cost, however spatial resolution is low when compared to other nanofabrication methods. Another widely used material class for nanofabrication via self-assembly is block copolymers. Based on intermolecular interactions between blocks and molecules, self-assembly of block copolymers leads to large-scale nanofabrication of 2D (thin film), 3D (bulk), and solution-based nanostructures with small feature size at low cost. Self-assembly of block copolymers is also used as a directing agent for nanofabrication of other functional materials including metals and oxides.

7. Nanomolding uses nanostructured templates (molds) to set the shape of the nanostructure. Materials are driven into the molds by various biases such as a pressure gradient. Nanomolding can fabricate nanostructures at high throughput and inherently controlled size and geometry. A wide range of materials including metals, non-metals, soft materials, and ordered phases are suitable for nanomolding. Limitations of nanomolding are the requirements of a mold which affects costs and also require a demolding processing step.

The various nanofabrication methods discussed here and summarized in Table 2 are compared in Fig. 26 by their fabrication throughput and by the material class that can be used.

5. Application of nanomolding

Today's development of nanoscience and nontechnology relies on the feasibility of nanofabrication methods. From the discussion above, nanofabrication through molding offers the ability to fabricate nanostructures that exhibit the following characteristics: *i)* vertically aligned nanowire/nanorod arrays and nanopatterns, *ii.)* precise control over size and geometry of the nanowire/nanorod, *iii.)* nanowire/nanorod are attached to a bulk reservoir. In principle, nanostructures with such specifics can also be fabricated with nanolithography techniques or direct writing methods (FIB). However, the former is limited to semiconductor materials and the latter suffers from the fundamental inability for scale-up. Nanomolding on the other hand can be carried out with metals, non-metals, solid solutions, and ordered phases in a highly scalable manner, hence, enables potential application in broad fields including:

Devices: Various electronic, photonic, and chemical devices rely on the utilization of nanowires due to their high surface-to-volume ratio or surface-to-footprint ratio [301,302]. In some cases, their functional properties originate from the size reduction [301,303-306]. Nanowires of functional materials that exhibit enhanced properties are widely used in a variety of fields including: *i.)* energy storage [307], where functional nanowires (e.g., metals, silicon-based materials, lithium titanium oxides, conducting polymers, and carbon materials) are used as electrodes for lithium-ion batteries [308,309], sodium-ion batteries [310], and supercapacitors [311]. Important requirements of such nanowires are their dimensional accuracy, control over chemistry, high-quality crystal structures, and fast electronic transport due to their small scale. *ii.)* Computing [301], where semiconductor nanowires (e.g., Si, Ge, and III-V semiconductors) are used for fabrication of nanowire field effect transistors (FETs) [312]. These nanowire FETs exhibit high performance and high electron mobility suggesting possibilities beyond wafer-based electronics. *iii.)* Detectors [313] and sensors [306,314]. The large surface-to-volume ratios and quantum size effects of nanowire devices offer promising applications for detectors and sensors. These application include optoelectronic sensors based on FET with semiconducting nanowires [315], conductometric sensors with metal, metal-oxide, and polymer nanowires [316,317], and surface-plasmon-resonance-based sensors with metal nanowires which allow for ultrasensitive and direct detection of chemical (e.g., H_2, CO, NH_3) and biological (e.g., DNA, RNA, ATP) species. Single-photon detectors based on superconducting and semiconducting nanowires are another promising application field by exhibiting high-speed, wide wavelength, high efficiency, and precise photon detecting. *iv.)* Energy conversion [318]. For example, light emitting diodes exhibit enhanced extraction efficiency when based on semiconducting nanowires due to the concentrated emission from the tip of the nanowires. *v.)* Quantum devices [196,305]. Owing to their large surface-to-volume ratio and high electron mobility, nanowires are also of significant interest for applications in quantum devices where the topological properties become important. These quantum devices based on topological materials are attractive for the fundamental understanding of topology and for future applications such as low-dissipation electronics and high-speed electronics. Main materials for nanowire quantum devices include topological materials such as topological insulators (e.g., SnTe) and topological semimetals (e.g., Cd_3As_2) [319]. Unlike single nanowires, which typically require tedious assembly for device application, nanomolding fabricates nanowire arrays attached to substrates that can be readily integrated into devices. Examples of such applications include: supercapacitors [311,320], magnetic memories [163], single-photon detectors [313,321], chemical sensors [322], and light emitting diodes (LED) [318,323].

Energy harvesting: Vertically aligned nanowire arrays are promising candidates for solar energy [324-326] and chemical energy harvesting [5,161,327-330]. Applications include photovoltaics/solar cells, and fuel cells. Due to their efficient antireflection to the incident light and short collection length for excited carriers, nanowire arrays made from semiconductors (e.g., silicon and compound semiconductors) enhance light absorption in solar cells and other photovoltaic applications [326]. For example, Si and GaAs nanowire arrays can be used for high-performance solar cells [331,332]. In addition, perovskite nanowire arrays also show application for solar cells with high photocurrent density and high power efficiency [333]. High performance of photovoltaics requires the nanowires to be single-crystalline materials with low defect densities, well controlled morphology and dimensions, and well-defined doping compositions [334]. Nanomolding as a method offering precise geometry control and high-quality nanowire arrays, is promising for required

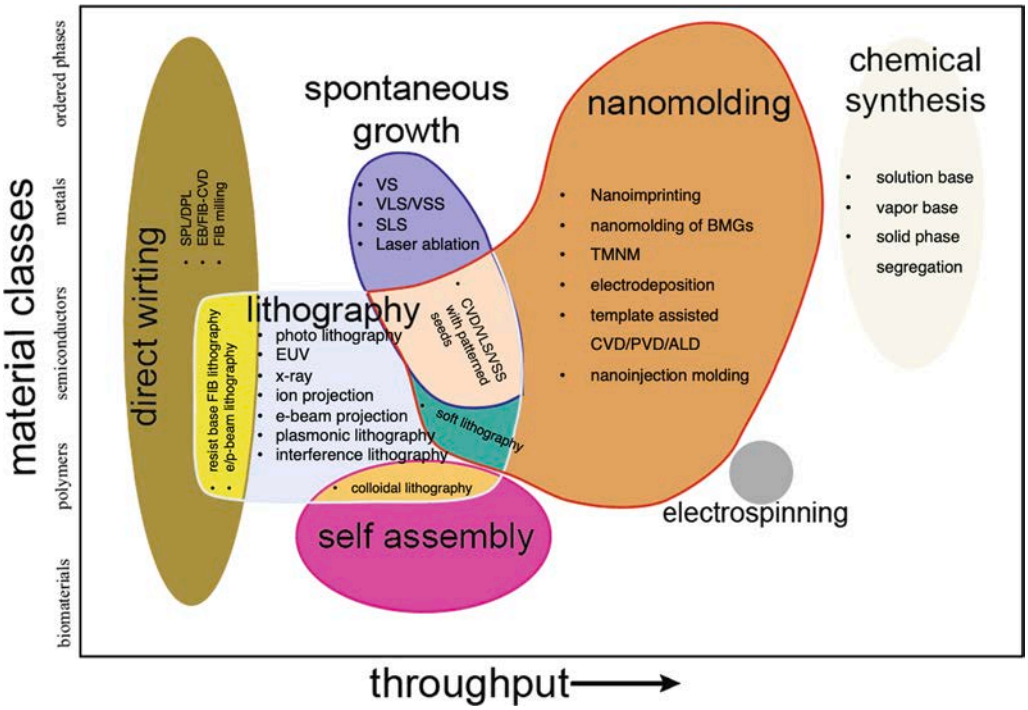

Fig. 26. Comparison of nanofabrication methods by the materials they can fabricate and the throughput of the process. Established nanofabrication methods are summarized into different categories by their fabrication principles. Defined by the features of each fabrication principle, these categories exhibit different fabrication throughput (horizonal axis) and covering different material classes (vertical axis). Some techniques combine more than one of these principles.

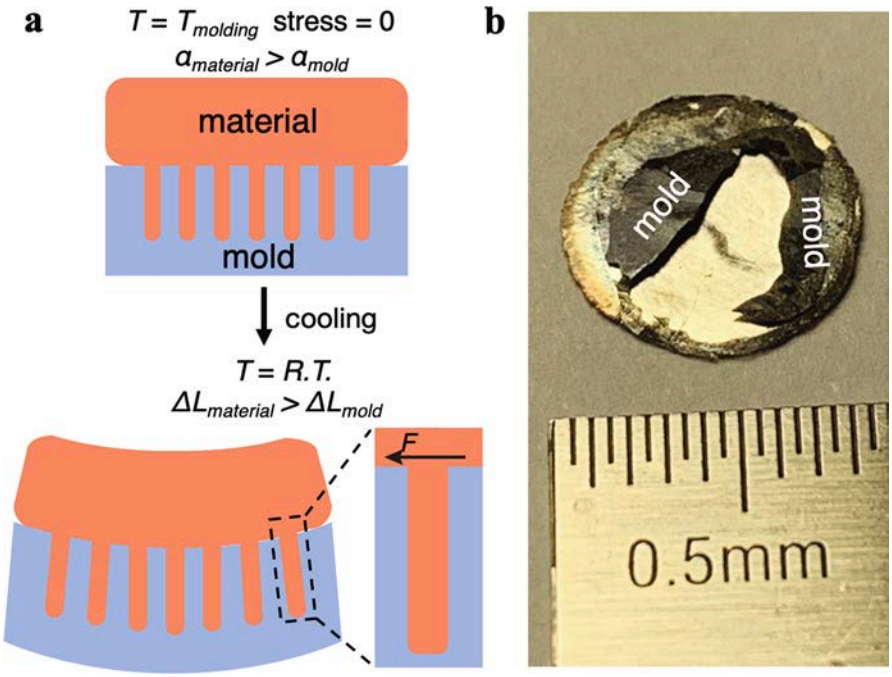

Fig. 27. Thermal stresses and resulting thermal deformation during nanomolding. (a) Due to the generally different thermal expansion coefficients of mold and moldable material, $\Delta\alpha = \alpha_{mold} - \alpha_{material}$, cooling down to room temperature from the molding temperature changes the length of mold and moldable material in different ways. Due to the "anchoring" of the moldable material into the mold in the nanocavities, stress is building up. Such stress acts as a force to resist mold release. It can bend the mold/moldable material combination and may even break it. (b) Example, where thermal stresses after TMNM of Ag into AAO nanomolds at 700°C cause the AAO mold to break when cooled to room temperature.

fabrication. Metal-based nanowire arrays (e.g., Pt-based, Ni-based alloys, and metallic glasses) are widely used in fuel cells for their high catalytic activity [5,85,161,328-330,335-337]. For example, Pt and Pt-Ru nanowires are demonstrated as catalysts for methanol fuel cells [338]. Ni-Co nanowire arrays are used in urea/hydrogen peroxide fuel cells [329]. Bulk metallic glass nanowire arrays fabricated by liquid base nanomolding also exhibit promising catalytic activity [5,161]. In general, it is the precise control over the wires' diameter and spacing that makes nanomolding a front runner in fabricating energy harvesting applications.

Chemical industry: One-dimensional nanowire arrays have shown enhanced efficiency for catalysis, electrochemistry [339-342], and photochemistry applications [343,344]. Efficient photocatalytic energy conversion requires high light absorption, high mobility for charge separation and collection, and fast mass transport of reactants. Nanowire photocatalysts, with their high absorption rate, small radial dimension, and large surface-to-volume ratio, become promising candidates. Semiconductor nanowire arrays (e.g., TiO_2, ZnO, $BiVO_4$, and other compound semiconductors) are widely used in photocatalysis processes. For example, it has been demonstrated that GaN nanowire arrays are promising candidates for photocatalyst, water splitting with a highly stable photocatalytic process [345] and CO_2 reductions [346]. For electrocatalysts, of great advantages are the high catalytic activity enabled by high surface-to-volume

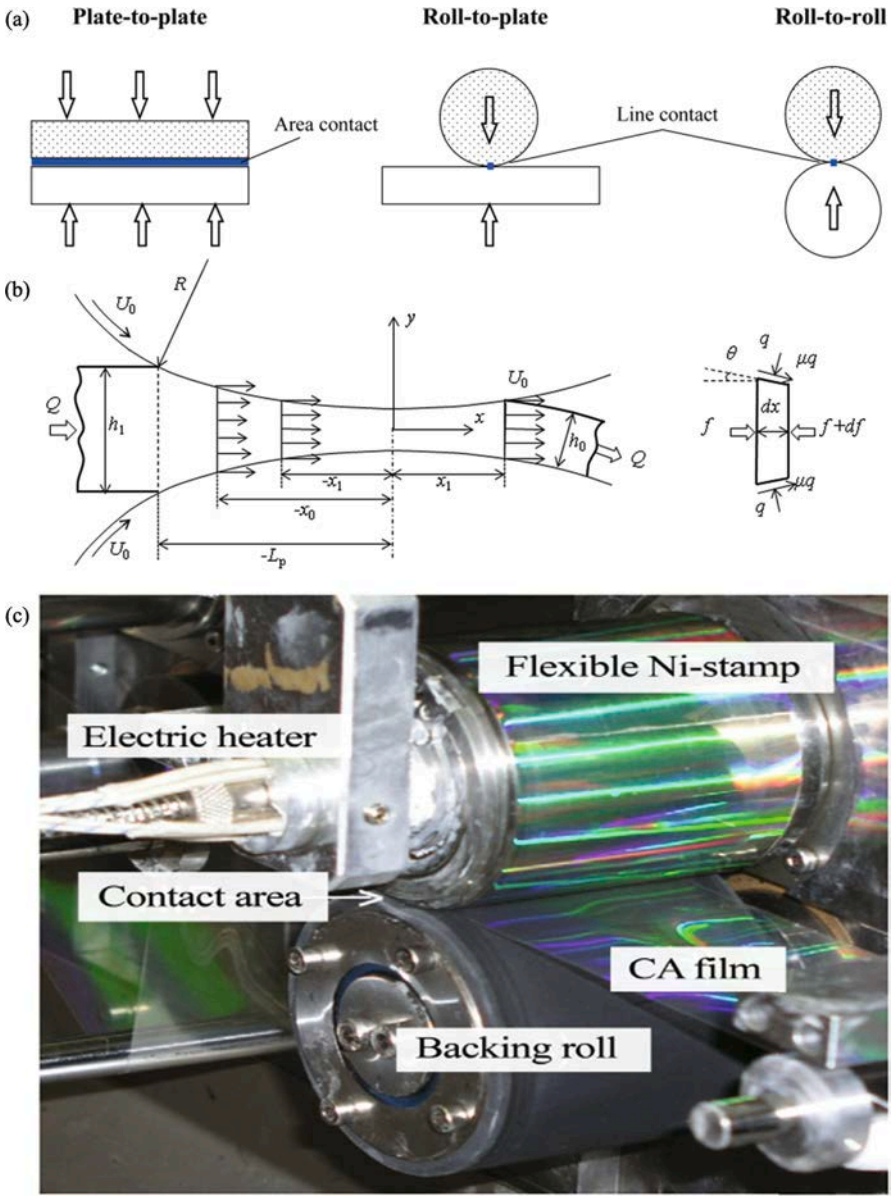

Fig. 28. Scaling-up strategies for nanomolding. (a) Schematics of plate-to-plate, roll-to-plate, and roll-to-roll. Whereas in plate-to-plate, the entire plate is distributing the applied force, for roll-to-plate and roll-to-roll, only a narrow contact line experiences the applied force. Hence, for the same applied force, a much higher pressure is experienced in the contact line, compared to the pressure within a plate-to-plate setup in the contact area. (b) Mechanical model for roll-to-roll molding. (c) Example of roll-to-roll nanoimprinting of a polymer film [392].

ratio an fast charge/carrier transfer during electrolysis within the nanowire arrays. Electrocatalysis utilizes mainly metal-based nanowires (e.g., Pt, Cu, FeP, and Ni-/Co– oxides). In this category, noble metals and bimetallic nanowires are typically used. For example, Pt and Ir nanostructures are used as high-performance electrocatalysts for water splitting [347,348]. In addition, metal-based nanowires, such as $NiCo_2O_4$ and Mo_2C, have been also demonstrated as low-cost and highly active electrocatalysts [349,350]. Nanomolding can be used as the fabrication method of catalysts nanowire arrays that are attached to conductive substrates for the use in chemical processes such as water splitting [343,344] and reduction of CO_2 [342,351].

Life science: Nanomaterials/nanowires, when compared to bulk materials generally show greatly enhanced biological, mechanical, and physicochemical properties. Their small scale, large surface area and biocompatibility, enhance or enable a variety of bio-applications. These applications include: *i.)* bio-sensors [19,352], where devices based on metallic and semiconducting nanowires are used as sensors to detect biomolecules and species, as discussed above. *ii.)* Bio-measurements [353] to probe signals from living bio-systems. For example, micro/nano electrode arrays are used to record electrical activities from living cells [354,355]. Typically, for electro-signal measurement, Au is used in the nanowires. *iii.)* Bacteria/cell adhesion [7,356,357]. Living cells can recognize and respond to nanoscale topographies, which has been observed by using vertically aligned nanowire arrays [358-360]. As a consequence, such arrays have been used for application in life science where they interface with cells and tissues [7,360-364]. Semiconductor nanowire arrays, including Si and ZnO [356,365], and metallic nanowires, such as Ag and BMGs [7,357] are typically used for cell adhesions. *iv.)* Bone and tissue engineering [366,367]. Natural bone surfaces usually contain features with a length scale of ~ 100 nm. To avoid rejection of the cells of artificial bone materials with a smoother surface nanostructured bone replacements are necessary [368]. For example, metallic nanowires and polymer nanofibers/nanowires are promising candidates for scaffolds in tissue engineering [369]. In general, to avoid a rejection by the human body materials must be bio-compatible, which has been shown to be the case for metals (e.g., Au and Ag), semiconductors (e.g., Si), polymers and metallic glasses (e.g., Pt-based BMG) [8,360].

Artificial surfaces and metamaterials: Artificial surfaces and metamaterials realize desired properties and functionalities with designed 2D/3D nanostructures [370]. They are of significant interest in optics [370], acoustics [371], mechanics [372,373], and related applications [374,375]. Functionality is generated through the geometry of the designed nanostructure. For example, optical metasurfaces use designed periodic subwavelength nanostructures to resonantly couple to incident electromagnetic fields. In such cases, precise fabrication of the designed functional nanostructure is critical to achieve the envisioned properties of these surfaces. Generally, any deviation from the designed nanopattern which originates from imperfections in the fabrication precision in shape of the individual nanofeature and the periodic arrangement of the nanofeatures leads to a drop in device performance [376-378]. These 2D/3D nanopatterns with precisely controlled geometry can be potentially achieved by nanomolding against a patterned hard mold. Examples of applications include: optical devices [379] (metals and dielectric materials), plasmonic devices [380,395] (metals), surface enhanced Raman scattering [381,396,397] (metals), and superhydrophobic surfaces [382-384] (polymers and metals).

Besides the application discussed above, nanomolding also offers solutions for the fabrication of nanostructures from materials which are generally difficult to synthesis on the nanoscale [64]. At least in principle any alloy and compound with any number of components can be molded. This includes highly ordered crystallographic structures such as ordered phases [64]. This recent success may also path the way for practical fabrication of quantum materials and devices.

6. Concluding remarks on nanomolding

Nanomolding is the underlying mechanism for a wide range of nanofabrication methods such as template-based deposition, extrusion, nanoembossing, soft lithography, nanoimprint lithography, thermomechanical nanomolding, and nanoimprinting.

It has established itself as a versatile toolbox for nanofabrication; Nanomolding is the nanofabrication technique of choice for a wide range of materials and states of matter. Its versatility surpasses all other nanofabrication methods. Nanomolding offers solutions for lithography techniques and for the fabrication of a wide range of materials that are needed for envisioned nanodevices and quantum material and device applications. The various specific nanomolding methods can be further categorized by their physical mechanisms underlying the processes which themselves are defined by the states of matter and the material classes.

While the technological readiness of nanomolding is generally high, in some cases the readiness has already reached a level that it has been commercially pursued, we want to point out critical research to accelerate and broaden commercial usage of nanomolding as an enabler for nanomaterials and devices. These are:

(i) Requirements and limitations of hard molds: In particular for the most versatile nanomolding methods that require elevated temperature and high pressure, only few mold materials and mold material fabrication methods have been established. By far most common are anodic aluminum oxide (AAO) and nanopatterned silicon. Both techniques and nano molds are commercially available. However, costs for nanoarray molds are high, for example, ~10 dollars per cm^2 for AAO research molds. Even though these costs can be significantly reduced in a large-scale production [385], it will be challenging to reduce cost by more than three orders of magnitude. Hence, for applications such as photovoltaic, most catalytic applications, and many plasmonic applications, these mold costs prevent nanomolding as a commercially viable process. Alternatives for AAO and silicon molds have been explored [143,144]. In order to mold lower melting temperature materials such as polymers, some metallic glasses and low temperature metals, instead of searching for inexpensive mold alternatives, reusable molds, made from highly durable metallic glasses have been pursued [143,223,386]. In general, a broader range of available molds which differentiate by mold costs, precision, shape and size would be highly beneficial to match the specifics of an application with the appropriate mold.

(ii) Mold release: For the majority of applications free standing nanowires/arrays are demanded, which requires the separation of the nanowire/array from the mold. This typically requires dissolution of the mold through an etching process. Mold dissolution is most commonly achieved through wet-etching using KOH. For many materials including metals and ordered phases, such KOH exposure

also results in (at least partially) dissolution of the formed nanowires. A careful optimization of the etching process including temperature and mechanical irritation may reduce the undesired dissolution of the nanowire. However, it will be difficult to entirely eliminate dissolution when using KOH. Alternative mold release strategies have to be developed. Here, first attempts based on mechanical demolding have been explored [143,189].

(iii) Thermal stresses during nanomolding: For the majority of nanomolding processes, molding is carried out at elevate temperatures. As mold and moldable material are different materials, they generally exhibit different thermal expansion coefficients, $\Delta\alpha = \alpha_{mold} - \alpha_{material}$. Such difference causes thermal stresses to evolve upon cooling mold and moldable material from the molding temperature down to room temperature. Such stresses resist mold release, can bend the mold/moldable material sandwich, or even break it (Fig. 27). For example, when TMNM of gold at 330°C ($\alpha(Au) = 1.4 \times 10^{-5}\ K^{-1}$) into AAO ($\alpha(AAO) = 8.2 \times 10^{-6}\ K^{-1}$) cause a thermal stress of $\Delta\alpha\Delta T \bullet G \sim 50$ MPa when cooled to room temperature. Such stress is significant when considering that the tensile strength of gold is ~ 120 MPa. Minimizing molding temperature for a given material and slow cooling after the molding process to enable some stress release may offer some possibilities for stress release. Most effective however will be to reduce these thermal stresses by identifying mold/moldable material combinations with minimal $\Delta\alpha$, making the need for a wider range of mold materials (i) even more important.

(iv) Ability to scale-up and enhance throughput. Many of the commercial applications demand large size nanowire arrays [385,387-390]. An effective strategy to scale-up nanoimprinting from a batch-to-batch process to a continuous process are based on rolling strategies. During such roll-to-roll-based nanoimprinting, the molding force, which is spread out over a contact area in plate-to-plate nanoimprinting, is concentrated to the "area" of the contact "line". This is the case for roll-to-plate [391] and roll-to-roll nanomolding [392-394] (Fig. 28). Due to the finite "line" contact regions between rollers, a much larger width can be achieved with the same molding force when compared to a plate-to-plate molding process, where force is distributed over the entire molded region (Fig. 28b). Further, when assuming a continuous feedstock, the length of the moldable material is unlimited during the rolling process. The molding force applied on the line contact during roll-to-roll molding is given by:

$$F = \frac{3\eta U_0\sqrt{R}}{(h_1)^{3/2}} f\left(\frac{h_0}{h_1}, \frac{h_m}{h_1}\right), \tag{8}$$

where f is a constant depending on the ratios of h_0/h_1 and h_m/h_1. R, h_m, and U_0 are the radius of the roller, the minimum gap between the two rollers, and the rolling speed, respectively (Fig. 28(b)). h_1 and h_0 are the thickness of the feedstock sheet before and after rolling, respectively. Eq. (8) indicates that the molding force is independent of the area of the feedstock sheet (to be patterned region). This is in contrast to plate-to-plate nanomolding, where the molding force is proportional to the to-be-patterned area of the feedstock sheet. It is important to mention that roll-to-roll molding involves both molding and demolding processes. The requirement for demolding limits the aspect ratio of molded nanofeatures to typically less than unity [394]. Moreover, the interface friction and adhesion during rolling introduces new challenges such as the mechanical instability and the durability of the roller mold [393,394]. The major limitation of roll-to-roll nanoimprinting in terms of material selection stems from its temperature limitation. Current systems can be operated at temperatures of up to ~ 200 °C. This temperature is sufficient for molding of most polymers but excludes most other materials from being processed through this technique. Hence, development of rolling machines that operate at higher temperatures is required to scale up nanomolding to enable the use of a roll-to-roll process for most materials.

Declaration of Competing Interest

The authors declare that they have no known competing financial interests or personal relationships that could have appeared to influence the work reported in this paper.

Acknowledgements

This work was supported by the National Science Foundation through the Advanced Manufacturing Program (CMMI 1901613), the National Natural Science Foundation of China (12172260 and 11632009), and the Wuhan Science and Technology Bureau of China (2019010701011390).

References

[1] Humplik T, Lee J, O'Hern SC, Fellman BA, Baig MA, Hassan SF, et al. Nanostructured materials for water desalination. Nanotechnology 2011;22:292001.
[2] Werber JR, Osuji CO, Elimelech M. Materials for next-generation desalination and water purification membranes. Nat Rev Mater 2016;1:16018.
[3] Bruce PG, Scrosati B, Tarascon J-M. Nanomaterials for Rechargeable Lithium Batteries. Angew Chem Int Ed 2008;47:2930–46.
[4] Liu N, Lu Z, Zhao J, McDowell MT, Lee H-W, Zhao W, et al. A pomegranate-inspired nanoscale design for large-volume-change lithium battery anodes. Nat Nanotechnol 2014;9:187.
[5] Sekol RC, Kumar G, Carmo M, Gittleson F, Hardesty-Dyck N, Mukherjee S, et al. Bulk Metallic Glass Micro Fuel Cell. Small 2013;9:2081–5.
[6] Stevens MM, George JH. Exploring and Engineering the Cell Surface Interface. Science 2005;310:1135–8.
[7] Padmanabhan J, Kinser ER, Stalter MA, Duncan-Lewis C, Balestrini JL, Sawyer AJ, et al. Engineering Cellular Response Using Nanopatterned Bulk Metallic Glass. ACS Nano 2014;8:4366–75.
[8] Liu Y, Padmanabhan J, Cheung B, Liu JB, Chen Z, Scanley BE, et al. Combinatorial development of antibacterial Zr-Cu-Al-Ag thin film metallic glasses. Sci Rep-Uk 2016;6.
[9] Feng L, Li S, Li Y, Li H, Zhang L, Zhai J, et al. Super-Hydrophobic Surfaces: From Natural to Artificial. Adv Mater 2002;14:1857–60.

[10] Feng X-Q, Gao X, Wu Z, Jiang L, Zheng Q-S. Superior Water Repellency of Water Strider Legs with Hierarchical Structures: Experiments and Analysis. Langmuir 2007;23:4892–6.
[11] Xia T, Li N, Wu Y, Liu L. Patterned superhydrophobic surface based on Pd-based metallic glass. Appl Phys Lett 2012;101:081601.
[12] Kreder MJ, Alvarenga J, Kim P, Aizenberg J. Design of anti-icing surfaces: smooth, textured or slippery? Nat Rev Mater 2016;1:15003.
[13] Schuller JA, Barnard ES, Cai W, Jun YC, White JS, Brongersma ML. Plasmonics for extreme light concentration and manipulation. Nat Mater 2010;9:193–204.
[14] Ozbay E. Plasmonics: Merging Photonics and Electronics at Nanoscale Dimensions. Science 2006;311:189–93.
[15] Mortensen NA, Raza S, Wubs M, Søndergaard T, Bozhevolnyi SI. A generalized non-local optical response theory for plasmonic nanostructures. Nat Commun 2014;5:3809.
[16] Brolo AG. Plasmonics for future biosensors Nat Photon 2012;6:709–13.
[17] He X, Gao F, Tu G, Hasko D, Hüttner S, Steiner U, et al. Formation of Nanopatterned Polymer Blends in Photovoltaic Devices. Nano Lett 2010;10:1302–7.
[18] Liu B, Li Y, Wan H, Wang L, Xu W, Zhu S, et al. High Performance, Multiplexed Lung Cancer Biomarker Detection on a Plasmonic Gold Chip. Adv Funct Mater 2016;26:7994–8002.
[19] Kinser ER, Padmanabhan J, Yu R, Corona SL, Li J, Vaddiraju S, et al. Nanopatterned Bulk Metallic Glass Biosensors. ACS Sensors 2017;2:1779–87.
[20] Huang X, Zhao Z, Cao L, Chen Y, Zhu E, Lin Z, et al. High-performance transition metal–doped Pt₃Ni octahedra for oxygen reduction reaction. Science 2015;348:1230–4.
[21] Li J, Doubek G, McMillon-Brown L, Taylor AD. Recent Advances in Metallic Glass Nanostructures: Synthesis Strategies and Electrocatalytic Applications. Adv Mater 2019;31:1802120.
[22] Jeong HE, Lee J-K, Kim HN, Moon SH, Suh KY. A nontransferring dry adhesive with hierarchical polymer nanohairs. Proc Natl Acad Sci 2009;106:5639–44.
[23] Rogers JA, Someya T, Huang Y. Materials and mechanics for stretchable electronics. Science 2010;327:1603–7.
[24] Jo A, Joo W, Jin W-H, Nam H, Kim JK. Ultrahigh-density phase-change data storage without the use of heating. Nat Nanotechnol 2009;4:727–31.
[25] Wang ZL, Song J. Piezoelectric Nanogenerators Based on Zinc Oxide Nanowire Arrays. Science 2006;312:242–6.
[26] Schneider GF, Dekker C. DNA sequencing with nanopores. Nat Biotechnol 2012;30:326–8.
[27] Uchic MD, Dimiduk DM, Florando JN, Nix WD. Sample dimensions influence strength and crystal plasticity. Science 2004;305:986–9.
[28] Rasmussen A, Gaitan M, Locascio LE, Zaghloul ME. Fabrication techniques to realize cmos-compatible microfluidic microchannels. J Microelectromech Syst 2001;10:286–97.
[29] Liu X, Osada M, Kitamura K, Nagata T, Si D. Ferroelectric-assisted gold nanoparticles array for centimeter-scale highly reproducible SERS substrates. Sci Rep 2017;7:3630.
[30] Zhang J, Zhang X, Chen S, Gong T, Zhu Y. Surface-enhanced Raman scattering properties of multi-walled carbon nanotubes arrays-Ag nanoparticles. Carbon 2016;100:395–407.
[31] Yang X, Yang M, Pang B, Vara M, Xia Y. Gold Nanomaterials at Work in Biomedicine. Chem Rev 2015;115:10410–88.
[32] Kildishev AV, Boltasseva A, Shalaev VM. Planar Photonics with Metasurfaces. Science 2013;339:1232009.
[33] Haruta M, Yamada N, Kobayashi T, Iijima S. Gold Catalysts Prepared by Coprecipitation for Low-Temperature Oxidation of Hydrogen and of Carbon-Monoxide. J Catal 1989;115:301–9.
[34] Daniel MC, Astruc D. Gold nanoparticles: Assembly, supramolecular chemistry, quantum-size-related properties, and applications toward biology, catalysis, and nanotechnology. Chem Rev 2004;104:293–346.
[35] Volkert CA, Lilleodden ET. Size effects in the deformation of sub-micron Au columns. Philos Mag 2006;86:5567–79.
[36] Detsi E, Punzhin S, Rao JC, Onck PR, De Hosson JTM. Enhanced Strain in Functional Nanoporous Gold with a Dual Microscopic Length Scale Structure. ACS Nano 2012;6:3734–44.
[37] Wang YM, Chen MW, Zhou FH, Ma E. High tensile ductility in a nanostructured metal. Nature 2002;419:912–5.
[38] Yu Q, Shan ZW, Li J, Huang XX, Xiao L, Sun J, et al. Strong crystal size effect on deformation twinning. Nature 2010;463:335–8.
[39] Frick CP, Clark BG, Orso S, Schneider AS, Arzt E. Size effect on strength and strain hardening of small-scale [111] nickel compression pillars. Mat Sci Eng a-Struct 2008;489:319–29.
[40] Arutyunov KY, Zavialov VV, Sedov EA, Golokolenov IA, Zarudneva AA, Shein KV, et al. Nanoarchitecture: Toward Quantum-Size Tuning of Superconductivity. Phys Status Solidi-R 2019;13.
[41] Njoki PN, Lim IIS, Mott D, Park HY, Khan B, Mishra S, et al. Size correlation of optical and spectroscopic properties for gold nanoparticles. J Phys Chem C 2007;111:14664–9.
[42] Faraday MX. The Bakerian Lecture. —Experimental relations of gold (and other metals) to light. Philos Trans R Soc Lond 1857;147:145–81.
[43] Sebastian EM, Jain SK, Purohit R, Dhakad S, Rana R. Nanolithography and its current advancements. Mater Today: Proc 2020.
[44] Wagner RS, Ellis WC. VAPOR-LIQUID-SOLID MECHANISM OF SINGLE CRYSTAL GROWTH. Appl Phys Lett 1964;4:89–90.
[45] Givargizov EI. Fundamental aspects of VLS growth. J Cryst Growth 1975;31:20–30.
[46] Seliger RL, Kubena RL, Olney RD, Ward JW, Wang V. High-resolution, ion-beam processes for microstructure fabrication. Journal of Vacuum Science and Technology 1979;16:1610–2.
[47] Broers AN, Molzen WW, Cuomo JJ, Wittels ND. Electron-beam fabrication of 80-Å metal structures. Appl Phys Lett 1976;29:596–8.
[48] Possin GE. A Method for Forming Very Small Diameter Wires. Rev Sci Instrum 1970;41:772–4.
[49] Sun L, Searson P, Chien C-L. Electrochemical deposition of nickel nanowire arrays in single-crystal mica films. Appl Phys Lett 1999;74:2803–5.
[50] Fojtík A, Henglein A. Laser ablation of films and suspended particles in a solvent : formation of cluster and colloid solutions Berichte der Bunsen-Gesellschaft 1993;97:3.
[51] Morales AM, Lieber CM. A laser ablation method for the synthesis of crystalline semiconductor nanowires. Science 1998;279:208–11.
[52] Zeng H, Du X-W, Singh SC, Kulinich SA, Yang S, He J, et al. Nanomaterials via Laser Ablation/Irradiation in Liquid: A Review. Adv Funct Mater 2012;22:1333–53.
[53] Chou SY, Krauss PR, Renstrom PJ. Imprint of sub-25 nm vias and trenches in polymers. Appl Phys Lett 1995;67:3114–6.
[54] Kim E, Xia Y, Whitesides GM. Polymer microstructures formed by moulding in capillaries. Nature 1995;376:4.
[55] Masuda H, Fukuda K. Ordered Metal Nanohole Arrays Made by a Two-Step Replication of Honeycomb Structures of Anodic Alumina. Science 1995;268:1466–8.
[56] Chou SY, Krauss PR, Renstrom PJ. Imprint Lithography with 25-Nanometer Resolution. Science 1996;272:85–7.
[57] Xia YN, Whitesides GM. Soft lithography. Annu Rev Mater Sci 1998;28:153–84.
[58] Pang SW, Tamamura T, Nakao M, Ozawa A, Masuda H. Direct nano-printing on Al substrate using a SiC mold. Journal of Vacuum Science & Technology B: Microelectronics and Nanometer Structures Processing, Measurement, and Phenomena 1998;16:1145–9.
[59] Piner RD, Zhu J, Xu F, Hong S, Mirkin CA. Dip-Pen. Nanolithography Science 1999;283:661–3.
[60] Kumar G, Tang HX, Schroers J. Nanomoulding with amorphous metals. Nature 2009;457:868.
[61] Liu Z. One-step fabrication of crystalline metal nanostructures by direct nanoimprinting below melting temperatures. Nat Commun 2017;8:14910.
[62] Liu Z, Han G, Sohn S, Liu N, Schroers J. Nanomolding of crystalline metals: The smaller the easier. Phys Rev Lett 2019;122:036101.
[63] Liu Z. Investigation of Temperature and Feature Size Effects on Deformation of Metals by Superplastic Nanomolding. Phys Rev Lett 2019;122:016101.
[64] Liu N, Xie Y, Liu G, Sohn S, Raj A, Han G, et al. General Nanomolding of Ordered Phases. Phys Rev Lett 2020;124:036102.
[65] Pérez-Juste J, Pastoriza-Santos I, Liz-Marzán LM, Mulvaney P. Gold nanorods: Synthesis, characterization and applications. Coord Chem Rev 2005;249:1870–901.
[66] Xia Y, Xiong Y, Lim B, Skrabalak SE. Shape-Controlled Synthesis of Metal Nanocrystals: Simple Chemistry Meets Complex Physics? Angew Chem Int Ed 2009;48:60–103.
[67] Ahmadi TS, Wang ZL, Green TC, Henglein A, El-Sayed MA. Shape-Controlled Synthesis of Colloidal Platinum Nanoparticles. Science 1996;272:1924–5.

[68] Pfeiffer HC. Recent advances in electron-beam lithography for the high-volume production of VLSI devices. IEEE Trans Electron Devices 1979;26:663–74.
[69] Martin CR. Nanomaterials: a membrane-based synthetic approach. Science 1994;266:1961–6.
[70] Hoyer P, Baba N, Masuda H. Small quantum-sized CdS particles assembled to form a regularly nanostructured porous film. Appl Phys Lett 1995;66:2700–2.
[71] John PMS, Craighead HG. Microcontact printing and pattern transfer using trichlorosilanes on oxide substrates. Appl Phys Lett 1996;68:1022–4.
[72] Whidden TK, Ferry DK, Kozicki MN, Kim E, Kumar A, Wilbur J, et al. Pattern transfer to silicon by microcontact printing and RIE. Nanotechnology 1996;7:447–51.
[73] Xia Y, Kim E, Zhao X-M, Rogers JA, Prentiss M, Whitesides GM. Complex Optical Surfaces Formed by Replica Molding Against Elastomeric Masters. Science 1996;273:347–9.
[74] Block ID, Chan LL, Cunningham BT. Large-area submicron replica molding of porous low-k dielectric films and application to photonic crystal biosensor fabrication. Microelectron Eng 2007;84:603–8.
[75] Thibault C, Severac C, Trévisiol E, Vieu C. Microtransfer molding of hydrophobic dendrimer. Microelectron Eng 2006;83:1513–6.
[76] Zhao X-M, Xia Y, Whitesides GM. Fabrication of three-dimensional micro-structures: Microtransfer molding. Adv Mater 1996;8:837–40.
[77] Ajayan PM. lijima S. Capillarity-induced filling of carbon nanotubes Nature 1993;361:333–4.
[78] King E, Xia Y, Zhao X-M, Whitesides GM. Solvent-assisted microcontact molding: A convenient method for fabricating three-dimensional structures on surfaces of polymers. Adv Mater 1997;9:651–4.
[79] Han L, Zhou J, Gong X, Gao C. Solvent-assisted polymer micro-molding. Chin Sci Bull 2009;54:2193–204.
[80] Ginger DS, Zhang H, Mirkin CA. The Evolution of Dip-Pen Nanolithography. Angew Chem Int Ed 2004;43:30–45.
[81] Kim D, Giermann AL, Thompson CV. Solid-state dewetting of patterned thin films. Appl Phys Lett 2009;95:251903.
[82] Mann S. Self-assembly and transformation of hybrid nano-objects and nanostructures under equilibrium and non-equilibrium conditions. Nat Mater 2009;8:781–92.
[83] Hasan M, Schroers J, Kumar G. Functionalization of Metallic Glasses through Hierarchical Patterning. Nano Lett 2015;15:963–8.
[84] Radha B, Lim SH, Saifullah MSM, Kulkarni GU. Metal hierarchical patterning by direct nanoimprint lithography. Sci Rep-Uk 2013;3.
[85] Mukherjee S, Sekol RC, Carmo M, Altman EI, Taylor AD, Schroers J. Tunable Hierarchical Metallic-Glass Nanostructures. Adv Funct Mater 2013;23:2708–13.
[86] Chou TP, Zhang QF, Fryxell GE, Cao GZ. Hierarchically structured ZnO film for dye-sensitized solar cells with enhanced energy conversion efficiency. Adv Mater 2007;19:2588-+..
[87] Lopes WA, Jaeger HM. Hierarchical self-assembly of metal nanostructures on diblock copolymer scaffolds. Nature 2001;414:735–8.
[88] Xie DG, Nie ZY, Shinzato S, Yang YQ, Liu FX, Ogata S, et al. Controlled growth of single-crystalline metal nanowires via thermomigration across a nanoscale junction. Nature. Communications 2019;10.
[89] Thoury M, Mille B, Séverin-Fabiani T, Robbiola L, Réfrégiers M, Jarrige JF, et al. High spatial dynamics-photoluminescence imaging reveals the metallurgy of the earliest lost-wax cast object. Nat Commun 2016;7:13356.
[90] Greer JR, De Hosson JTM. Plasticity in small-sized metallic systems: Intrinsic versus extrinsic size effect. Prog Mater Sci 2011;56:654–724.
[91] Hegyi ÁI, Ispánovity PD, Knapek M, Tüzes D, Máthis K, Chmelík F, et al. Micron-Scale Deformation: A Coupled In Situ Study of Strain Bursts and Acoustic Emission. Microsc Microanal 2017;23:1076–81.
[92] Chisholm C, Bei H, Lowry MB, Oh J, Syed Asif SA, Warren OL, et al. Dislocation starvation and exhaustion hardening in Mo alloy nanofibers. Acta Mater 2012;60:2258–64.
[93] Li X, Wei Y, Lu L, Lu K, Gao H. Dislocation nucleation governed softening and maximum strength in nano-twinned metals. Nature 2010;464:877–80.
[94] Zhu T, Li J. Ultra-strength materials. Prog Mater Sci 2010;55:710–57.
[95] Saotome Y, Tao ZAI. Microforming of Mems Parts with Amorphous Alloys. Mrs Proceedings 1998;554:385–90.
[96] Gao H, Hu Y, Xuan Y, Li J, Yang Y, Martinez RV, et al. Large-scale nanoshaping of ultrasmooth 3D crystalline metallic structures. Science 2014;346:1352–6.
[97] Shao Z, Gopinadhan M, Kumar G, Mukherjee S, Liu YH, O'Hern CS, et al. Size-dependent viscosity in the super-cooled liquid state of a bulk metallic glass. Appl Phys Lett 2013;102.
[98] Sohn S, Jung Y, Xie YJ, Osuji C, Schroers J, Cha JJ. Nanoscale size effects in crystallization of metallic glass nanorods. Nat Commun 2015;6.
[99] Rowland HD, King WP, Pethica JB, Cross GLW. Molecular Confinement Accelerates Deformation of Entangled Polymers During Squeeze Flow. Science 2008;322:720–4.
[100] Kumar G, Desai A, Schroers J. Bulk Metallic Glass: The Smaller the Better. Adv Mater 2011;23:461–76.
[101] Frost HJ, Ashby MF. Deformation-mechanism maps : the plasticity and creep of metals and ceramics. Pergamon Press; 1982.
[102] Liu Z, Schroers J. General nanomoulding with bulk metallic glasses. Nanotechnology 2015;26.
[103] Busch R, Schroers J, Wang WH. Thermodynamics and kinetics of bulk metallic glass. Mrs Bull 2007;32:620–3.
[104] Green JL, Ito K, Xu K, Angell CA. Fragility in liquids and polymers: New, simple quantifications and interpretations. J Phys Chem B 1999;103:3991–6.
[105] Duan G, Wiest A, Lind ML, Li J, Rhim WK, Johnson WL. Bulk metallic glass with benchmark thermoplastic processability. Adv Mater 2007;19:4272-+..
[106] Gallino I, Schroers J, Busch R. Kinetic and thermodynamic studies of the fragility of bulk metallic glass forming liquids. J Appl Phys 2010;108.
[107] Schroers J. On the formability of bulk metallic glass in its supercooled liquid state. Acta Mater 2008;56:471–8.
[108] Soejima H, Nishiyama N, Takehisa H, Shimanuki M, Inoue A. Viscous flow forming of Zr-based bulk metallic glasses for industrial applications. J Metastable Nanocryst Mater 2005;24:531.
[109] Pitt EB, Kumar G, Schroers J. Temperature dependence of the thermoplastic formability in bulk metallic glasses. J Appl Phys 2011;110.
[110] Blodgett ME, Egami T, Nussinov Z, Kelton KF. Proposal for universality in the viscosity of metallic liquids. Sci Rep-Uk 2015;5.
[111] Angell CA. Relaxation in Liquids, Polymers and Plastic Crystals - Strong Fragile Patterns and Problems. J Non-Cryst Solids 1991;131:13–31.
[112] Urakawa O, Swallen SF, Ediger MD, von Meerwall ED. Self-diffusion and viscosity of low molecular weight polystyrene over a wide temperature range. Macromolecules 2004;37:1558–64.
[113] Schroers J. Bulk Metallic Glasses. Phys Today 2013;66:32.
[114] Zhang B, Zhao DQ, Pan MX, Wang WH, Greer AL. Amorphous metallic plastic. Phys Rev Lett 2005;94:-..
[115] Schroers J. Processing of Bulk Metallic Glass. Adv Mater 2010;22:1566–97.
[116] Johnson WL, Kaltenboeck G, Demetriou MD, Schramm JP, Liu X, Samwer K, et al. Beating Crystallization in Glass-Forming Metals by Millisecond Heating and Processing. Science 2011;332:828–33.
[117] Wu FF, Zhang ZF, Mao SX, Eckert J. Effect of sample size on ductility of metallic glass. Phil Mag Lett 2009;89:178–84.
[118] Yi J, Wang WH, Lewandowski JJ. Sample size and preparation effects on the tensile ductility of Pd-based metallic glass nanowires. Acta Mater 2015;87:1–7.
[119] Volkert CA, Donohue A, Spaepen F. Effect of sample size on deformation in amorphous metals. J Appl Phys 2008;103:-..
[120] Magagnosc DJ, Ehrbar R, Kumar G, He MR, Schroers J, Gianola DS. Tunable Tensile Ductility in Metallic Glasses. Sci Rep-Uk 2013;3:1096.
[121] Magagnosc DJ, Kumar G, Schroers J, Gianola DS. Effect of Ion Irradiation on Tensile Ductility, Strength, and Fictive Temperature in Metallic Glass Nanowires. Acta Mater 2014;74:165.
[122] Magagnosc DJ, Chen W, Kumar G, Schroers J, Gianola DS. Thermomechanical Behavior of Molded Metallic Glass Nanowires. Sci Rep-Uk 2016;6.
[123] Csikor FF, Motz C, Weygand D, Zaiser M, Zapperi S. Dislocation Avalanches, Strain Bursts, and the Problem of Plastic Forming at the Micrometer Scale. Science 2007;318:251–4.
[124] Meduri C, Hasan M, Adam S, Kumar G. Effect of temperature on shear bands and bending plasticity of metallic glasses. J Alloy Compd 2018;732:922–7.
[125] Hasan M, Kumar G. High-throughput drawing and testing of metallic glass nanostructures. Nanoscale 2017;9:3261–8.
[126] Han G, Xu L, Liu Z. Controlled fabrication of hierarchical metal nanostructures. Mater Lett 2019;241:160–3.
[127] Xia Y, Yang P, Sun Y, Wu Y, Mayers B, Gates B, et al. One-dimensional nanostructures: synthesis, characterization, and applications. Adv Mater 2003;15:353–89.

[128] Zhang Z, Shimizu T, Chen L, Senz S, Gösele U. Bottom-Imprint Method for VSS Growth of Epitaxial Silicon Nanowire Arrays with an Aluminium Catalyst. Adv Mater 2009;21:4701–5.
[129] Routkevitch D, Bigioni T, Moskovits M, Xu JM. Electrochemical fabrication of CdS nanowire arrays in porous anodic aluminum oxide templates. The Journal of Physical Chemistry 1996;100:14037–47.
[130] Matsui S, Kaito T, Fujita J-i, Komuro M, Kanda K, Haruyama Y. Three-dimensional nanostructure fabrication by focused-ion-beam chemical vapor deposition. Journal of Vacuum Science & Technology B: Microelectronics and Nanometer Structures Processing, Measurement, and Phenomena 2000;18:3181–4.
[131] Mark AG, Gibbs JG, Lee T-C, Fischer P. Hybrid nanocolloids with programmed three-dimensional shape and material composition. Nat Mater 2013;12:802–7.
[132] Liu Y, Liu J, Sohn S, Li Y, Cha JJ, Schroers J. Metallic glass nanostructures of tunable shape and composition. Nat Commun 2015;6:7043.
[133] Yao Y, Huang Z, Xie P, Lacey SD, Jacob RJ, Xie H, et al. Carbothermal shock synthesis of high-entropy-alloy nanoparticles. Science 2018;359:1489–94.
[134] Mårtensson T, Carlberg P, Borgström M, Montelius L, Seifert W, Samuelson L. Nanowire arrays defined by nanoimprint lithography. Nano Lett 2004;4:699–702.
[135] Liu X, Chen N, Gu J-L, Yang G-N, Mussler G, Yao K-F. Die imprinting of MGs: A one-step approach for large-area metallic photonic crystals. Mater Des 2015;87:1018–21.
[136] Lei Y, Zhang LD, Meng GW, Li GH, Zhang XY, Liang CH, et al. Preparation and photoluminescence of highly ordered TiO2 nanowire arrays. Appl Phys Lett 2001;78:1125–7.
[137] Guo LJ. Nanoimprint lithography: Methods and material requirements. Adv Mater 2007;19:495–513.
[138] Li R, Chen Z, Datye A, Simon GH, Ketkaew J, Kinser E, et al. Atomic imprinting into metallic glasses. Communications Physics 2018;1:75.
[139] Zhang FX, Low HY. Ordered three-dimensional hierarchical nanostructures by nanoimprint lithography. Nanotechnology 2006;17:1884–90.
[140] Chou SY. Nanoimprint Lithography Nanofabrication Handbook 2012:187–206.
[141] Xia QF, Keimel C, Ge HX, Yu ZN, Wu W, Chou SY. Ultrafast patterning of nanostructures in polymers using laser assisted nanoimprint lithography. Appl Phys Lett 2003;83:4417–9.
[142] Pfeiffer K, Reuther F, Fink M, Gruetzner G, Carlberg P, Maximov I, et al. A comparison of thermally and photochemically cross-linked polymers for nanoimprinting. Microelectron Eng 2003;67–8:266–73.
[143] Singer JP, Gopinadhan M, Shao Z, Taylor AD, Schroers J, Osuji CO. Nanoimprinting Sub-100 nnn Features in a Photovoltaic Nanocomposite using Durable Bulk Metallic Glass Molds. Acs Appl Mater Inter 2015;7:3456–61.
[144] Hasan M, Shajahan I, Gopinadhan M, Ketkaew J, Anesgart A, Cho C, et al. Three-Dimensional Compatible Sacrificial Nanoimprint Lithography for Tuning the Wettability of Thermoplastic Materials. J Micro Nano-Manuf 2018;6.
[145] Cheng M, Wert JA. Modeling of microimprinting of bulk metallic glasses. J Mater Sci Technol 2006;22:851–4.
[146] Chang YC, Wu TT, Chen MF, Lee CJ, Huang JC, Pan CT. Finite element simulation of micro-imprinting in Mg-Cu-Y amorphous alloy. Mat Sci Eng a-Struct 2009;499:153–6.
[147] Kumar G, Blawzdziewicz J, Schroers J. Controllable nanoimprinting of metallic glasses: effect of pressure and interfacial properties. Nanotechnology 2013;24.
[148] Browne DJ, Stratton D, Gilchrist MD, Byrne CJ. Bulk Metallic Glass Multiscale Tooling for Molding of Polymers with Micro to Nano Features. A Review Metall Mater Trans A 2013;44a:2021–30..
[149] Bardt JA, Bourne GR, Schmitz TL, Ziegert JC, Sawyer WG. Micromolding three-dimensional amorphous metal structures. J Mater Res 2007;22:339–43.
[150] Pan CT, Wu TT, Chen MF, Chang YC, Lee CJ, Huang JC. Hot embossing of micro-lens array on bulk metallic glass. Sensors and Actuators a-Physical 2008;141:422–31.
[151] Schroers J, Nguyen T, O'Keeffe S, Desai A. Thermoplastic forming of bulk metallic glass - Applications for MEMS and microstructure fabrication. Mat Sci Eng a-Struct 2007;449:898–902.
[152] Li R, Chen Z, Datye A, Simon GH, Ketkaew J, Kinser E, et al. Atomic imprinting into metallic glasses. Commun Phys 2018;1.
[153] Zhang N, Chu JS, Byrne CJ, Browne DJ, Gilchrist MD. Replication of micro/nano-scale features by micro injection molding with a bulk metallic glass mold insert. J Micromech Microeng 2012;22.
[154] Schroers J, Pham Q, Desai A. Thermoplastic forming of bulk metallic glass - A technology for MEMS and microstructure fabrication. J Microelectromech S 2007;16:240–7.
[155] Hu ZL, Meduri CS, Blawzdziewicz J, Kumar G. Nanoshaping of glass forming metallic liquids by stretching: evading lithography. Nanotechnology 2019;30.
[156] Schroers J, Samwer K, Szuecs F, Johnson WL. Characterization of the interface between the bulk glass forming alloy Zr41Ti14Cu12Ni10Be23 with pure metals and ceramics. J Mater Res 2000;15:1617–21.
[157] Ding SY, Kong J, Schroers J. Wetting of bulk metallic glass forming liquids on metals and ceramics. J Appl Phys 2011;110.
[158] Chiu HM, Kumar G, Blawzdziewicz J, Schroers J. Thermoplastic extrusion of bulk metallic glass. Scr Mater 2009;61:28–31.
[159] Takenaka K, Saidoh N, Nishiyama N, Inoue A. Fabrication and nano-imprintabilities of Zr-, Pd- and Cu-based glassy alloy thin films. Nanotechnology 2011;22:-..
[160] Zhou C, Datye A, Chen Z, Simon GH, Wang X, Schroers J, et al. Atomic imprinting in the absence of an intrinsic length scale. Apl Mater 2020;8:111104.
[161] Carmo M, Sekol RC, Ding SY, Kumar G, Schroers J, Taylor AD. Bulk Metallic Glass Nanowire Architecture for Electrochemical Applications. ACS Nano 2011;5:2979–83.
[162] Hasan M, Kahler N, Kumar G. Shape-Controlled Metal-Metal and Metal-Polymer Janus Structures by Thermoplastic Embossing. Acs Appl Mater Inter 2016;8:11084–90.
[163] Dong Q, Li G, Ho CL, Faisal M, Leung CW, Pong PWT, et al. A Polyferroplatinyne Precursor for the Rapid Fabrication of L10-FePt-type Bit Patterned Media by Nanoimprint Lithography. Adv Mater 2012;24:1034–40.
[164] Chao CY, Guo LJ. Polymer microring resonators fabricated by nanoimprint technique. J Vac Sci Technol B 2002;20:2862–6.
[165] Xia QF, Robinett W, Cumbie MW, Banerjee N, Cardinali TJ, Yang JJ, et al. Memristor-CMOS Hybrid Integrated Circuits for Reconfigurable Logic. Nano Lett 2009;9:3640–5.
[166] Lee KT, Jang JY, Park SJ, Ji CG, Yang SM, Guo LJ, et al. Angle-Insensitive and CMOS-Compatible Subwavelength Color Printing. Adv Opt Mater 2016;4:1696–702.
[167] Suh KY, Kim YS, Lee HH. Capillary force lithography. Adv Mater 2001;13:1386–9.
[168] Suh KY, Park MC, Kim P. Capillary force lithography: a versatile tool for structured biomaterials interface towards cell and tissue engineering. Adv Funct Mater 2009;19:2699–712.
[169] Lakshmi BB, Patrissi CJ, Martin CR. Sol− gel template synthesis of semiconductor oxide micro-and nanostructures. Chem Mater 1997;9:2544–50.
[170] Chou SY, Krauss PR, Renstrom PJ. Nanoimprint lithography. J Vac Sci Technol B 1996;14:4129–33.
[171] Krauss PR, Chou SY. Nano-compact disks with 400 Gbit/in(2) storage density fabricated using nanoimprint lithography and read with proximal probe. Appl Phys Lett 1997;71:3174–6.
[172] Hirai Y, Harada S, Isaka S, Kobayashi M, Tanaka Y. Nano-imprint lithography using replicated mold by Ni electro plating. Microprocesses and Nanotechnology 2001, Digest of Papers. 2001:182-3 318.
[173] Zankovych S, Hoffmann T, Seekamp J, Bruch JU, Torres CMS. Nanoimprint lithography: challenges and prospects. Nanotechnology 2001;12:91–5.
[174] Chou SY. Special Issue: Nanoimprint Lithography: 20 years Foreword. Appl Phys a-Mater. 2015;121:317-8.
[175] Okada N, Egami T, Miyoshi S, Inomoto R, Yamane K, Tadatomo K, et al. InGaN-Based Light-Emitting Diodes Fabricated on Nano Patterned Sapphire Substrates with Pillar Height of More than 600 nm by Nanoimprint Lithography. Jpn J Appl Phys 2013;52.
[176] Mills E, Cannarella J, Zhang Q, Bhadra S, Arnold CB, Chou SY. Silicon nanopillar anodes for lithium-ion batteries using nanoimprint lithography with flexible molds. J Vac Sci Technol B 2014;32.
[177] Ok JG, Shin YJ, Park HJ, Guo LJ. A step toward next-generation nanoimprint lithography: extending productivity and applicability. Appl Phys a-Mater 2015;121:343–56.

[178] Schift H. Nanoimprint lithography: An old story in modern times? A review. J Vac Sci Technol B 2008;26:458–80.
[179] Fang TH, Li WL, Tao NR, Lu K. Revealing Extraordinary Intrinsic Tensile Plasticity in Gradient Nano-Grained Copper. Science 2011;331:1587–90.
[180] Greer JR, Nix WD. Nanoscale gold pillars strengthened through dislocation starvation. Physical Review B 2006;73:245410.
[181] Shan ZW, Mishra RK, Syed Asif SA, Warren OL, Minor AM. Mechanical annealing and source-limited deformation in submicrometre-diameter Ni crystals. Nat Mater 2008;7:115–9.
[182] Coble RL. A Model for Boundary Diffusion Controlled Creep in Polycrystalline Materials. J Appl Phys 1963;34:1679–82.
[183] Zhu TT, Bushby AJ, Dunstan DJ. Materials mechanical size effects: a review. Mater Technol 2008;23:193–209.
[184] Ashby MF. A first report on deformation-mechanism maps. Acta Metall 1972;20:887–97.
[185] Liu N, Liu G, Raj A, Sohn S, Morales-Acosta MD, Liu J, et al. Unleashing nanofabrication through thermomechanical nanomolding. Science Advances 2021;7 (47):eabi4567. https://doi.org/10.1126/sciadv.abi4567.
[186] Gupta D. Grain-Boundary Self-Diffusion in Au by Ar Sputtering Technique. J Appl Phys 1973;44:4455–8.
[187] Raj A, Liu NJ, Liu GN, Sohn S, Xiang JX, Liu Z, et al. Nanomolding of Gold and Gold-Silicon Heterostructures at Room Temperature. ACS Nano 2021;15: 14275–84.
[188] Hoffman RE, Turnbull D. Lattice and Grain Boundary Self-Diffusion in Silver. J Appl Phys 1951;22:634–9.
[189] Xu L, Shui L, Zhang Y, Peng Q, Xue L, Liu Z. Robust and reproducible fabrication of large area aluminum (Al) micro/nanorods arrays by superplastic nanomolding at room temperature. Appl Phys Express 2020;13:036503.
[190] Südkamp T, Bracht H. Self-diffusion in crystalline silicon: A single diffusion activation enthalpy down to 755◦ C. Physical Review B 2016;94:125208.
[191] Cui B, Keimel C, Chou SY. Ultrafast direct imprinting of nanostructures in metals by pulsed laser melting. Nanotechnology 2010;21:045303.
[192] Sohn SW, Liu YH, Liu JB, Gong P, Prades-Rodel S, Blatter A, et al. Noble metal high entropy alloys. Scripta Mater 2017;126:29–32.
[193] Paglione J, Greene RL. High-temperature superconductivity in iron-based materials. Nat Phys 2010;6:645.
[194] Chen J, Yu P, Stenger J, Hocevar M, Car D, Plissard SR, et al. Experimental phase diagram of zero-bias conductance peaks in superconductor/semiconductor nanowire devices. Sci Adv 2017;3:e1701476.
[195] Zhang E, Zhi J, Zou Y-C, Ye Z, Ai L, Shi J, et al. Signature of quantum Griffiths singularity state in a layered quasi-one-dimensional superconductor. Nat Commun 2018;9:4656.
[196] Gazibegovic S, Car D, Zhang H, Balk SC, Logan JA, de Moor MW, et al. Epitaxy of advanced nanowire quantum devices. Nature 2017;548:434.
[197] Plissard SR, Van Weperen I, Car D, Verheijen MA, Immink GW, Kammhuber J, et al. Formation and electronic properties of InSb nanocrosses. Nat Nanotechnol 2013;8:859.
[198] Tao Y, Degen CL. Growth of magnetic nanowires along freely selectable⟨ hkl⟩ crystal directions. Nat Commun 2018;9:339.
[199] Yue Z, Cai B, Wang L, Wang X, Gu M. Intrinsically core-shell plasmonic dielectric nanostructures with ultrahigh refractive index. Sci Adv 2016;2:e1501536.
[200] Rao F, Ding K, Zhou Y, Zheng Y, Xia M, Lv S, et al. Reducing the stochasticity of crystal nucleation to enable subnanosecond memory writing. Science 2017; 358:1423–7.
[201] Salinga M, Kersting B, Ronneberger I, Jonnalagadda VP, Vu XT, Le Gallo M, et al. Monatomic phase change memory. Nat Mater 2018;17:681.
[202] Xie Y, Kim W, Kim Y, Kim S, Gonsalves J, BrightSky M, et al. Self-healing of a confined phase change memory device with a metallic surfactant layer. Adv Mater 2018;30:1705587.
[203] Fatemi V, Wu S, Cao Y, Bretheau L, Gibson QD, Watanabe K, et al. Electrically tunable low-density superconductivity in a monolayer topological insulator. Science 2018;362:926–9.
[204] Pribiag VS, Beukman AJ, Qu F, Cassidy MC, Charpentier C, Wegscheider W, et al. Edge-mode superconductivity in a two-dimensional topological insulator. Nat Nanotechnol 2015;10:593.
[205] Jauregui LA, Pettes MT, Rokhinson LP, Shi L, Chen YP. Magnetic field-induced helical mode and topological transitions in a topological insulator nanoribbon. Nat Nanotechnol 2016;11:345.
[206] Flueli M, Borel JP. Surface-Energy Anisotropy Measurements on a Small Cuboctahedron of Gold Observed by High-Resolution Electron-Microscopy (Hrem). J Cryst Growth 1988;91:67–70.
[207] Yao Z, Wang C, Li Y, Kim N-Y. AAO-assisted synthesis of highly ordered, large-scale TiO 2 nanowire arrays via sputtering and atomic layer deposition. Nanoscale Res Lett 2015;10:166.
[208] Zhang L, Zhang P, Fang Y. Magnetron sputtering of silver nanowires using anodic aluminum oxide template: A new active substrate of surface enhanced Raman scattering and an investigation of its enhanced mechanism. Anal Chim Acta 2007;591:214–8.
[209] Li X, Meng G, Xu Q, Kong M, Zhu X, Chu Z, et al. Controlled synthesis of germanium nanowires and nanotubes with variable morphologies and sizes. Nano Lett 2011;11:1704–9.
[210] Zhao Q, Wen G, Liu Z, Fan Y, Zou G, Li L, et al. Synthesis of dense, single-crystalline CrO2 nanowire arrays using AAO template-assisted chemical vapor deposition. Nanotechnology 2011;22:125603.
[211] Li Y, Meng G, Zhang L, Phillipp F. Ordered semiconductor ZnO nanowire arrays and their photoluminescence properties. Appl Phys Lett 2000;76:2011–3.
[212] Jang D, Li X, Gao H, Greer JR. Deformation mechanisms in nanotwinned metal nanopillars. Nat Nanotechnol 2012;7:594.
[213] Che G, Lakshmi B, Martin C, Fisher E, Ruoff RS. Chemical vapor deposition based synthesis of carbon nanotubes and nanofibers using a template method. Chem Mater 1998;10:260–7.
[214] Hamrakulov B, In-Soo K, Lee M, Park B. Electrodeposited Ni, Fe, Co and Cu single and multilayer nanowire arrays on anodic aluminum oxide template. Transactions of Nonferrous Metals Society of China 2009;19:s83–7.
[215] Lew K-K, Redwing JM. Growth characteristics of silicon nanowires synthesized by vapor–liquid–solid growth in nanoporous alumina templates. J Cryst Growth 2003;254:14–22.
[216] Barbero DR, Saifullah MS, Hoffmann P, Mathieu HJ, Anderson D, Jones GA, et al. High-Resolution Nanoimprinting with a Robust and Reusable Polymer Mold. Adv Funct Mater 2007;17:2419–25.
[217] Liang CC, Lin CH, Cheng TC, Shieh J, Lin HH. Nanoimprinting of flexible polycarbonate sheets with a flexible polymer mold and application to superhydrophobic surfaces. Adv Mater Interfaces 2015;2:1500030.
[218] Mukherjee S, Carmo M, Kumar G, Sekol RC, Taylor AD, Schroers J. Palladium nanostructures from multi-component metallic glass. Electrochim Acta 2012;74: 145–50.
[219] Tavakoli MM, Waleed A, Gu L, Zhang D, Tavakoli R, Lei B, et al. A non-catalytic vapor growth regime for organohalide perovskite nanowires using anodic aluminum oxide templates. Nanoscale 2017;9:5828–34.
[220] Wang C, Li M, Pan S, Li H. Well-aligned carbon nanotube array membrane synthesized in porous alumina template by chemical vapor deposition. Chin Sci Bull 2000;45:1373–6.
[221] Kuo C, Gau C. Vapor–solid–solid growth of crystalline silicon nanowires using anodic aluminum oxide template. Thin Solid Films 2011;519:3603–7.
[222] Chen B, Xu Q, Zhao X, Zhu X, Kong M, Meng G. Branched Silicon Nanotubes and Metal Nanowires via AAO-Template-Assistant Approach. Adv Funct Mater 2010;20:3791–6.
[223] Liu X, Shao Y, Li J-F, Chen N, Yao K-F. Large-area and uniform amorphous metallic nanowire arrays prepared by die nanoimprinting. J Alloy Compd 2014;605: 7–11.
[224] Chu J, Wijaya H, Wu C, Tsai T, Wei C, Nieh T, et al. Nanoimprint of gratings on a bulk metallic glass. Appl Phys Lett 2007;90:034101.
[225] Gong P, Kou H, Wang S, Deng L, Wang X, Jin J. Research on thermoplastic formability and nanomoulding mechanism of lightweight Ti-based bulk metallic glasses. J Alloy Compd 2019;801:267–76.
[226] Gong P, Wang S, Liu Z, Chen W, Li N, Wang X, et al. Lightweight Ti-based bulk metallic glasses with superior thermoplastic formability. Intermetallics 2018;98: 54–9.
[227] Khang D-Y, Kang H, Kim T-I, Lee HH. Low-pressure nanoimprint lithography. Nano Lett 2004;4:633–7.

[228] Schulz H, Scheer H-C, Hoffmann T, Sotomayor Torres C, Pfeiffer K, Bleidiessel G, et al. New polymer materials for nanoimprinting. Journal of Vacuum Science & Technology B: Microelectronics and Nanometer Structures Processing, Measurement, and Phenomena 2000;18:1861–5.
[229] Pfeiffer K, Fink M, Bleidiessel G, Gruetzner G, Schulz H, Scheer H-C, et al. Novel linear and crosslinking polymers for nanoimprinting with high etch resistance. Microelectron Eng 2000;53:411–4.
[230] He X, Gao F, Tu G, Hasko DG, Hüttner S, Greenham NC, et al. Formation of well-ordered heterojunctions in polymer: PCBM photovoltaic devices. Adv Funct Mater 2011;21:139–46.
[231] Yang Y, Mielczarek K, Aryal M, Zakhidov A, Hu W. Nanoimprinted polymer solar cell ACS nano 2012;6:2877–92.
[232] Kim Y, Suh K, Lee HH. Fabrication of three-dimensional microstructures by soft molding. Appl Phys Lett 2001;79:2285–7.
[233] John J, Tang Y, Rothstein JP, Watkins JJ, Carter KR. Large-area, continuous roll-to-roll nanoimprinting with PFPE composite molds. Nanotechnology 2013;24:505307.
[234] Liu Y, Weiss DN, Li J. Rapid nanoimprinting and excellent piezoresponse of polymeric ferroelectric nanostructures. ACS Nano 2009;4:83–90.
[235] Khang D-Y, Lee HH. Sub-100 nm patterning with an amorphous fluoropolymer mold. Langmuir 2004;20:2445–8.
[236] Sirringhaus H, Brown P, Friend R, Nielsen MM, Bechgaard K, Langeveld-Voss B, et al. Two-dimensional charge transport in self-organized, high-mobility conjugated polymers. Nature 1999;401:685.
[237] Rolland JP, Hagberg EC, Denison GM, Carter KR, De Simone JM. High-resolution soft lithography: enabling materials for nanotechnologies. Angew Chem Int Ed 2004;43:5796–9.
[238] Li Z, Gu Y, Wang L, Ge H, Wu W, Xia Q, et al. Hybrid nanoimprint– soft lithography with sub-15 nm resolution. Nano Lett 2009;9:2306–10.
[239] Hagberg EC, Malkoch M, Ling Y, Hawker CJ, Carter KR. Effects of modulus and surface chemistry of thiol-ene photopolymers in nanoimprinting. Nano Lett 2007;7:233–7.
[240] Chiu C-H, Kuo H-L, Chen P-C, Wen C-H, Liu Y-C, Chen H-M-P. Nanoimprinting-lithography-induced self-aligned liquid crystals for novel multifunctional optical films. Appl Phys Lett 2006;88(7):073509.
[241] Liu C, Yiu W, Au F, Ding J, Lee C, Lee S. Electrical properties of zinc oxide nanowires and intramolecular p–n junctions. Appl Phys Lett 2003;83:3168–70.
[242] Liu C, Zapien JA, Yao Y, Meng X, Lee CS, Fan S, et al. High-Density, ordered ultraviolet light-emitting ZnO nanowire arrays. Adv Mater 2003;15:838–41.
[243] Fan HJ, Lee W, Scholz R, Dadgar A, Krost A, Nielsch K, et al. Arrays of vertically aligned and hexagonally arranged ZnO nanowires: a new template-directed approach. Nanotechnology 2005;16:913.
[244] Feng H, Zhuo R, Chen J, Yan D, Feng J, Li H, et al. Axial periodical nanostructures of Sb-doped SnO2 grown by chemical vapor deposition. Physica E 2009;41:1640–4.
[245] Zhao Q, Wen G, Liu Z, Yuan J, Li D, Zou G, et al. High-density, vertically aligned crystalline CrO 2 nanorod arrays derived from chemical vapor deposition assisted by AAO templates. Chem Commun 2009;3949–51.
[246] Liu J, Yan P, Yue G, Kong L, Zhuo R, Qu D. Synthesis of doped ZnS one-dimensional nanostructures via chemical vapor deposition. Mater Lett 2006;60:3471–6.
[247] Ding J, Zapien J, Chen W, Lifshitz Y, Lee S, Meng X. Lasing in ZnS nanowires grown on anodic aluminum oxide templates. Appl Phys Lett 2004;85:2361–3.
[248] Wu Q, Ren S, Deng S, Chen J, Xu N. Growth of aligned Cu 2 S nanowire arrays with AAO template and their field-emission properties. Journal of Vacuum Science & Technology B: Microelectronics and Nanometer Structures Processing, Measurement, and Phenomena 2004;22:1282–5.
[249] Zhang J, Jin L, Li S, Xie J, Yang F, Duan J, et al. Fabrication of two types of ordered InP Nanowire Arrays on a single anodic aluminum oxide template and its application in solar cells. J Mater Sci Technol 2015;31:634–8.
[250] Wang X, Sun X, Fairchild M, Hersee SD. Fabrication of GaN nanowire arrays by confined epitaxy. Appl Phys Lett 2006;89:233115.
[251] Li Z, Zhang J, Meng A, Guo J. Large-area highly-oriented SiC nanowire arrays: synthesis, Raman, and photoluminescence properties. J Phys Chem B 2006;110:22382–6.
[252] Tseng AA. Recent developments in nanofabrication using focused ion beams. Small 2005;1:924–39.
[253] Kim C-S, Ahn S-H, Jang D-Y. Developments in micro/nanoscale fabrication by focused ion beams. Vacuum 2012;86:1014–35.
[254] Dhawan A, Gerhold M, Vo-Dinh T. Theoretical simulation and focused ion beam fabrication of gold nanostructures for surface-enhanced Raman scattering (SERS). NanoBiotechnology 2007;3:164–71.
[255] Volkert CA, Minor AM. Focused ion beam microscopy and micromachining. Mrs Bull 2007;32:389–95.
[256] Tseng AA, Chen K, Chen CD, Ma KJ. Electron beam lithography in nanoscale fabrication: recent development. IEEE Trans Electron Packag Manuf 2003;26:141–9.
[257] Chen Y. Nanofabrication by electron beam lithography and its applications: A review. Microelectron Eng 2015;135:57–72.
[258] van Kan JA, Bettiol AA, Watt F. Three-dimensional nanolithography using proton beam writing. Appl Phys Lett 2003;83:1629–31.
[259] Watt F, Breese MB, Bettiol AA, van Kan JA. Proton beam writing Mater Today 2007;10:20–9.
[260] Tseng AA, Notargiacomo A, Chen TP. Nanofabrication by scanning probe microscope lithography: A review. J Vac Sci Technol B 2005;23:877–94.
[261] Matsui S, Ichihashi T. I nsitu observation on electron-beam-induced chemical vapor deposition by transmission electron microscopy. Appl Phys Lett 1988;53:842–4.
[262] Xue CF, Zhao J, Wu YQ, Yu HN, Yang SM, Wang LS, et al. Fabrication of large-area high-aspect-ratio periodic nanostructures on various substrates by soft X-ray interference lithography. Appl Surf Sci 2017;425:553–7.
[263] Baglin JEE. Ion beam nanoscale fabrication and lithography-A review. Appl Surf Sci 2012;258:4103–11.
[264] Wua BQ, Kumar A. Extreme ultraviolet lithography: A review. J Vac Sci Technol B 2007;25:1743–61.
[265] Hong F., Blaikie R. Plasmonic Lithography: Recent Progress. Adv Opt Mater 2019;7(14):1801653.
[266] Mojarad N, Gobrecht J, Ekinci Y. Interference lithography at EUV and soft X-ray wavelengths: Principles, methods, and applications. Microelectron Eng 2015;143:55–63.
[267] Zhang JH, Li YF, Zhang XM, Yang B. Colloidal Self-Assembly Meets Nanofabrication: From Two-Dimensional Colloidal Crystals to Nanostructure Arrays. Adv Mater 2010;22:4249–69.
[268] Wu H, Pan W, Lin DD, Li HP. Electrospinning of ceramic nanofibers: Fabrication, assembly and applications. J Adv Ceram 2012;1:2–23.
[269] Reneker DH, Chun I. Nanometre diameter fibres of polymer, produced by electrospinning. Nanotechnology 1996;7:216–23.
[270] Turkevich J, Stevenson PC, Hillier J. A study of the nucleation and growth processes in the synthesis of colloidal gold. Discuss Faraday Soc 1951;11:55–75.
[271] Murray CB, Norris DJ, Bawendi MG. Synthesis and Characterization of Nearly Monodisperse Cde (E = S, Se, Te) Semiconductor Nanocrystallites. J Am Chem Soc 1993;115:8706–15.
[272] Stöber W, Fink A, Bohn E. Controlled growth of monodisperse silica spheres in the micron size range. J Colloid Interface Sci 1968;26:62–9.
[273] Guozhong C. Nanostructures and nanomaterials: synthesis, properties and applications. World scientific; 2004.
[274] Sercel PC, Saunders WA, Atwater HA, Vahala KJ, Flagan RC. Nanometer-Scale Gaas Clusters from Organometallic Precursors. Appl Phys Lett 1992;61:696–8.
[275] Uchida K, Kaneko S, Omi S, Hata C, Tanji H, Asahara Y, et al. Optical Nonlinearities of a High-Concentration of Small Metal Particles Dispersed in Glass - Copper and Silver Particles. J Opt Soc Am B 1994;11:1236–43.
[276] Sears GW. A Mechanism of Whisker Growth. Acta Metall Mater 1955;3:367–9.
[277] Heath JR, Legoues FK. A Liquid Solution Synthesis of Single-Crystal Germanium Quantum Wires. Chem Phys Lett 1993;208:263–8.
[278] Sun YG, Gates B, Mayers B, Xia YN. Crystalline silver nanowires by soft solution processing. Nano Lett 2002;2:165–8.
[279] Gudiksen MS, Lieber CM. Diameter-selective synthesis of semiconductor nanowires. J Am Chem Soc 2000;122:8801–2.
[280] Trentler TJ, Hickman KM, Goel SC, Viano AM, Gibbons PC, Buhro WE. Solution-Liquid-Solid Growth of Crystalline Iii-V Semiconductors - an Analogy to Vapor-Liquid-Solid Growth. Science 1995;270:1791–4.
[281] Yu D, Lee C, Bello I, Sun X, Tang Y, Zhou G, et al. Synthesis of nano-scale silicon wires by excimer laser ablation at high temperature. Solid State Commun 1998;105:403–7.
[282] Whitesides GM, Grzybowski B. Self-assembly at all scales. Science 2002;295:2418–21.

[283] Yan X, Yao JM, Lu G, Li X, Zhang JH, Han K, et al. Fabrication of non-close-packed arrays of colloidal spheres by soft lithography. J Am Chem Soc 2005;127:7688–9.
[284] Aizenberg J, Braun PV, Wiltzius P. Patterned colloidal deposition controlled by electrostatic and capillary forces. Phys Rev Lett 2000;84:2997–3000.
[285] Ozin GA, Hou K, Lotsch BV, Cademartiri L, Puzzo DP, Scotognella F, et al. Nanofabrication by self-assembly Mater Today 2009;12:12–23.
[286] Thurn-Albrecht T, Schotter J, Kastle CA, Emley N, Shibauchi T, Krusin-Elbaum L, et al. Ultrahigh-density nanowire arrays grown in self-assembled diblock copolymer templates. Science 2000;290:2126–9.
[287] Kim SO, Solak HH, Stoykovich MP, Ferrier NJ, de Pablo JJ, Nealey PF. Epitaxial self-assembly of block copolymers on lithographically defined nanopatterned substrates. Nature 2003;424:411–4.
[288] Cummins C, Lundy R, Walsh JJ, Ponsinet V, Fleury G, Morris MA. Enabling Future Nanomanufacturing through Block Copolymer Self-Assembly: A review. Nano Today 2020;35:100936.
[289] Tan KW, Jung B, Werner JG, Rhoades ER, Thompson MO, Wiesner U. Transient laser heating induced hierarchical porous structures from block copolymer-directed self-assembly. Science 2015;349:54–8.
[290] Templin M, Franck A, DuChesne A, Leist H, Zhang YM, Ulrich R, et al. Organically modified aluminosilicate mesostructures from block copolymer phases. Science 1997;278:1795–8.
[291] Zhao DY, Feng JL, Huo QS, Melosh N, Fredrickson GH, Chmelka BF, et al. Triblock copolymer syntheses of mesoporous silica with periodic 50 to 300 angstrom pores. Science 1998;279:548–52.
[292] Zou YD, Zhou XR, Ma JH, Yang XY, Deng YH. Recent advances in amphiphilic block copolymer templated mesoporous metal-based materials: assembly engineering and applications. Chem Soc Rev 2020;49:1173–208.
[293] Robbins SW, Beaucage PA, Sai H, Tan KW, Werner JG, Sethna JP, et al. Block copolymer self-assembly-directed synthesis of mesoporous gyroidal superconductors. Science Advances 2016;2(1):e1501119.
[294] Robbins SW, Sai H, DiSalvo FJ, Gruner SM, Wiesner U. Monolithic Gyroidal Mesoporous Mixed Titanium-Niobium Nitrides. ACS Nano 2014;8:8217–23.
[295] Thedford RP, Beaucage PA, Susca EM, Chao CA, Nowack KC, Van Dover RB, et al. Superconducting Quantum Metamaterials from High Pressure Melt Infiltration of Metals into Block Copolymer Double Gyroid Derived Ceramic Templates. Adv Funct Mater 2021;31(23):2100469.
[296] Hu Y, Gu M, Liu X, Zhang J, Huang S, Liu B. Sol-Gel Template Synthesis and Characterization of Lu2O3: Eu3+ Nanowire Arrays. Micromachines 2018;9:601.
[297] Limmer SJ, Seraji S, Forbess MJ, Wu Y, Chou TP, Nguyen C, et al. Electrophoretic growth of lead zirconate titanate nanorods. Adv Mater 2001;13:1269–72.
[298] Miao Z, Xu D, Ouyang J, Guo G, Zhao X, Tang Y. Electrochemically induced sol− gel preparation of single-crystalline TiO2 nanowires. Nano Lett 2002;2:717–20.
[299] Yue G, Yan P, Fan X, Wang M, Qu D, Yan D, et al. Characterization of the single crystalline iron sulfide nanowire array synthesis by pulsed electrodeposition. J Appl Phys 2006;100:124313.
[300] Moshonov M, Frey GL. Directing Hybrid Structures by Combining Self-Assembly of Functional Block Copolymers and Atomic Layer Deposition: A Demonstration on Hybrid Photovoltaics. Langmuir 2015;31:12762–9.
[301] Li Y, Qian F, Xiang J, Lieber CM. Nanowire electronic and optoelectronic devices. Mater Today 2006;9:18–27.
[302] Routkevitch D, Tager AA, Haruyama J, Almawlawi D, Moskovits M, Xu JM. Nonlithographic nano-wire arrays: Fabrication, physics, and device applications. Ieee T Electron Dev 1996;43:1646–58.
[303] Hayden O, Agarwal R, Lu W. Semiconductor nanowire devices. Nano Today 2008;3:12–22.
[304] Lin H, Huang CP, Li W, Ni C, Shah SI, Tseng YH. Size dependency of nanocrystalline TiO2 on its optical property and photocatalytic reactivity exemplified by 2-chlorophenol. Appl Catal B-Environ 2006;68:1–11.
[305] Gul O, Zhang H, Bommer JDS, de Moor MWA, Car D, Plissard SR, et al. Ballistic Majorana nanowire devices. Nat Nanotechnol 2018;13:192–7.
[306] Ramgir NS, Yang Y, Zacharias M. Nanowire-Based Sensors. Small 2010;6:1705–22.
[307] Yu KS, Pan XL, Zhang GB, Liao XB, Zhou XB, Yan MY, et al. Nanowires in Energy Storage Devices: Structures, Synthesis, and Applications. Adv Energy Mater 2018;8(32):1802369.
[308] Li YG, Tan B, Wu YY. Mesoporous CO3O4 nanowire arrays for lithium ion batteries with high capacity and rate capability. Nano Lett 2008;8:265–70.
[309] Huang JY, Zhong L, Wang CM, Sullivan JP, Xu W, Zhang LQ, et al. In Situ Observation of the Electrochemical Lithiation of a Single SnO2 Nanowire Electrode. Science 2010;330:1515–20.
[310] Cao YL, Xiao LF, Wang W, Choi DW, Nie ZM, Yu JG, et al. Reversible Sodium Ion Insertion in Single Crystalline Manganese Oxide Nanowires with Long Cycle Life. Adv Mater 2011;23:3155–60.
[311] Wang K, Wu HP, Meng YN, Wei ZX. Conducting Polymer Nanowire Arrays for High Performance Supercapacitors. Small 2014;10:14–31.
[312] McAlpine MC, Friedman RS, Lieber DM. Nanoimprint lithography for hybrid plastic electronics. Nano Lett 2003;3:443–5.
[313] Dauler EA, Grein ME, Kerman AJ, Marsili F, Miki S, Nam SW, et al. Review of superconducting nanowire single-photon detector system design options and demonstrated performance. Opt Eng 2014;53:081907.
[314] Yogeswaran U, Chen SM. A review on the electrochemical sensors and biosensors composed of nanowires as sensing material. Sensors-Basel 2008;8:290–313.
[315] Cui Y, Wei QQ, Park HK, Lieber CM. Nanowire nanosensors for highly sensitive and selective detection of biological and chemical species. Science 2001;293:1289–92.
[316] Murray BJ, Walter EC, Penner RM. Amine vapor sensing with silver mesowires. Nano Lett 2004;4:665–70.
[317] McAlpine MC, Agnew HD, Rohde RD, Blanco M, Ahmad H, Stuparu AD, et al. Peptide-nanowire hybrid materials for selective sensing of small molecules. J Am Chem Soc 2008;130:9583–9.
[318] Lai E, Kim W, Yang PD. Vertical Nanowire Array-Based Light Emitting Diodes. Nano Res 2008;1:123–8.
[319] Liu PZ, Wilhams JR, Cha JJ. Topological nanomaterials Nat Rev Mater 2019;4:479–96.
[320] Xia XH, Tu JP, Mai YJ, Wang XL, Gu CD, Zhao XB. Self-supported hydrothermal synthesized hollow Co3O4 nanowire arrays with high supercapacitor capacitance. J Mater Chem 2011;21:9319–25.
[321] Gibson SJ, van Kasteren B, Tekcan B, Cui YC, van Dam D, Haverkort JEM, et al. Tapered InP nanowire arrays for efficient broadband high-speed single-photon detection. Nat Nanotechnol 2019;14:473–9.
[322] Talin AA, Hunter LL, Leonard F, Rokad B. Large area, dense silicon nanowire array chemical sensors. Appl Phys Lett 2006;89:153102.
[323] Xu S, Xu C, Liu Y, Hu YF, Yang RS, Yang Q, et al. Ordered Nanowire Array Blue/Near-UV Light Emitting Diodes. Adv Mater 2010;22:4749–53.
[324] Hu L, Chen G. Analysis of optical absorption in silicon nanowire Arrays for photovoltaic applications. Nano Lett 2007;7:3249–52.
[325] Li JS, Yu HY, Wong SM, Li XC, Zhang G, Lo PGQ, et al. Design guidelines of periodic Si nanowire arrays for solar cell application. Appl Phys Lett 2009;95:243113.
[326] Lin CX, Povinelli ML. Optical absorption enhancement in silicon nanowire arrays with a large lattice constant for photovoltaic applications. Opt Express 2009;17:19371–81.
[327] Zhang X, Lu W, Da J, Wang H, Zhao D, Webley PA. Porous platinum nanowire arrays for direct ethanol fuel cell applications. Chem Commun 2009,:195–7.
[328] Qiao Y, Li CM. Nanostructured catalysts in fuel cells. J Mater Chem 2011;21:4027–36.
[329] Guo F, Cheng K, Ye K, Wang G, Cao D. Preparation of nickel-cobalt nanowire arrays anode electro-catalyst and its application in direct urea/hydrogen peroxide fuel cell. Electrochim Acta 2016;199:290–6.
[330] Xu C, Wang H, Shen PK, Jiang SP. Highly ordered Pd nanowire arrays as effective electrocatalysts for ethanol oxidation in direct alcohol fuel cells. Adv Mater 2007;19:4256–9.
[331] Peng KQ, Wang X, Lee ST. Silicon nanowire array photoelectrochemical solar cells. Appl Phys Lett 2008;92:163103.
[332] Aberg I, Vescovi G, Asoli D, Naseem U, Gilboy JP, Sundvall C, et al. A GaAs Nanowire Array Solar Cell with 15.3% Efficiency at 1 Sun. EEE Journal of photovoltaics 2015;6(1):185–90.
[333] Im JH, Luo JS, Franckevicius M, Pellet N, Gao P, Moehl T, et al. Nanowire Perovskite Solar Cell. Nano Lett 2015;15:2120–6.

[334] Tian B, Kempa TJ, Lieber CM. Single nanowire photovoltaics. Chem Soc Rev 2009;38:16–24.
[335] Doubek G, Sekol RC, Li JY, Ryu WH, Gittleson FS, Nejati S, et al. Guided Evolution of Bulk Metallic Glass Nanostructures: A Platform for Designing 3D Electrocatalytic Surfaces. Adv Mater 2016;28:1940–9.
[336] Chang FF, Yu G, Shan SY, Skeete Z, Wu JF, Luo J, et al. Platinum-nickel nanowire catalysts with composition-tunable alloying and faceting for the oxygen reduction reaction. J Mater Chem A 2017;5:12557–68.
[337] Choi WC, Woo SI. Bimetallic Pt–Ru nanowire network for anode material in a direct-methanol fuel cell. J Power Sources 2003;124:420–5.
[338] Pan CF, Wu H, Wang C, Wang B, Zhang L, Cheng ZD, et al. Nanowire-based high performance "micro fuel cell": One nanowire, one fuel cell. Adv Mater 2008;20 (9):1644–8.
[339] Jiang P, Liu Q, Liang Y, Tian J, Asiri AM, Sun X. A cost-effective 3D hydrogen evolution cathode with high catalytic activity: FeP nanowire array as the active phase. Angew Chem 2014;126:13069–73.
[340] Lu BA, Cao DX, Wang P, Wang GL, Gao YY. Oxygen evolution reaction on Ni-substituted Co3O4 nanowire array electrodes. Int J Hydrogen Energ 2011;36: 72–8.
[341] Tang C, Gan L, Zhang R, Lu W, Jiang X, Asiri AM, et al. Ternary Fe x Co1–x P nanowire array as a robust hydrogen evolution reaction electrocatalyst with Pt-like activity: experimental and theoretical insight. Nano Lett 2016;16:6617–21.
[342] Ma M, Djanashvili K, Smith WA. Controllable Hydrocarbon Formation from the Electrochemical Reduction of CO2 over Cu Nanowire Arrays. Angew Chem Int Edit 2016;55:6680–4.
[343] Su JZ, Guo LJ, Yoriya S, Grimes CA. Aqueous Growth of Pyramidal-Shaped BiVO4 Nanowire Arrays and Structural Characterization: Application to Photoelectrochemical Water Splitting. Cryst Growth Des 2010;10:856–61.
[344] Ai GJ, Li HX, Liu SP, Mo R, Zhong JX. Solar Water Splitting by TiO2/CdS/Co-Pi Nanowire Array Photoanode Enhanced with Co-Pi as Hole Transfer Relay and CdS as Light Absorber. Adv Funct Mater 2015;25:5706–13.
[345] Wang DF, Pierre A, Kibria MG, Cui K, Han XG, Bevan KH, et al. Wafer-Level Photocatalytic Water Splitting on GaN Nanowire Arrays Grown by Molecular Beam Epitaxy. Nano Lett 2011;11:2353–7.
[346] AlOtaibi B, Fan SZ, Wang DF, Ye JH, Mi ZT. Wafer-Level Artificial Photosynthesis for CO2 Reduction into CH4 and CO Using GaN Nanowires. Acs Catal 2015;5: 5342–8.
[347] Gao J, Sahli F, Liu CJ, Ren D, Guo XY, Werner J, et al. Solar Water Splitting with Perovskite/Silicon Tandem Cell and TiC-Supported Pt Nanocluster Electrocatalyst. Joule 2019;3:2930–41.
[348] Fu LH, Yang FL, Cheng GZ, Luo W. Ultrathin Ir nanowires as high-performance electrocatalysts for efficient water splitting in acidic media. Nanoscale 2018;10: 1892–7.
[349] Peng Z, Jia DS, Al-Enizi AM, Elzatahry AA, Zheng GF. From Water Oxidation to Reduction: Homologous Ni-Co Based Nanowires as Complementary Water Splitting Electrocatalysts. Adv Energy Mater 2015;5.
[350] Liao L, Wang SN, Xiao JJ, Bian XJ, Zhang YH, Scanlon MD, et al. A nanoporous molybdenum carbide nanowire as an electrocatalyst for hydrogen evolution reaction. Energy Environ Sci 2014;7:387–92.
[351] Wang PL, Wang SC, Wang HQ, Wu ZB, Wang LZ. Recent Progress on Photo-Electrocatalytic Reduction of Carbon Dioxide. Part Part Syst Char 2018;35.
[352] Gao ZQ, Agarwal A, Trigg AD, Singh N, Fang C, Tung CH, et al. Silicon nanowire arrays for label-free detection of DNA. Anal Chem 2007;79:3291–7.
[353] Hai A, Shappir J, Spira ME. In-cell recordings by extracellular microelectrodes. Nat Methods 2010;7(3):200–2.
[354] Hochberg LR, Serruya MD, Friehs GM, Mukand JA, Saleh M, Caplan AH, et al. Neuronal ensemble control of prosthetic devices by a human with tetraplegia. Nature 2006;442:164–71.
[355] Nicolelis MAL, Lebedev MA. OPINION Principles of neural ensemble physiology underlying the operation of brain-machine interfaces. Nat Rev Neurosci 2009; 10:530–40.
[356] Qi SJ, Yi CQ, Ji SL, Fong CC, Yang MS. Cell Adhesion and Spreading Behavior on Vertically Aligned Silicon Nanowire Arrays. Acs Appl Mater Inter 2009;1: 30–4.
[357] Jones RS, Draheim RR, Roldo M. Silver Nanowires: Synthesis, Antibacterial Activity and Biomedical Applications. Appl Sci 2018;8(5):673.
[358] Hochbaum AI, Aizenberg J. Bacteria Pattern Spontaneously on Periodic Nanostructure Arrays. Nano Lett 2010;10:3717–21.
[359] Bucaro MA, Vasquez Y, Hatton BD, Aizenberg J. Fine-Tuning the Degree of Stem Cell Polarization and Alignment on Ordered Arrays of High-Aspect-Ratio Nanopillars. ACS Nano 2012;6:6222–30.
[360] Schroers J, Kumar G, Hodges TM, Chan S, Kyriakides TR. Bulk metallic glasses for biomedical applications. Jom 2009;61:21–9.
[361] Elnathan R, Kwiat M, Patolsky F, Voelcker NH. Engineering vertically aligned semiconductor nanowire arrays for applications in the life sciences. Nano Today 2014;9:172–96.
[362] Padmanabhan J, Augelli MJ, Cheung B, Kinser ER, Cleary B, Kumar P, et al. Regulation of cell-cell fusion by nanotopography. Sci Rep 2016;6(1):1–9.
[363] Loye AM, Kinser ER, Bensouda S, Shayan M, Davis R, Wang R, et al. Regulation of Mesenchymal Stem Cell Differentiation by Nanopatterning of Bulk Metallic Glass. Sci Rep 2018;8(1):1–11.
[364] Shayan M, Padmanabhan J, Morris AH, Cheung B, Smith R, Schroers J, et al. Nanopatterned bulk metallic glass-based biomaterials modulate macrophage polarization. Acta Biomater 2018;75:427–38.
[365] Lee JY, Kang BS, Hicks B, Chancellor TF, Chu BH, Wang HT, et al. The control of cell adhesion and viability by zinc oxide nanorods. Biomaterials 2008;29: 3743–9.
[366] Porter JR, Henson A, Popat KC. Biodegradable poly (ε-caprolactone) nanowires for bone tissue engineering applications. Biomaterials 2009;30:780–8.
[367] Chan BP, Leong KW. Scaffolding in tissue engineering: general approaches and tissue-specific considerations. Eur Spine J 2008;17:S467–79.
[368] Salata OV. Applications of nanoparticles in biology and medicine. Journal of nanobiotechnology 2004;2:1–6.
[369] Dvir T, Timko BP, Kohane DS, Langer R. Nanotechnological strategies for engineering complex tissues. Nat Nanotechnol 2011;6:13–22.
[370] Chen HT, Taylor AJ, Yu NF. A review of metasurfaces: physics and applications. Rep Prog Phys 2016;79:076401.
[371] Assouar B, Liang B, Wu Y, Li Y, Cheng JC, Jing Y. Acoustic metasurfaces Nat Rev Mater 2018;3:460–72.
[372] Li XM, Reinhoudt D, Crego-Calama M. What do we need for a superhydrophobic surface? A review on the recent progress in the preparation of superhydrophobic surfaces. Chem Soc Rev 2007;36:1529-..
[373] Yu XL, Zhou J, Liang HY, Jiang ZY, Wu LL. Mechanical metamaterials associated with stiffness, rigidity and compressibility: A brief review. Prog Mater Sci 2018;94:114–73.
[374] Zheludev NI, Kivshar YS. From metamaterials to metadevices. Nat Mater 2012;11:917–24.
[375] Cummer SA, Christensen J, Alu A. Controlling sound with acoustic metamaterials. Nat Rev Mater 2016;1(3):1–13.
[376] Lassaline N, Brechbuhler R, Vonk SJW, Ridderbeek K, Spieser M, Bisig S, et al. Optical Fourier surfaces. Nature 2020;582:506–10.
[377] Li ZC, Liu WW, Cheng H, Chen SQ, Tian JG. Realizing Broadband and Invertible Linear-to-circular Polarization Converter with Ultrathin Single-layer Metasurface. Sci Rep-Uk 2015;5:1–9.
[378] Luo XG. Subwavelength Optical Engineering with Metasurface Waves. Adv. Opt Mater 2018;6:1701201.
[379] Yu NF, Capasso F. Flat optics with designer metasurfaces. Nat Mater 2014;13:139–50.
[380] Guo X, Ma YG, Wang YP, Tong LM. Nanowire plasmonic waveguides, circuits and devices. Laser Photonics Rev 2013;7:855–81.
[381] Wang AX, Kong XM. Review of Recent Progress of Plasmonic Materials and Nano-Structures for Surface-Enhanced Raman Scattering. Materials 2015;8: 3024–52.
[382] Lv PY, Xue YH, Shi YP, Lin H, Duan HL. Metastable States and Wetting Transition of Submerged Superhydrophobic Structures. Phys Rev Lett 2014;112:196101.
[383] Xiang YL, Huang SL, Lv PY, Xue YH, Su Q, Duan HL. Ultimate Stable Underwater Superhydrophobic State. Phys Rev Lett 2017;119:134501.
[384] Wen RF, Li Q, Wu JF, Wu GS, Wang W, Chen YF, et al. Hydrophobic copper nanowires for enhancing condensation heat transfer. Nano Energy 2017;33: 177–83.

[385] Lei Y, Cai WP, Wilde G. Highly ordered nanostructures with tunable size, shape and properties: A new way to surface nano-patterning using ultra-thin alumina masks. Prog Mater Sci 2007;52:465–539.
[386] schroers J, Kumar G, Tang H. Method for Imprinting and Erasing Amorphous Metal Alloys. US20140186648A1.
[387] Wu MH, Wen LY, Lei Y, Ostendorp S, Chen K, Wilde G. Ultrathin Alumina Membranes for Surface Nanopatterning in Fabricating Quantum-Sized Nanodots. Small 2010;6:695–9.
[388] Lei Y, Yang SK, Wu MH, Wilde G. Surface patterning using templates: concept, properties and device applications. Chem Soc Rev 2011;40:1247–58.
[389] Yang SK, Xu F, Ostendorp S, Wilde G, Zhao H, Lei Y. Template-Confined Dewetting Process to Surface Nanopatterns: Fabrication, Structural Tunability, and Structure-Related Properties. Adv Funct Mater 2011;21:2446–55.
[390] Hasannaeimi V, Wang X, Salloom R, Xia Z, Schroers J, Mukherjee S. Nanomanufacturing of Non-Noble Amorphous Alloys for Electrocatalysis. ACS Applied Energy Materials 2020;3(12):12099–107.
[391] Tan H, Gilbertson A, Chou SY. Roller nanoimprint lithography. Journal of Vacuum Science & Technology B: Microelectronics and Nanometer Structures Processing, Measurement, and Phenomena 1998;16:3926–8.
[392] Kooy N, Mohamed K, Pin LT, Guan OS. A review of roll-to-roll nanoimprint lithography. Nanoscale Res Lett 2014;9:320.
[393] Ahn SH, Guo LJ. High-speed roll-to-roll nanoimprint lithography on flexible plastic substrates. Adv Mater 2008;20:2044–9.
[394] Ahn SH, Guo LJ. Large-Area Roll-to-Roll and Roll-to-Plate Nanoimprint Lithography: A Step toward High-Throughput Application of Continuous Nanoimprinting. ACS Nano 2009;3:2304–10.
[395] Deng F, Xiang J, Liu Z, Ding T. Dynamic and reversible tuning of pixelated plasmonic cluster arrays. J. Mater. Chem. C 2021;9:15927–31.
[396] Xiang J, Wang Y, Wu Y, Fang H, Shui L, Liu Z, et al. Ordered Hierarchical Ag Nanostructures as Surface-Enhanced Raman Scattering Platforms for (Bio) chemical Sensing and Pollutant Monitoring. ACS Appl. Nano Mater. 2021. https://doi.org/10.1021/acsanm.1c02200.
[397] Xiang J, Wang Y, Wu Y, Peng Q, Shui L, Ouyang W, et al. Superplastic Nanomolding of Highly Ordered Metallic Sub-Micrometer Pillars Arrays for Surface Enhanced Raman Scattering. Advanced Materials Technologies 2021:2100891.
[398] Liu G, Sohn S, Liu N, Raj A, Schwarz U, Schroers J. Single-Crystal Nanostructure Arrays Forming Epitaxially through Thermomechanical Nanomolding. Nano Lett. 2021. https://doi.org/10.1021/acs.nanolett.1c03744.